UNIVERSITAT POLITÈCNICA DE VALÈNCIA

Departamento de Máquinas y Motores Térmicos

DOCTORAL THESIS:

Analysis and optimization of the transient operation of gasoline turbocharged direct injection engines under high EGR conditions

---

Presented by: Mr. David González Domínguez
Supervised by: Dr. Héctor Climent Puchades

in fulfillment of the requirements for the degree of

Doctor of Philosophy

Valencia, March 2023

Doctoral Thesis

Analysis and optimization of the transient operation of gasoline turbocharged direct injection engines under high EGR conditions

Presented by: Mr. David González Domínguez
Supervised by: Dr. Héctor Climent Puchades

THESIS EXAMINERS

Dr. Alain Maiboom
Dr. Jacobo Porteiro Fresco
Dr. Francisco Vera García

DEFENSE COMMITTEE

Chairman: Dr. José Manuel Luján Martínez
Secretary: Dr. María de los Reyes García Contreras
Member: Dr. Jacobo Porteiro Fresco

Valencia, March 2023

Abstract

Road transport is a major contributor to climate change. However, given the lack of competitiveness of fossil fuel-free alternatives, it does not seem possible to reduce the dependence on the internal combustion engine (ICE) as rapidly as planned by the authorities. Advanced gasoline engines will therefore hold a high market share in the automobile industry in the following years, at least during the next decade, either working in conventional or hybrid powertrains. Hence it is essential to keep improving these engines to reduce the negative impact of light-duty vehicles on the environment.

The most used strategy to reduce fuel consumption and CO_2 emissions in current spark-ignition (SI) gasoline engines is downsizing combined with direct injection (DI). Besides, downsizing must go hand in hand with turbocharging to maintain peak power. It is also proven that exhaust gas recirculation (EGR) can improve fuel economy in SI engines by 3-6% at medium and high loads. As a disadvantage, extracting the full benefit from EGR requires operating with high recirculation rates (close to the EGR dilution limit), leading to some issues under transient conditions. In this thesis, it is demonstrated that high EGR operation through long-route systems in turbocharged engines can potentially originate combustion instabilities and poor engine response during load-decrease (tip-out) and load-increase (tip-in) maneuvers, respectively.

Transient operations are especially important for manufacturers since the implementation of the Worldwide harmonized Light vehicle Test Procedure (WLTP). The present thesis is therefore devoted to analyzing and optimizing the gasoline engine performance under high EGR conditions during relevant transient maneuvers. To this end, a Euro-6 1.3L turbocharged DI SI gasoline engine with a variable geometry turbine was employed. A 1D model of this ICE was developed to assess fluid dynamics and transport phenomena. Engine tests were also performed to validate the 1D model and evaluate torque response, combustion stability, and raw exhaust emissions.

Before addressing the study of transient maneuvers, the engine calibration with EGR was carried out, and 0D conventional and hybrid vehicle simulations were done to determine the EGR benefit in fuel economy under WLTP driving conditions. Finally, tip-in and tip-out results revealed that some air management strategies are effective in meeting the transient EGR challenges in SI engines, but at the expense of increased complexity and costs.

Keywords: EGR; SI gasoline engine; transient operation; air management; 1D engine model; experimental data

Resumen

El transporte por carretera es uno de los sectores que más contribuyen al cambio climático. Por ello, muchos gobernantes a nivel mundial están promoviendo una transición hacia medios de transporte sostenibles que no dependan de combustibles fósiles. Sin embargo, debido a la falta de competitividad de las alternativas actuales, no parece factible, en el corto plazo, reducir significativamente el uso de los motores de combustión. Así pues, es probable que los motores de gasolina (MEP) mantengan su papel dominante en el sector automotriz durante los próximos años. De ahí que sea crucial seguir mejorando estos motores a fin de reducir su huella de carbono.

Actualmente, es habitual fabricar motores MEP de pequeña cilindrada ("downsizing") con sistemas de sobrealimentación e inyección directa, a fin de reducir el consumo de combustible y las emisiones de CO_2. Además, en la última década, se ha demostrado que la recirculación de gases de escape (EGR) puede mejorar la eficiencia de los motores MEP entre un 3 % y un 6 %, dependiendo del grado de carga. Como desventaja, para poder extraer todo el potencial de la estrategia EGR, es necesario trabajar con altas tasas de EGR, lo que puede causar ciertos problemas en condiciones transitorias. En esta tesis, se ha demostrado que el uso de altas tasas de EGR a través de sistemas de baja presión en motores MEP turboalimentados puede ralentizar la respuesta del motor y provocar fallos de encendido durante maniobras de aceleración y desaceleración, respectivamente.

Con la entrada en vigor de nuevos procedimientos de homologación de vehículos, como el WLTP (Worldwide harmonized Light vehicle Test Procedure), donde las operaciones transitorias tienen un peso importante, los fabricantes buscan que sus motores consuman y emitan menos en un amplio rango de condiciones de operación, tanto estacionarias como transitorias. Por ello, el objetivo principal de esta tesis es analizar y optimizar el funcionamiento, en condiciones transitorias, de los motores MEP que operan con altas tasas de EGR. Para ello, se ha empleado un motor de gasolina (Euro 6) de 1.3l turboalimentado con inyección directa, distribución variable y turbina de geometría variable. Se ha desarrollado un modelo unidimensional (1D) del motor para el estudio de la fluidodinámica y los fenómenos de transporte en su interior. Por otro lado, se ha ensayado el motor para calibrar el modelo 1D y evaluar aspectos difícilmente predecibles con dicho modelo, como las emisiones contaminantes y la estabilidad de la combustión.

Previo al estudio en condiciones transitorias, el motor fue calibrado con EGR, y se realizaron simulaciones para determinar el consumo de un vehículo convencional y otro híbrido, ambos con EGR, durante un ciclo WLTP. Finalmente, se concluyó que ciertas estrategias orientadas a mejorar el proceso de renovación de la carga pueden resolver la problemática del uso del EGR en condiciones transitorias. Eso sí, implementar dichas estrategias conllevaría un aumento en complejidad y costes.

Resum

El transport per carretera és un dels sectors que més contribueixen al canvi climàtic. Per això, molts governants a nivell mundial estan promovent una transició cap a mitjans de transport sostenibles que no depenguen de combustibles fòssils. No obstant això, a causa de la falta de competitivitat de les alternatives actuals, no sembla factible, en el curt termini, reduir significativament l'ús dels motors de combustió. Així doncs, és probable que els motors de gasolina (MEP) mantinguen el seu paper dominant en el sector automotriu durant els pròxims anys. D'ací ve que siga crucial continuar millorant aquests motors a fi de reduir la seua petjada de carboni.

Actualment, és habitual fabricar motors MEP de xicoteta cilindrada ("downsizing") amb sistemes de sobrealimentació i injecció directa, a fi de reduir el consum de combustible i les emissions de CO_2. A més, en l'última dècada, s'ha demostrat que la recirculació de gasos d'escapament (EGR) pot millorar l'eficiència dels motors MEP entre un 3% i un 6%, depenent del grau de càrrega. Com a desavantatge, per a poder extraure tot el potencial de l'estratègia EGR, és necessari treballar amb altes taxes de EGR, la qual cosa pot causar uns certs problemes en condicions transitòries. En aquesta tesi, s'ha demostrat que l'ús d'altes taxes de EGR a través de sistemes de baixa pressió en motors MEP turboalimentats pot alentir la resposta del motor i provocar fallades d'encesa durant maniobres d'acceleració i desacceleració, respectivament.

Amb l'entrada en vigor de nous procediments d'homologació de vehicles, com el WLTP (Worldwide harmonized Light vehicle Test Procedure), on les operacions transitòries tenen un pes important, els fabricants busquen que els seus motors consumisquen i emeten menys en un ampli rang de condicions d'operació, tant estacionàries com transitòries. Per això, l'objectiu principal d'aquesta tesi és analitzar i optimitzar el funcionament, en condicions transitòries, dels motors MEP que operen amb altes taxes de EGR. Per a això, s'ha emprat un motor de gasolina (Euro 6) de 1.3l turboalimentat amb injecció directa, distribució variable i turbina de geometria variable. S'ha desenvolupat un model unidimensional (1D) del motor per a l'estudi de la fluidodinàmica i els fenòmens de transport en el seu interior. D'altra banda, s'ha assajat el motor per a calibrar el model 1D i avaluar aspectes difícilment predictibles amb aquest model, com les emissions contaminants i l'estabilitat de la combustió.

Previ a l'estudi en condicions transitòries, el motor va ser calibrat amb

EGR, i es van realitzar simulacions per a determinar el consum d'un vehicle convencional i un altre híbrid, tots dos amb EGR, durant un cicle WLTP. Finalment, es va concloure que unes certes estratègies orientades a millorar el procés de renovació de la càrrega poden resoldre la problemàtica de l'ús del EGR en condicions transitòries. Això sí, implementar aquestes estratègies comportaria un augment en complexitat i costos.

List of publications

The Ph.D. candidate, David González Domínguez, has co-authored the six scientific publications presented in this section with Prof. Héctor Climent Puchades and other members of the I.U.I. CMT-Motores Térmicos. All the published studies come from the research activities carried out during the candidate's Ph.D. degree. The candidate's contribution to these publications includes: developing methods, creating models, performing experimental and modeling activities, analyzing results, and writing and reviewing manuscripts. Besides, the Ph.D. candidate is the corresponding author in five of their six publications. The role of the rest of the co-authors is specified in each of the respective publications. In addition, the Universitat Politècnica de València and the I.U.I. CMT-Motores Térmicos provided all resources required for each research activity, such as facilities, materials, testing rigs, and software licenses.

It should be stated that the innovative aspects and main results of this thesis have already been presented in the candidate's publications. Those results and figures taken from the cited publications have been improved, ordered, linked, completed, and further discussed in the present document.

Finally, it should be clarified that the Ph.D. candidate was positioned in the author list of each publication based on seniority, as determined by the I.U.I. CMT-Motores Térmicos. The candidate's publications are listed below:

[1] J. Serrano, H. Climent, R. Navarro, and D. González-Domínguez. "Methodology to Standardize and Improve the Calibration Process of a 1D Model of a GTDI Engine". *SAE Technical Paper 2020-01-1008* (2020). DOI: 10.4271/2020-01-1008. URL: https://www.sae.org/content/2020-01-1008/

[2] J. Galindo, H. Climent, J. de la Morena, D. González-Domínguez, S. Guilain, and T. Besançon. "Experimental and modeling analysis on the optimization of combined VVT and EGR strategies in turbocharged direct-injection gasoline engines with VNT". *Proceedings of the Institution of Mechanical Engineers, Part D: Journal of Automobile Engineering* 235.(10-11) (2021). DOI: 10.1177/09544070211004502

[3] J. Galindo, H. Climent, J. de la Morena, D. González-Domínguez, S. Guilain, and T. Besançon. "Assessment of air-management strategies to improve the transient performance of a gasoline engine under high EGR conditions during load-decrease operation". *International Journal of Engine Research* (2021). DOI: 10.1177/14680874211055578

[4] J. Galindo, H. Climent, J. de la Morena, D. González-Domínguez, S. Guilain, and T. Besançon. "Compressor Surge Mitigation in Turbocharged Spark-Ignition Engines without an Anti-Surge Control System during Load-Decrease Operation". *Applied Sciences* 12.(3) (2022), p. 1751. DOI: 10.3390/app12031751. URL: https://www.mdpi.com/2076-3417/12/3/1751

[5] H. Climent, V. Dolz, B. Pla, and D. González-Domínguez. "Analysis on the potential of EGR strategy to reduce fuel consumption in hybrid powertrains based on advanced gasoline engines under simulated driving cycle conditions". *Energy Conversion and Management* 266 (2022), p. 115830. DOI: 10.1016/j.enconman.2022.115830

[6] J. Galindo, H. Climent, J. de la Morena, D. González-Domínguez, and S. Guilain. "Assessment of air management strategies to improve the transient response of advanced gasoline engines operating under high EGR conditions". *Energy* 262 (2023), p. 125586. DOI: 10.1016/j.energy.2022.125586. URL: https://linkinghub.elsevier.com/retrieve/pii/S0360544222024720

Agradecimientos

En primer lugar, me gustaría reconocer la dedicación de mi tutor Héctor, quien me ha apoyado de principio a fin y me ha dado siempre un espacio para proponer y ser creativo. Sinceramente, me alegro de haber tomado la decisión de ser tu doctorando. Quiero reconocer también el gran trabajo de Joaquín de la Morena, guiándome en muchos momentos y siempre con algo interesante que aportar. En general, me gustaría agradecer la ayuda de todos aquellos profesores y técnicos que, de una u otra forma, han participado en la elaboración de esta tesis, con especial mención a Vicente Esteve. Y al I.U.I. CMT-Motores Térmicos por proporcionar todos los medios necesarios.

Además, quiero dar las gracias a mis compañeros de despacho por recibirme con los brazos abiertos. Gracias a Roberto, Vishnu, María, Vitor, Aditya y Juan. Y en especial, gracias a Rafa, Bárbara y Alex, con quienes he compartido inumerables momentos, charlas y reuniones. Todos ellos son culpables de que guarde un bonito recuerdo de este duro camino de cuatro años.

Por supuesto, no voy a olvidarme de mi club de fans, formado por mis padres, Tere y José, y mi hermana Elena, a quienes les agradezco su apoyo incondicional y dedico esta tesis. Por último, quiero agradecer a toda mi familia y amigos simplemente por haberme acompañado durante estos 4 años.

"La utopía está en el horizonte. Me acerco dos pasos, ella se aleja dos pasos. Camino diez pasos y el horizonte se mueve diez pasos más allá. Por mucho que yo camine, nunca la alcanzaré. ¿Para qué sirve la utopía? Para eso sirve, para caminar."

Fernando Birri.

Contents

List of Tables

List of Figures

List of symbols

Latin characters

C	combustion efficiency (in the Wiebe function)
c_p, c_v	heat capacities at constant pressure and volume, respectively
E_{oc}	open circuit voltage (related to the battery of the hybrid SUV)
f_C	cut-off frequency
F_{ICE}	engine friction torque
F_{ae}, F_g, F_{rr}	aerodynamic, gravity, and rolling resistance forces, respectively
i	instantaneous current (related to the battery of the hybrid SUV)
I_a, I_d	moments of inertia of the axles and driveshaft, respectively
I_{it}, I_{ot}	moments of inertia of the transmission input and output sides, respectively
m	exponent in the Wiebe function
M_v	vehicle mass
$\dot{m}_f$	fuel mass flow rate
p	pressure
$\widetilde{p}$	filtered pressure (low-pass, $f_C = 30$ Hz)
$\overline{p}$	moving average pressure (low-pass, $f_C = 5$ Hz)
$\widetilde{\overline{p}}$	difference between $\widetilde{p}$ and $\overline{p}$
P_{bat}	power supplied by the battery of the hybrid SUV
Q_f	heat released by the fuel
Q_w	heat transfer through the cylinder walls
r_w	wheel radius
R_d, R_t	differential and transmission ratios, respectively
$\dot{R}_t$	time derivative of R_t
t	time
T	temperature
T_C	duration of one engine cycle

v	vehicle speed
V	volume
w_d	driveline speed at the clutch output
$\dot{w}_d$	time derivative of w_d
w_h	difference between v_{up} and v_{low} (or hysteresis width)
w_i	width of the SOC interval ($SOC_{max} - SOC_{min}$)
$\dot{W}_{eng}$	power delivered by the engine
$\dot{W}_{sys}$	power supplied by the auxiliary boosting system
X_{fb}	mass fraction of fuel burned

Greek characters

α	instantaneous crank angle
α_0	crank angle at which the combustion starts
Δ	variation/increment
$\Delta\alpha$	combustion duration
η_c	Coulomb efficiency (related to the battery of the hybrid SUV)
κ	constant parameter that replaces the ratio of specific heats
λ	air-to-fuel equivalence ratio
τ_d, τ_{req}	torque demand or request by the driver
τ^*_{ICE}	engine torque at which the BSFC is minimum (for a given speed)
ϕ	fuel-to-air equivalence ratio
Ω_{int}	internal resistance (related to the battery of the hybrid SUV)

Subscripts

1, 2	related to the compressor inlet and outlet conditions, respectively
cc	related to the combustion chamber conditions
corr	corrected variable
exh	related to the exhaust manifold conditions
int	related to the intake manifold conditions

min, *max*	minimum and maximum, respectively (related to the battery SOC)
tank	related to PAT conditions
up, *low*	upper and lower limit (of the vehicle speed), respectively

Acronyms

0D	zero-dimensional
1D	one-dimensional
AFR	air-to-fuel ratio
AHR	apparent heat release
AHRR	apparent heat release rate
AMF	air mass flow
ANN	artificial neural network
ASV	anti-surge valve
BC	battery capacity
BEV	battery electric vehicle
BMEP	brake mean effective pressure
BSFC	brake-specific fuel consumption
CA50	crank angle at which the 50% of the heat is released
CAD	crank-angle degrees
CO	carbon monoxide
CO_2	carbon dioxide
COV	coefficient of variation
CR	compression ratio
DI	direct injection
DOE	design of experiments
DTC	delayed throttle closure
ECU	engine control unit
EGR	exhaust gas recirculation
EM	electric motor
EMS	energy management strategy

EVC	exhaust valve closing
FM	friction multiplier
FMEP	friction mean effective pressure
FSM	finite-state machine
GHG	greenhouse gas
GPF	gasoline particulate filter
HC	hydrocarbon
HEV	hybrid electric vehicle
HP	high-pressure
HTM	heat transfer multiplier
ICE	internal combustion engine
IMEP	indicated mean effective pressure
IVC	intake valve closing
IVO	intake valve opening
LDV	light-duty vehicle
LP	low-pressure
MAPE	mean absolute percentage error
MAPO	maximum amplitude of pressure oscillations
MF	mass flow
NOx	nitrogen oxides
O_2	molecular oxygen
PAT	pressurized air tank
PFI	port fuel injection
PHEV	plug-in hybrid electric vehicle
PI	proportional-integral
PM	particulate matter
RDE	Real Driving Emissions
RGF	residual gas fraction
rpm	revolution per minute
SAP	secondary air path
SI	spark ignition

SOC	state of charge
SUV	sport utility vehicle
TAM	trapped air mass
TWC	three-way catalyst
VGT	variable geometry turbine
VVA	variable valve actuation
VVT	variable valve timing
WCAC	water charge air cooler
WG	waste-gate
WLTP	Worldwide harmonized Light vehicle Test Procedure

Chapter 1

Introduction

Contents

1.1 Background and motivation

Environmental awareness has substantially increased in the last decades, mainly in the most developed countries [7], promoting ambitious policies to fight climate change and air pollution. An example of this is the new emission regulations for on-road vehicles. Road transport is responsible for 12% of global greenhouse gas (GHG) emissions [8] and is the biggest contributor to nitrogen oxide (NOx) emissions [9, 10]. Hence many governments have established more stringent requirements for new vehicle sales: reducing the allowed tailpipe emission levels, defining new vehicle certification procedures, and even imposing some bans on the use of fossil fuels in the future. The present thesis is focused on the study of gasoline engines, and these are predominantly used in light-duty vehicles (LDVs). So, first and foremost, it is essential to know the current status of the LDV emission standards in the leading markets [11]:

- All new LDV sold in the European Union (EU) from September 2018 must be homologated according to the Worldwide harmonized Light vehicle Test Procedure (WLTP). This procedure is more realistic than the preceding one, the New European Driving Cycle (NEDC), which was designed in 1993. It is estimated that the deviation between the laboratory and real-life CO_2 emissions is reduced from around 35% with the NEDC [12] to 13% with the WLTP [13]. In order to eliminate this discrepancy, the WLTP is complemented with Real Driving Emissions (RDE) tests, in which the vehicle emissions are measured during actual road routes. In addition, the European Parliament recently voted in favor of a proposal to reduce CO_2 emissions in 2030 by 55% and 50% from new cars and vans, respectively, compared to the 2021 targets [14]. This proposal also calls for a CO_2 emission reduction of 100% by 2035, thus banning the sales of LDV powered by fossil fuels in the EU from that year. Regarding air pollutants, great efforts have been made in the last two decades to decrease such emissions. The Euro 5 and Euro 6 standards have resulted, since the application of the former until 2019, in a 35% reduction in both NOx and particulate matter (PM) emissions from road transport [15]. The Euro 7 regulation is under discussion and will include: new limits on previously non-regulated species; lower NOx, CO, and PM limits; and changes in test procedures [11].

- In the United States of America (USA), the Environmental Protection

Agency (EPA) has updated the federal GHG emission standards for LDV to set more stringent requirements in each model year from 2023 to 2026 [16]. The EPA has agreed to increase 2026's target values of fuel economy by 23%, compared to the previous rule (Safer Affordable Fuel-Efficient), and to establish a series of incentives to accelerate the production of zero and near-zero tailpipe emission vehicles. The EPA has also defined exigent limits for air pollutant emissions through the Tier 3 standard. Every manufacturer must gradually reduce its fleet average NOx + NMOG (non-methane organic gas) emissions until reaching 19 mg/km in 2025, 65% less than in 2017; and the 100% of the new cars must generate less than 1.9 mg PM/km since 2021. These limit values are in line with the California LEV III regulation. Concerning vehicle certification procedures, the EPA has not lately introduced any changes. The Federal Test Procedure and the Highway Fuel Economy Test are used to comply with GHG and air-pollutant emission targets [16].

- The fuel economy and CO_2 emissions in the Chinese LDV market are regulated by the rule of Parallel Management of Corporate Average Fuel Consumption (CAFC) and New Energy Vehicle (NEV) credits, also known as the Dual-Credit policy. Updated in January 2021, this regulation aims to improve the fuel economy of gasoline and diesel cars while promoting the sale of NEVs, a term referring to battery electric vehicles, plug-in hybrid electric vehicles, and fuel cell electric vehicles [17]. Every manufacturer must achieve a specific amount of credits by producing or importing NEVs. In the case of a NEV credit surplus at the end of the year, manufacturers can either sell the excess to other companies or employ it to offset their CAFC deficit if they have not complied with the CAFC target. The China 5 standard sets a fleet-average fuel consumption target of 4 WLTP L/100 km by 2025 and 3.2 WLTP L/100 km by 2030 for new LDV registrations [18]. Besides, the China 6 standard, in effect since July 2020, establishes stricter limits on air pollutant emissions than Euro 6 and replaces the NEDC with WLTP. RDE tests are included in China 6 as well [19].

- Japan and South Korea have also updated their fuel economy targets for passenger cars by 2030 [11]. Japan plans to achieve a fleet-average CO_2 emission of around 85 g/km under WLTP conditions, 23% lower than in 2015. South Korea is more ambitious and proposes a 50% reduction from 140 (2015) to 70 g CO_2/km (2030).

In view of all these environmental policies, most manufacturers are putting much faith in vehicle electrification to achieve GHG emission objectives. However, it does not seem easy to reduce the dependence on the internal combustion engine (ICE) at the pace planned by the authorities. The battery electric vehicle (BEV) is the most solid alternative to fossil fuels but still has major limitations: high production costs, short driving ranges, long charging times, and polluting battery manufacturing. In addition, BEV's benefit in the well-to-wheel CO_2 emissions is unclear and may evaporate depending on the energy mix [20, 21]. Such limitations explain why only 10% and 6% of the new cars sold in the EU and USA in 2022 are BEVs. A more advanced situation is found in China, where the BEV share in the new LDV registrations has risen to 19% in the first half of 2022 [22]. Some predictions show that at least 50% of the cars on the road in 2050 will be based on ICEs and that the sales of plug-in cars, including BEVs and plug-in hybrid electric vehicles (PHEVs), will not be predominant until 2040 [23]. Other more optimistic studies foresee that half of the cars sold by 2030 will be plug-in vehicles [24]. In any case, the ICE will still play an important, even leading, role in the automotive sector over the following decades. Therefore, in order to further reduce vehicle emissions, it is critical to keep dedicating resources and efforts to improve ICEs.

Spark ignition (SI) engines working in conventional and, mostly, hybrid powertrains are the main LDV propulsion system currently. Over the last decade, SI engines, commonly fueled with gasoline, have gained much weight in the automotive sector because of the increased complexity and costs of diesel after-treatment systems and the "diesel-gate" scandal. Focusing on gasoline engines, most manufacturers opt for downsizing with direct fuel injection to reduce fuel consumption [25, 26], closely related to CO_2 emissions, while pollutant emissions are usually under control using a three-way catalyst (TWC) followed by a gasoline particulate filter (GPF). Besides, downsized engines need turbocharging to maintain peak power. Another worthwhile fuel-saving strategy in SI engines is exhaust gas recirculation (EGR). High rates of cooled low-pressure EGR can provide fuel savings higher than 5% depending on the operating conditions [27]. EGR also avoids fuel enrichment to decrease the turbine inlet temperature at high engine loads.

However, the combination of high EGR rates with long transport delays, inherent to long-route EGR systems, can penalize the transient engine performance in terms of response, combustion stability, and fuel economy. Firstly, during load-decrease and deceleration maneuvers, high EGR operation can

result in misfire events due to an over-dilution of the air-fuel mixture in the final working conditions. This over-dilution is, in turn, caused by a slow EGR evacuation from the intake system [3]. Misfiring is undesired as it brings about some negative effects: unstable output torque, higher unburned hydrocarbon emissions, thermal damage to the catalyst, and crankshaft torsional vibration. Secondly, in the case of load-increase and acceleration maneuvers, operating with high EGR levels can lead to poor engine response due to a longer turbocharger lag [6]. Introducing high EGR rates while keeping the load constant involves increasing the intake manifold pressure, so the dependence on the turbocharger is greater. This fact can significantly delay the increase in engine airflow required when demanding more power.

The present thesis arises from the need to solve these transient EGR challenges. Since the adoption of new vehicle homologation procedures, such as WLTP and RDE, the management of transient maneuvers is even more important for manufacturers. Some of them decide not to exploit the full potential of the EGR strategy by decreasing recirculation rates, simplifying the transient engine operation control in return. Hence improving the transient engine performance under high EGR conditions is essential to obtain the maximum reduction in fuel consumption and CO_2 emissions. The present thesis is therefore devoted to studying and optimizing the transient operation of gasoline engines with EGR.

1.2 Objectives

The objective of the present Ph.D. thesis is twofold. The first purpose is to analyze the influence of the low-pressure EGR strategy on the transient behavior of a Euro-6 downsized turbocharged SI gasoline engine with variable valve timing (VVT) and variable geometry turbine (VGT) systems. The main variables to be analyzed are engine response, combustion stability, and fuel economy. Once the main issues derived from using EGR are identified, the second objective is to provide and assess a set of air management solutions to improve engine operation with high EGR rates during relevant transient maneuvers.

1.3 Methodology

The whole procedure followed to accomplish the objectives defined in Section 1.2 has been divided into five chapters, whose content is described below:

- **Chapter 2** gives a comprehensive literature review on the state-of-the-art. This chapter examines the technological advances that have improved gasoline engines in the last decades, mostly in terms of fuel economy and CO_2 emissions. The EGR strategy and technologies integrated into the used SI gasoline engine have been especially reviewed.
- **Chapter 3** describes the experimental and modeling tools. A 1D engine model and an engine test stand have been employed in this thesis. Engine simulations were used to analyze fluid dynamics and transport phenomena, while experimental tests were performed to calibrate the engine model and assess the combustion process and exhaust emissions. In addition, 0D vehicle models were developed to evaluate the impact of the EGR strategy on fuel consumption under driving conditions.
- **Chapter 4** is devoted to optimizing ICE operation with EGR from the fuel consumption perspective. It was required before addressing the study of transient maneuvers, given that the gasoline engine employed in this thesis was not initially designed to operate with EGR. Thus, the EGR rate, VVT settings, and spark timing were optimized for several steady-state operating conditions deliberately selected. The optimization method is characterized by a high number of engine simulations and a reduced experimental workload. After the engine calibration, the fuel economy improvement achieved with EGR was quantified not only for each of the selected steady-state operating points, but also during a WLTP driving cycle by means of conventional and hybrid powertrain simulations.
- **Chapter 5** consists of three studies and is fully dedicated to analyzing the transient engine operation under high EGR conditions. The first two studies are focused on evaluating the EGR impact on torque response during tip-in (load-increase) and tip-out (load-decrease) maneuvers at 1500 rpm, in which the fuel consumption in the former and the combustion stability in the latter are also considered. In these studies, different technical solutions, such as a secondary air path, a pressurized

air tank, and an electric supercharger, are researched to improve engine performance. In addition, a third study on compressor surge control was performed under transient EGR conditions. In the engine utilized, installing a throttle valve at the compressor inlet duct (upstream of the EGR joint) is required to achieve high EGR rates. By taking advantage of this valve, the viability of preventing compressor surge during aggressive tip-outs without the anti-surge valve is analyzed. This way, the compressor manufacturing costs could be reduced.

- Finally, **Chapter 6** provides the main conclusions and the potential future studies derived from the research carried out in the present thesis.

Chapter 1 references

[3] J. Galindo, H. Climent, J. de la Morena, D. González-Domínguez, S. Guilain, and T. Besançon. "Assessment of air-management strategies to improve the transient performance of a gasoline engine under high EGR conditions during load-decrease operation". *International Journal of Engine Research* (2021). DOI: 10.1177/14680874211055578 (cit. on pp. xii, 5).

[6] J. Galindo, H. Climent, J. de la Morena, D. González-Domínguez, and S. Guilain. "Assessment of air management strategies to improve the transient response of advanced gasoline engines operating under high EGR conditions". *Energy* 262 (2023), p. 125586. DOI: 10.1016/j.energy.2022.125586. URL: https://linkinghub.elsevier.com/retrieve/pii/S0360544222024720 (cit. on pp. xii, 5).

[7] C. Flynn, E. Yamasumi, S. Fisher, D. Snow, Z. Grant, M. Kirby, P. Browning, M. Rommerskirchen, and I. Russell. *Peoples' Climate Vote*. Tech. rep. United Nations Development Programme, University of Oxford and Browning Environmental Communications, 2021. URL: https://www.undp.org/publications/peoples-climate-vote (cit. on p. 2).

[8] H. Ritchie, M. Roser, and P. Rosado. "CO2 and Greenhouse Gas Emissions: by sector". *Our World in Data* (2020). URL: https://ourworldindata.org/emissions-by-sector (cit. on p. 2).

[9] Statista. *Emissions in the European Union*. Tech. rep. 2022. URL: https://www.statista.com/study/56124/emissions-in-the-european-union/ (cit. on p. 2).

[10] Statista. *Emissions in the United States*. Tech. rep. 2022. URL: https://www.statista.com/study/40176/us-ghg-emissions-statista-dossier/ (cit. on p. 2).

[11] A. Joshi. "Review of Vehicle Engine Efficiency and Emissions". *SAE Technical Paper 2021-01-0575* (2021). DOI: 10.4271/2021-01-0575. URL: https://www.sae.org/content/2021-01-0575/ (cit. on pp. 2, 3, 23).

[12] G. Fontaras, N.-G. Zacharof, and B. Ciuffo. "Fuel consumption and CO2 emissions from passenger cars in Europe – Laboratory versus real-world emissions". *Progress in Energy and Combustion Science* 60 (2017), pp. 97–131. DOI: 10.1016/j.pecs.2016.12.004. URL: https:

//linkinghub.elsevier.com/retrieve/pii/S0360128516300442 (cit. on p. 2).

[13] G. Fontaras, B. Ciuffo, N. Zacharof, S. Tsiakmakis, A. Marotta, J. Pavlovic, and K. Anagnostopoulos. "The difference between reported and real-world CO2 emissions: How much improvement can be expected by WLTP introduction?" *Transportation Research Procedia* 25 (2017), pp. 3933–3943. DOI: 10.1016/j.trpro.2017.05.333. URL: https://linkinghub.elsevier.com/retrieve/pii/S2352146517306403 (cit. on p. 2).

[14] European Parliament. *Fit for 55: MEPs back objective of zero emissions for cars and vans in 2035*. Tech. rep. 2022. URL: https://www.europarl.europa.eu/news/en/press-room/20220603IPR32129/fit-for-55-meps-back-objective-of-zero-emissions-for-cars-and-vans-in-2035 (cit. on p. 2).

[15] Statista. *Transportation emissions in the European Union*. Tech. rep. 2021. URL: https://www.statista.com/study/89825/eu-transportation-emissions/ (cit. on p. 2).

[16] U.S. Environmental Protection Agency (EPA). *Revised 2023 and Later Model Year Light-Duty Vehicle Greenhouse Gas Emissions Standards*. 2021. URL: https://www.epa.gov/regulations-emissions-vehicles-and-engines/final-rule-revise-existing-national-ghg-emissions (cit. on p. 3).

[17] H. Zhang, F. Zhao, H. Hao, and Z. Liu. "Effect of Chinese Corporate Average Fuel Consumption and New Energy Vehicle Dual-Credit Regulation on Passenger Cars Average Fuel Consumption Analysis". *International Journal of Environmental Research and Public Health* 18.(14) (2021), p. 7218. DOI: 10.3390/ijerph18147218. URL: https://www.mdpi.com/1660-4601/18/14/7218 (cit. on p. 3).

[18] Y. Li, Z. Wang, K. Wang, and B. Zhang. "Fuel economy of Chinese light-duty car manufacturers: An efficiency analysis perspective". *Energy* 220 (2021), p. 119622. DOI: 10.1016/j.energy.2020.119622. URL: https://linkinghub.elsevier.com/retrieve/pii/S0360544220327298 (cit. on p. 3).

[19] M. Lyu, X. Bao, R. Zhu, and R. Matthews. "State-of-the-art outlook for light-duty vehicle emission control standards and technologies in China". *Clean Technologies and Environmental Policy* 22.(4) (2020),

pp. 757–771. DOI: 10.1007/s10098-020-01834-x. URL: http://link.springer.com/10.1007/s10098-020-01834-x (cit. on p. 3).

[20] T. Burton, S. Powers, C. Burns, G. Conway, F. Leach, and K. Senecal. "A Data-Driven Greenhouse Gas Emission Rate Analysis for Vehicle Comparisons". *SAE International Journal of Electrified Vehicles* 12.(1) (2022). DOI: 10.4271/14-12-01-0006. URL: https://www.sae.org/content/14-12-01-0006/ (cit. on p. 4).

[21] Q. Qiao, F. Zhao, Z. Liu, S. Jiang, and H. Hao. "Comparative Study on Life Cycle CO2 Emissions from the Production of Electric and Conventional Vehicles in China". In: *Energy Procedia*. Vol. 105. 2017, pp. 3584–3595. DOI: 10.1016/j.egypro.2017.03.827 (cit. on p. 4).

[22] P. Mock and Z. Yang. *A 2022 update on electric car sales: China taking the lead, the U.S. catching up, and Europe falling behind*. 2022. URL: https://theicct.org/2022-update-ev-sales-us-eu-ch-aug22/ (cit. on p. 4).

[23] P. Senecal and F. Leach. "Diversity in transportation: Why a mix of propulsion technologies is the way forward for the future fleet". *Results in Engineering* 4 (2019), p. 100060. DOI: 10.1016/j.rineng.2019.100060. URL: https://linkinghub.elsevier.com/retrieve/pii/S259012301930060X (cit. on p. 4).

[24] I. Boudway. *More Than Half of US Car Sales Will Be Electric by 2030*. 2022. URL: https://www.bloomberg.com/news/articles/2022-09-20/more-than-half-of-us-car-sales-will-be-electric-by-2030 (cit. on p. 4).

[25] N. Fraser, H. Blaxill, G. Lumsden, and M. Bassett. "Challenges for Increased Efficiency through Gasoline Engine Downsizing". *SAE International Journal of Engines* 2.(1) (2009), pp. 991–1008. DOI: 10.4271/2009-01-1053. URL: https://www.sae.org/content/2009-01-1053/ (cit. on pp. 4, 15).

[26] D. Coltman, J. Turner, R. Curtis, D. Blake, B. Holland, R. J. Pearson, A. Arden, and H. Nuglisch. "Project Sabre: A Close-Spaced Direct Injection 3-Cylinder Engine with Synergistic Technologies to Achieve Low CO2 Output". *SAE International Journal of Engines* 1.(1) (2008), pp. 129–146. DOI: 10.4271/2008-01-0138. URL: https://www.sae.org/content/2008-01-0138/ (cit. on pp. 4, 15).

[27] J. Luján, H. Climent, R. Novella, and M. Rivas-Perea. "Influence of a low pressure EGR loop on a gasoline turbocharged direct injection engine". *Applied Thermal Engineering* 89 (2015), pp. 432–443. DOI: 10.1016/j.applthermaleng.2015.06.039 (cit. on pp. 4, 17, 24).

Chapter 2

Literature review

Contents

2.1 Introduction

The current status of the technology in SI gasoline engines has been thoroughly reviewed in this chapter, with particular emphasis on the most common strategies employed by manufacturers to reduce fuel consumption and emissions. Secondly, a detailed literature review of the EGR strategy is given. The following aspects related to the use of EGR in SI engines are examined: possible configurations, benefit in fuel economy, and impact on pollutant emissions. In addition, in order to define the starting point of the present thesis, the available literature on transient SI engine operation with EGR has been consulted.

2.2 State of the art in SI gasoline engines

As stated in Section 1.1, downsizing with direct injection (DI) is the favorite choice of manufacturers to improve fuel economy in gasoline engines, while turbocharging is used not to lose power. Some predictions have estimated that more than 90% of new gasoline engines will be downsized and turbocharged by 2025 in China, Europe, and the USA [28]. In the case of the USA, this prediction is too optimistic as the Environmental Protection Agency reported that only 35% of new LDVs sold in 2020 were powered by turbocharged engines [29]. Modern gasoline engines also include other interesting fuel-saving strategies, such as variable valve actuation, cylinder deactivation, variable compression ratio, and water injection. Besides, current SI engines utilize an after-treatment system composed of a TWC and GPF to control the four main pollutants: NOx, CO, hydrocarbons, and particulate matter. All these strategies and technologies have been reviewed in this section.

2.2.1 Downsizing

Downsizing consists in reducing the engine displacement by decreasing the number of cylinders or their size. The rationale behind this is basically to shift the engine operation to a better thermal efficiency zone, given that a downsized engine must operate at higher loads to provide the same output power [30]. Downsizing also results in lower friction losses due to smaller moving parts and, possibly, shorter strokes [31]. This strategy has been widely studied since the

early 1980's [32] and used for mass production since the late 2000's. Depending on the downsizing degree, fuel economy improvements higher than 20% can be obtained [33]. Coltman et al. [26] revealed that fuel savings of around 15% were achieved during an NEDC test by downsizing a 2.2l DI SI engine by 32%. A few years later, Turner et al. [34] evaluated the performance of a 60% downsized 2.0l SI engine and its naturally aspirated counterpart under NEDC conditions, reporting a CO_2 emission reduction of 21%.

However, the implementation of high downsizing degrees is also subject to some issues, such as drivability penalty and increased knocking risk. The former can be enhanced with VGT turbochargers [35] or electrical superchargers [36], and the latter can be reduced in different ways, e. g., direct fuel injection [25], EGR [37], variable valve actuation [38], and water injection [39], among others. Besides, the packaging of the valves, injector, and spark plug can become challenging if the cylinder size is significantly decreased.

2.2.2 Direct fuel injection

Japanese manufacturers were the first to utilize direct fuel injection in SI gasoline engines in the late 1990's. Injecting the fuel directly into the cylinders leads to lower in-cylinder temperature values than doing it into the intake ports, due to the higher heat absorbed by the in-cylinder trapped gases during the fuel evaporation. In turn, reducing the in-cylinder temperature results in lower heat losses [40], better volumetric efficiency [41], and decreased knocking risk [25]. This last point is key to increasing the compression ratio (or improving the combustion phasing) and, consequently, thermal efficiency [42]. According to the extensive literature review by Zhao et al. [43], the compression ratio (CR) in SI engines with early DI strategy can be up to 1.5 units higher than in comparable engines with port fuel injection. This CR increase, along with the rest of the direct injection advantages, can translate into fuel savings close to 25% depending on the test cycle [43].

These improvements match the results obtained by Graham [44], who tested two light-duty vehicles with DI SI engines under EPA Federal Test Procedure (FTP) conditions using a chassis dynamometer. Graham compared the fuel consumption of these two with the median value of a sample of LDVs with similar characteristics and port fuel injection (PFI) technology; concluding that the vehicles with DI used between 20% and 30% less fuel. However,

other researchers have stated that the contribution of the DI strategy to fuel economy is not as high as the estimated one by Zhao et al. [43] and Graham [44]. Confer et al. [45] determined that the DI strategy was responsible for only a 4% fuel saving after they performed EPA vehicle homologation tests on a rolling road. In particular, Confer et al. tested a PFI engine vehicle and a newer version of the same vehicle with some upgrades, like a start-stop system, a more aerodynamic chassis, and the direct injection, EGR and variable valve actuation strategies.

Furthermore, some studies have evaluated the potential of dual injection systems (DI + PFI) to reduce the knocking tendency further, obtaining positive [46] but also negative [47] results. Golzari et al. [46] stated that combining PFI and late DI strategies in a boosted single-cylinder SI engine resulted in 9% fuel improvement at 1000 rpm and partial load, compared with using only DI. In contrast, the same authors [46] observed no benefits at 2000 and 3000 rpm.

In terms of pollutant emissions, the direct injection strategy has some drawbacks. The air-fuel mixture heterogeneity associated with DI systems [48], coupled with lower combustion temperature values, can give rise to incomplete combustion. This explains why DI engines usually emit much more particulate matter than PFI engines [49] and why automotive manufacturers have included GPF systems in their new cars. Braisher et al. [50] reported that the PM emissions in a DI gasoline vehicle were an order of magnitude higher than in a similar PFI vehicle, based on chassis dynamometer tests under NEDC conditions. Gasoline engines with DI also generate greater amounts of CO and HC emissions than with PFI [48]. Nevertheless, the high performance of current TWC devices leads to no significant differences in CO and HC emissions between DI and PFI vehicles [51].

2.2.3 Turbocharging

Turbocharging enables the engine to be downsized without losing power, thus improving fuel economy. Another benefit of turbocharging is altitude compensation. Mansouri and Ommi [52] found via modeling that the brake power of an aircraft turbocharged SI engine with waste-gate (WG) at nominal speed was only reduced by 8% at 5000 meters above sea level, despite the 43% drop in the ambient air density. On the other hand, the use of turbochargers in

gasoline engines is also subject to the following issues: higher pumping losses, gas temperature limitation at the turbine inlet, drivability penalty due to turbocharger lag, and compressor surge.

Traditionally, the exhaust gas temperature at the turbine inlet has been controlled through fuel enrichment, that is, injecting more fuel than the stoichiometric value. However, this strategy is clearly undesired from the fuel economy perspective. Many studies have proven that the EGR strategy can assume the role of fuel enrichment, thus avoiding additional fuel consumption [27, 53]. Regarding drivability problems, some improvements have been introduced to minimize turbocharger lag, such as low-viscosity oils [54], advanced bearing technologies [55], mechanical [56] and electric [36] superchargers, and variable geometry turbines [35]. Besides, VGT turbochargers usually have an advantage in pumping losses over WG ones. Serrano et al. [57] stated that the VGT technology led to gasoline savings of up to 7.5% at full load in a downsized SI engine with a VVT system, compared to the fuel used with WG.

The most limiting issue of the ones associated with turbochargers is compressor surge. It consists in the stalling of the air (or intake gases) when the mass flow through the compressor is lower than a critical value [58]. This stalling phenomenon leads to flow reversal and recirculation within the compressor, which, in turn, can have multiple consequences: local instabilities, noise, large flow oscillations, efficiency loss, and damage to bearings, seals and impellers [59]. Surge appearance depends on the compressor design [60], the upstream and downstream duct geometries [61], and the flow pulsation [62] and transience [63]. Galindo et al. [64] stated that reducing the downstream volume may modify the surge dynamics from a low-frequency deep to a high-frequency mild surge. In addition, Galindo et al. found that the surge margin can be improved using either a tapered duct upstream of the compressor [65] or inlet vanes to generate a swirling flow [66].

Even though these improvements are implemented, compressor surge usually appears in turbocharged SI engines during gear shifts and fast throttle closings, in which the engine airflow is quickly reduced. Under such circumstances, the most extended solution for surge avoidance is installing a recirculation loop where an anti-surge valve (ASV) is opened when the compressor is getting close to the surge limit, thus connecting its inlet and outlet [67].

2.2.4 Variable valve actuation

The scavenging in four-stroke engines is typically carried out through two camshafts responsible for opening and closing the intake and exhaust valves. Figure 2.1 shows a generic valve lift diagram where the main parameters relative to valve actuation are specified. Initially, camshafts did not enable any modification of the valve lift, phase, or opening duration. Over the years, vehicle manufacturers have implemented variable valve actuation (VVA) systems due to their potential to reduce fuel consumption and tailpipe emissions. Several VVA technologies can be found depending on the valve parameter controlled: VVT (phase), VMVL (lift), VVEL (lift and duration), VVD (duration), and i-VTEC (lift, phase, and duration), among others. These technologies are defined in Figure 2.2 and reviewed below.

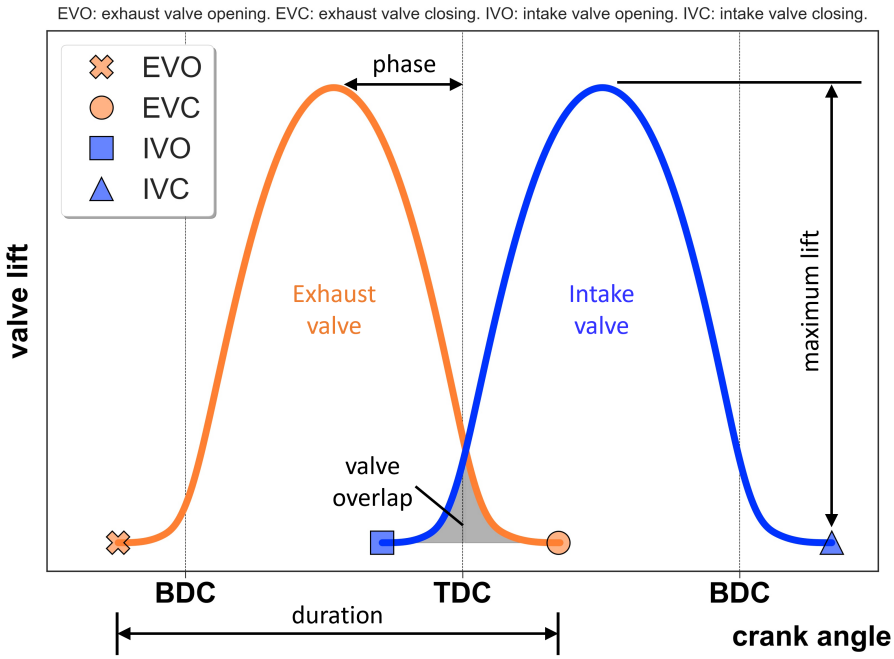

Figure 2.1: Generic valve lift diagram.

Current variable valve timing (VVT) systems allow continuous change of the valve phase without modifying the lift or event [68]. In turbocharged SI engines under throttling conditions, the VVT settings are generally chosen

to provide long valve overlaps, that is, late exhaust valve closings followed by early intake valve openings [69]. This way, the scavenging is worsened, so the intake pressure must be increased through de-throttling to keep the engine load constant. In consequence, pumping losses and fuel consumption are decreased. However, if VVT and EGR strategies are combined, again in throttling conditions, short valve overlaps are used to increase EGR tolerance by reducing internal burnt gas recirculation (IGR). Piqueras et al. [70] showed that minimizing the valve overlap was key to operating with cooled EGR rates close to 30%, thus achieving lower heat and pumping losses and better fuel economy.

Under turbocharged conditions, the valve overlap is shortened if the intake pressure is lower than the exhaust pressure, and vice versa. In other words, the VVT system is configured to improve scavenging and minimize residual gas fraction. The latter results in better volumetric efficiency, lower in-cylinder temperature, and decreased knocking risk [57]. Additionally, in the case of having more pressure at the intake manifold than at the exhaust manifold, increasing the valve overlap reduces the turbine inlet temperature, enabling fuel enrichment to be avoided at high engine loads [57].

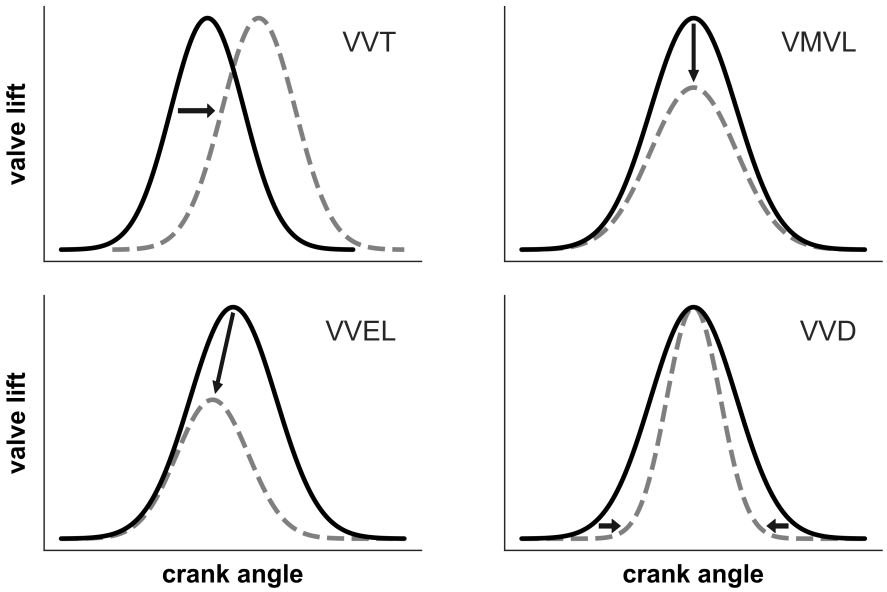

Figure 2.2: VVA concepts.

Variable valve lift and event (VVEL) systems, often referred to as variable valve lift (VVL), allow discrete or continuous change of the valve lift and opening duration (Figure 2.2). Another less-used technology is variable maximum valve lift (VMVL), by which only the lift is varied [71]. In VVEL systems, lift and duration are proportional, that is, they cannot be adjusted separately. If their adjustment is continuous, the throttle can be removed from SI engines, in which case the intake manifold pressure is always close to (or higher than, if turbocharged) the ambient pressure [72]. Li et al. [73] tested three turbocharged DI SI engines, two with dual VVT and one with intake VVL and exhaust VVT. They concluded that the VVL engine consumed up to 13% less fuel than the VVT ones at 2000 rpm and low loads. Li et al. also showed that the advantage of VVL over VVT was gradually reduced as the engine load was increased, even turning into a disadvantage at 1000 rpm and medium loads.

Some manufacturers have designed other more complex technologies, such as CVVD (continuously variable valve duration) and i-VTEC (intelligent variable valve timing and lift electronic control). The Hyundai's CVVD mechanism consists of an electro-mechanical actuator that moves the rotation axis of the cam lobes, enabling them to turn faster or slower than the camshaft, which, in turn, is translated into shorter and longer valve openings [74]. For its part, Honda introduced the dual overhead camshaft VTEC engine in 1989, which included two lobe profiles, one optimized for stability and fuel economy at low engine speeds and the other designed to give more power at high speeds. Switching from the former lobe profile, with low lift and short duration, to the latter, with high lift and long duration, is carried out using a hydraulically-driven locking pin. One decade later, Honda launched the i-VTEC technology combining VTEC with a continuously variable cam phasing system [75].

2.2.5 Other fuel consumption reduction strategies

Over the years, many other strategies have been used in gasoline engines to improve fuel economy. Three of the most interesting ones at present have been reviewed in this section: variable compression ratio (VCR), water injection, and cylinder deactivation.

Increasing the CR of an engine improves its thermal efficiency [76]. However, the compression ratio has an upper limit defined by the knock resistance of the fuel, so selecting a single CR represents a compromise between econ-

omy and performance. The VCR technology allows the compression ratio to be changed depending on the engine running conditions: at partial loads (where knocking risk is lower), high CR values are used to improve fuel efficiency; and at high loads, lower values are utilized to maintain the peak power. Automotive manufacturers have developed multiple VCR concepts, such as moving cylinder head, variable combustion chamber volume using a valve or secondary piston, variable connecting rod geometry, and variable height piston [77]. Wittek et al. [78] tested a turbocharged 1.0L DI SI engine with a two-stage VCR connecting rod system over a wide range of steady-state operating conditions. They determined that increasing the CR from 9.6 to 12.1 at partial loads led to fuel savings of up to 5%. In addition to the advantage in fuel economy, it should be remarked that VCR engines also have great fuel flexibility.

Another method to reduce fuel consumption at partial loads is cylinder deactivation. It basically consists in cutting fuel injection in some of the cylinders while increasing the load in the active ones. This way, pumping losses are reduced because of lower throttling. According to the review of Fridrichová et al. [79], cylinder deactivation can result in fuel savings higher than 20%. The fuel injection cut in the inactive cylinders must go hand in hand with valve deactivation. If not, the oxygen excess in the final exhaust gases may penalize the NOx conversion efficiency of the three-way catalyst [80].

Thirdly, some research studies have revealed the benefit of water injection in fuel economy [81]. The water can be injected at the intake ports [82] or directly into the cylinders [83]. The idea behind this is to reduce the in-cylinder temperature because of not only water evaporation but also the increased heat capacity of the trapped charge. As commented previously, decreasing the in-cylinder temperature leads to lower heat losses, knocking tendency, and turbine inlet temperature. Golzari et al. [81] performed engine tests at six steady-state operating points to evaluate the influence of intake port water injection on the performance of a boosted 1.2L DI SI engine. They reported that net indicated efficiency was improved by 5% and 15% at medium and high loads, respectively.

2.2.6 Pollutant emission control

Three-way catalysts are the after-treatment system utilized in SI gasoline engines since the early 1980's. TWCs are characterized by their compact design, low costs, and high conversion efficiency of NOx, CO and HC emissions [84]. These devices are composed of a honeycomb-structured monolith of cordierite, a high surface area washcoat, catalysts, and catalytic promoters [85]. The washcoat is a thin coating that covers the internal surface of the monolith and consists of a doped alumina-based material (Al_2O_3) with structural (BaO) and oxygen storage (CeO_2) promoters. Platinum group metals (Pt, Pd, and Rh) are used as oxidation and reduction catalysts. The main drawback of TWC systems is that high conversion rates can only be achieved in a narrow range of air-to-fuel ratio (AFR) values around the stoichiometric one. This explains why the AFR in SI engines is continuously oscillating between slightly-rich and slightly-lean values. Figure 2.3 shows, based on the information provided in [86, 87], the typical conversion efficiency values of a TWC as a function of the air-to-fuel equivalence ratio (λ).

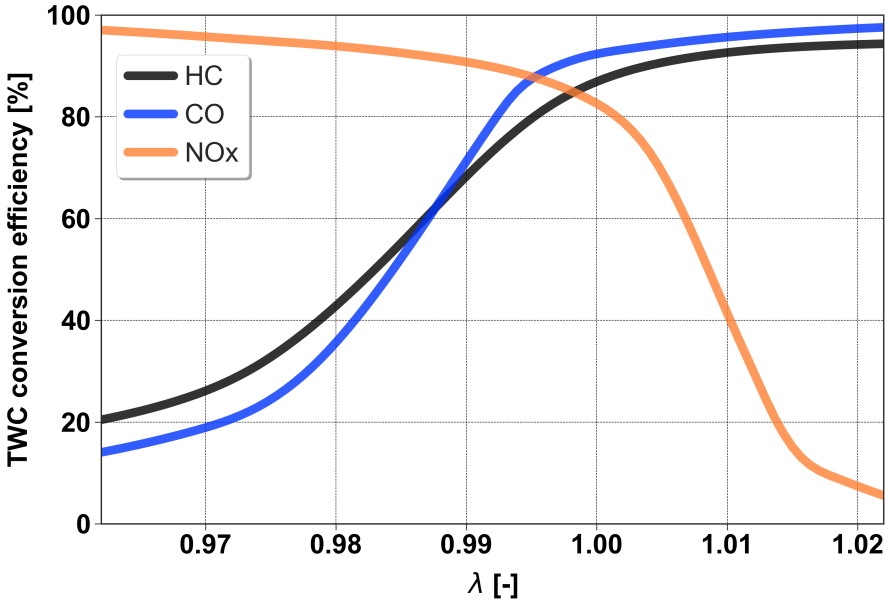

Figure 2.3: Typical conversion efficiency values of a three-way catalyst as a function of the air-to-fuel equivalence ratio. Adapted from [86, 87].

In addition, new emission regulations have forced manufacturers to reduce particulate matter emissions [11]. To this end, a gasoline particulate filter is installed downstream of the three-way catalyst. GPFs have the same operation principle as diesel particulate filters but require ceramic materials with higher thermal shock resistance [88].

2.3 Exhaust gas recirculation (EGR) in SI gasoline engines

2.3.1 EGR systems

The EGR strategy is used in turbocharged engines mainly through high-pressure (HP) and low-pressure (LP) systems. In the first ones, the exhaust gases are recirculated from the turbine inlet duct to the intake manifold; while, in the second ones, the gases are extracted downstream of the after-treatment devices and reintroduced upstream of the compressor. Figure 2.4 illustrates the single-line diagram of a turbocharged DI SI engine with a cooled low- (a) and high-pressure (b) EGR loop. Cooled EGR systems are composed of pipes, a cooler, and a valve to regulate the recirculation of exhaust gases. In addition, in the low-pressure configuration, it is usually required to install an additional valve upstream of the EGR joint or at the exhaust line, in order to guarantee a pressure difference (between the exhaust and intake lines) enough to achieve the desired recirculation rate.

The LP configuration has some advantages over the HP one. LP-EGR gases are introduced into the cylinders at a lower temperature than HP-EGR gases, mostly thanks to the intercooler located downstream of the compressor [89]. Potteau et al. [37] stated that this factor is critical for knock suppression and fuel enrichment avoidance. Another key parameter affecting knocking is the NOx emission levels in the recirculated gas flow, which are much lower when using LP systems (exhaust gases extracted after the TWC). Kawataba et al. [90] confirmed by testing that the knock probability in SI engines decreases as the NOx concentration in the trapped charge does. The HP-EGR strategy is also associated with cylinder-to-cylinder EGR dispersion [91] and major interferences with the turbocharger [92]. In contrast, LP-EGR systems are characterized by significant gas transport delays because of the large distance between the cylinders and the EGR valve. This means that any change in the

LP-EGR valve opening is not noticed in the cylinders until after some engine cycles, complicating engine control under transient conditions [93].

Some researchers [92, 94] have also investigated an alternative EGR loop configuration resulting from combining the LP- and HP-EGR systems: the mixed pressure loop. In this case, the exhaust gases are extracted upstream of the turbine and carried to the compressor inlet pipe.

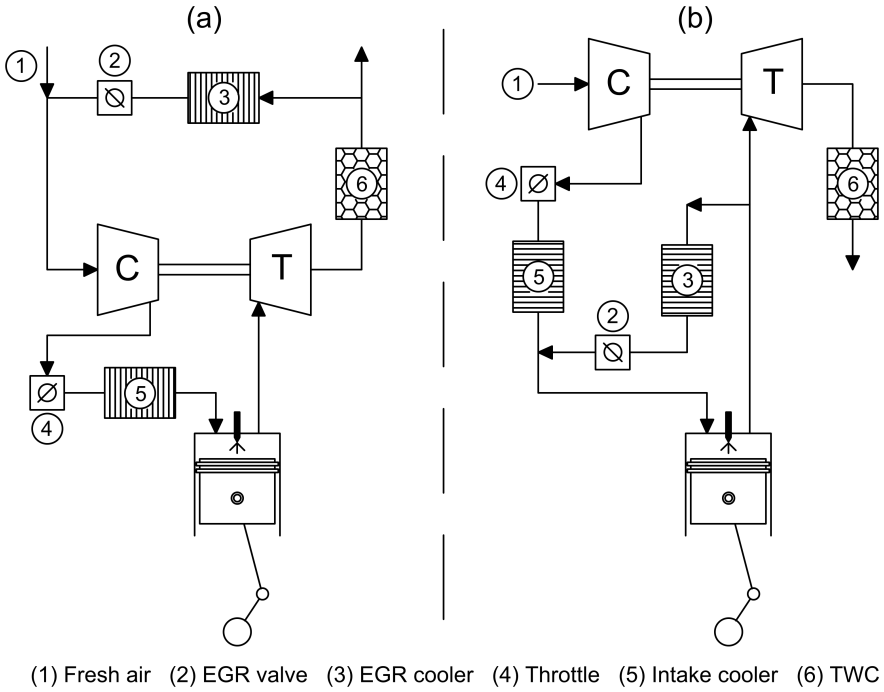

Figure 2.4: Single-line diagram of a turbocharged DI SI engine with a cooled low- (a) and high-pressure (b) EGR loop.

2.3.2 Impact on fuel consumption and engine-out emissions

Exhaust gas recirculation in SI gasoline engines reduces pumping losses (under throttling conditions), heat losses, knocking risk, and turbine inlet gas temperature [27, 95]. Alger et al. [53] added low- and high-pressure EGR loops to a boosted 1.6L DI SI engine. Both EGR systems were equipped with by-passable coolers. The conclusions from the engine tests performed by Al-

ger et al. are given below. Firstly, uncooled HP-EGR rates of up to 20% at partial loads resulted in a 3% fuel economy improvement due to a reduction in pumping losses mainly. Secondly, fuel savings higher than 25% were achieved at high loads with cooled LP EGR because of lower heat losses, improved combustion phasing, and fuel enrichment avoidance. Thirdly, engine-out CO emissions were decreased with EGR due to reduced CO_2 dissociation at partial loads (as a result of lower combustion temperature values) and higher air-to-fuel ratios at high loads. Fourthly and finally, the combustion temperature reduction also led to an abatement of engine-out NOx emissions.

These findings by Alger et al. [53] match the ones found in the works of Siokos et al. [96] and Piqueras et al. [70]. These two research works were performed by testing a turbocharged DI SI engine with a cooled low-pressure EGR loop. Siokos et al. [96] concluded that cooled LP EGR led to fuel efficiency benefits of around 4% at partial loads. Besides, Siokos et al. showed that fuel consumption at 2000 rpm and 6 bar BMEP was minimized by increasing the EGR-to-IGR ratio to 5. However, as the engine load was decreased, lower EGR-to-IGR ratios were more favorable. Piqueras et al. [70] optimized the EGR rate and VVT settings to improve fuel economy at 1500 rpm and 6 bar BMEP. They determined that the indicated efficiency was optimized by combining a minimum valve overlap with an EGR rate close to 30%. Comparing the optimized ICE operation with and without EGR, Piqueras et al. [70] observed that engine-out CO and NOx emissions were reduced by 15% and 80% with EGR, but HC emissions were increased by 60%.

As reported in the research studies mentioned above, obtaining the maximum benefit of the EGR strategy requires operating with high recirculation levels, except for very low engine loads. Although the turbocharger performance can be the main limitation at high loads and low speeds [57], increasing the EGR rate is usually limited by combustion instabilities (excessive dilution of the air-fuel mixture). On this matter, some advances in the field of ignition systems have been made in the last few years to extend the EGR tolerance in gasoline engines. Shimura et al. [97] and Pilla et al. [98] stated that the recirculation rate could be increased to 27% and 31% at high and low load conditions, respectively, using high-energy dual-coil ignition systems, thus improving fuel economy.

2.3.3 Transient operation with low-pressure EGR

High EGR operation through LP systems can lead to combustion stability issues during transient maneuvers, mainly due to the long transport delays inherent to these systems. These issues may occur particularly for aggressive throttle tip-outs in which the EGR dilution tolerance in the final operating point is much lower than in the initial one [99]. Throttle tip-outs are referred to the engine load decrease at a quasi-constant speed that happens in the first moments after the driver sharply lifts the accelerator pedal. Once the throttle is closed, the intake manifold pressure is substantially reduced, increasing the internal burnt gas recirculation during the valve overlap. This phenomenon, together with the slow evacuation of high EGR rates accumulated all through the intake path (from the LP-EGR valve to the intake ports), may cause misfires because of an excessive dilution of the air-fuel mixture (over-dilution).

A usual technique that calibration engineers use to manage fast tip-outs is fuel injection cutoff. However, this practice can negatively affect the NOx conversion efficiency of the TWC when restarting the injection, given that the oxygen storage capacity of the catalyst becomes saturated during the fuel cutoff [100]. In order to recondition the TWC surface, the engine operates with fuel-rich mixtures for some cycles after the restart despite the fuel economy penalty [99]. Fuel cutoff can also result in thermal damage to the catalyst [100].

Few alternatives to the fuel cutoff strategy can be found in the literature. Sarlashkar et al. [101] optimized the valve synchronization and spark timing to prevent misfiring during a 20-cycle tip-out in a dedicated EGR engine, in which only the exhaust gases from a cylinder are recirculated. Wiese et al. [102] utilized the VVT system to generate a short-circuit flow to quickly evacuate the EGR accumulated in the intake system, just before reducing the engine load. This solution is valid only under specific boosted conditions, and its implementation requires applying a delay between the throttle closure and driver demand. Siokos et al. [99] investigated the capability of a secondary air path to mitigate over-dilution during an aggressive tip-out (load reduction requested by a 0.1-second ramp). This secondary air path bypasses the main intake line, from the air filter outlet (upstream of the LP-EGR junction) to the intake manifold, to rapidly provide fresh air to the cylinders.

The use of high EGR levels can also give rise to poor drivability. Operating with EGR in downsized SI engines increases the dependence on the turbocharger, given that a higher pressure value at the intake manifold is needed to reach a specific load. Therefore, turbocharger lag becomes much more relevant, and this may lead to slow engine response during acceleration and tip-in maneuvers. A throttle tip-in is the opposite maneuver of a tip-out (previously defined). The drivability penalty can be partially compensated using VGT turbochargers [35], electric superchargers [103], and other strategies, which will be addressed in the present thesis. Another key point regarding engine control is estimating the LP-EGR rate accurately in transient conditions [104]. A precise estimation of the EGR gases entering the cylinders is critical to adjusting the spark timing and, thus, avoiding knocking and misfiring.

In summary, operating with high LP-EGR rates (close to the dilution limit) reduces fuel consumption in SI gasoline engines but is associated with some transient challenges. Researching and proposing solutions to these transient EGR challenges are the main focus of the present thesis.

Chapter 2 references

[11] A. Joshi. "Review of Vehicle Engine Efficiency and Emissions". *SAE Technical Paper 2021-01-0575* (2021). DOI: 10.4271/2021-01-0575. URL: https://www.sae.org/content/2021-01-0575/ (cit. on pp. 2, 3, 23).

[25] N. Fraser, H. Blaxill, G. Lumsden, and M. Bassett. "Challenges for Increased Efficiency through Gasoline Engine Downsizing". *SAE International Journal of Engines* 2.(1) (2009), pp. 991–1008. DOI: 10.4271/2009-01-1053. URL: https://www.sae.org/content/2009-01-1053/ (cit. on pp. 4, 15).

[26] D. Coltman, J. Turner, R. Curtis, D. Blake, B. Holland, R. J. Pearson, A. Arden, and H. Nuglisch. "Project Sabre: A Close-Spaced Direct Injection 3-Cylinder Engine with Synergistic Technologies to Achieve Low CO2 Output". *SAE International Journal of Engines* 1.(1) (2008), pp. 129–146. DOI: 10.4271/2008-01-0138. URL: https://www.sae.org/content/2008-01-0138/ (cit. on pp. 4, 15).

[27] J. Luján, H. Climent, R. Novella, and M. Rivas-Perea. "Influence of a low pressure EGR loop on a gasoline turbocharged direct injection engine". *Applied Thermal Engineering* 89 (2015), pp. 432–443. DOI: 10.1016/j.applthermaleng.2015.06.039 (cit. on pp. 4, 17, 24).

[28] G. Xiao, Z. Yang, and A. Isenstadt. "Fuel-efficiency technology trend assessment for LDVs in China: Advanced engine technology". 2018. URL: https://theicct.org/publication/fuel-efficiency-technology-trend-assessment-for-ldvs-in-china-advanced-engine-technology/ (cit. on p. 14).

[29] U.S. Environmental Protection Agency (EPA). *The 2021 EPA Automotive Trends Report. Greenhouse Gas Emissions, Fuel Economy, and Technology since 1975*. Tech. rep. 2021. URL: https://www.epa.gov/automotive-trends (cit. on p. 14).

[30] B. Lecointe and G. Monnier. "Downsizing a Gasoline Engine Using Turbocharging with Direct Injection". *SAE Technical Paper 2003-01-0542* (2003). DOI: 10.4271/2003-01-0542. URL: https://www.sae.org/content/2003-01-0542/ (cit. on p. 14).

[31] R. Nozawa, Y. Morita, and M. Shimizu. "Effects of engine downsizing on friction losses and fuel economy". *Tribology International* 27.(1) (1994), pp. 31–37. DOI: 10.1016/0301-679X(94)90060-4. URL: https://linkinghub.elsevier.com/retrieve/pii/0301679X94900604 (cit. on p. 14).

[32] H. C. Watson, E. E. Milkins, K. Roberts, and W. Bryce. "Turbocharging for Fuel Efficiency". *SAE Technical Paper 830014* (1983). DOI: 10.4271/830014. URL: https://www.sae.org/content/830014/ (cit. on p. 15).

[33] G. Lumsden, D. OudeNijeweme, N. Fraser, and H. Blaxill. "Development of a Turbocharged Direct Injection Downsizing Demonstrator Engine". *SAE International Journal of Engines* 2.(1) (2009), pp. 1420–1432. DOI: 10.4271/2009-01-1503. URL: https://www.sae.org/content/2009-01-1503/ (cit. on p. 15).

[34] J. Turner et al. "Ultra Boost for Economy: Extending the Limits of Extreme Engine Downsizing". *SAE International Journal of Engines* 7.(1) (2014), pp. 387–417. DOI: 10.4271/2014-01-1185. URL: https://www.sae.org/content/2014-01-1185/ (cit. on p. 15).

[35] G. Ericsson, H.-E. Angstrom, and F. Westin. "Optimizing the Transient of an SI-Engine Equipped with Variable Cam Timing and Variable Turbine". *SAE International Journal of Engines* 3.(1) (2010), pp. 903–915. DOI: 10.4271/2010-01-1233. URL: https://www.sae.org/content/2010-01-1233/ (cit. on pp. 15, 17, 27).

[36] M. Bassett, J. Hall, B. Hibberd, S. Borman, S. Reader, K. Gray, and B. Richards. "Heavily Downsized Gasoline Demonstrator". *SAE International Journal of Engines* 9.(2) (2016), pp. 729–738. DOI: 10.4271/2016-01-0663. URL: https://www.sae.org/content/2016-01-0663/ (cit. on pp. 15, 17).

[37] S. Potteau, P. Lutz, S. Leroux, S. Moroz, and E. Tomas. "Cooled EGR for a Turbo SI Engine to Reduce Knocking and Fuel Consumption". *SAE Technical Paper 2007-01-3978* (2007). DOI: 10.4271/2007-01-3978. URL: https://www.sae.org/content/2007-01-3978/ (cit. on pp. 15, 23).

[38] Y. Wang, G. Conway, J. McDonald, and A. Birckett. "Predictive GT-Power Simulation for VNT Matching to EIVC Strategy on a 1.6 L Turbocharged GDI Engine". *SAE Technical Paper 2019-01-0192* (2019).

DOI: 10.4271/2019-01-0192. URL: https://www.sae.org/content/2019-01-0192/ (cit. on p. 15).

[39] A. Li, Z. Zheng, and T. Peng. "Effect of water injection on the knock, combustion, and emissions of a direct injection gasoline engine". *Fuel* 268 (2020), p. 117376. DOI: 10.1016/j.fuel.2020.117376. URL: https://linkinghub.elsevier.com/retrieve/pii/S0016236120303719 (cit. on p. 15).

[40] Z. Han, R. D. Reitz, J. Yang, and R. W. Anderson. "Effects of Injection Timing on Air-Fuel Mixing in a Direct-Injection Spark-Ignition Engine". *SAE Technical Paper 970625* (1997). DOI: 10.4271/970625. URL: https://www.sae.org/content/970625/ (cit. on p. 15).

[41] L. P. Wyszynski, C. R. Stone, and G. T. Kalghatgi. "The Volumetric Efficiency of Direct and Port Injection Gasoline Engines with Different Fuels". *SAE Technical Paper 2002-01-0839* (2002). DOI: 10.4271/2002-01-0839. URL: https://www.sae.org/content/2002-01-0839/ (cit. on p. 15).

[42] D. Akihisa and S. Daisaku. "Research on Improving Thermal Efficiency through Variable Super-High Expansion Ratio Cycle". *SAE Technical Paper 2010-01-0174* (2010). DOI: 10.4271/2010-01-0174. URL: https://www.sae.org/content/2010-01-0174/ (cit. on p. 15).

[43] F Zhao, M.-C Lai, and D. L Harrington. "Automotive spark-ignited direct-injection gasoline engines". *Progress in Energy and Combustion Science* 25.(5) (1999), pp. 437–562. DOI: 10.1016/S0360-1285(99)00004-0. URL: https://linkinghub.elsevier.com/retrieve/pii/S0360128599000040 (cit. on pp. 15, 16).

[44] L. Graham. "Chemical characterization of emissions from advanced technology light-duty vehicles". *Atmospheric Environment* 39.(13) (2005), pp. 2385–2398. DOI: 10.1016/j.atmosenv.2004.10.049. URL: https://linkinghub.elsevier.com/retrieve/pii/S1352231005000774 (cit. on pp. 15, 16).

[45] K. A. Confer, J. Kirwan, and N. Engineer. "Development and Vehicle Demonstration of a Systems-Level Approach to Fuel Economy Improvement Technologies". *SAE Technical Paper 2013-01-0280* (2013). DOI: 10.4271/2013-01-0280. URL: https://www.sae.org/content/2013-01-0280/ (cit. on p. 16).

[46] R. Golzari, Y. Li, and H. Zhao. "Impact of Port Fuel Injection and In-Cylinder Fuel Injection Strategies on Gasoline Engine Emissions and Fuel Economy". *SAE Technical Paper 2016-01-2174* (2016). DOI: 10.4271/2016-01-2174. URL: https://www.sae.org/content/2016-01-2174/ (cit. on p. 16).

[47] T. Han, G. Lavoie, M. Wooldridge, and A. Boehman. "Dual Fuel Injection (DI + PFI) for Knock and EGR Dilution Limit Extension in a Boosted SI Engine". *SAE Technical Paper 2018-01-1735* (2018). DOI: 10.4271/2018-01-1735. URL: https://www.sae.org/content/2018-01-1735/ (cit. on p. 16).

[48] V. Knop and E. Essayem. "Comparison of PFI and DI Operation in a Downsized Gasoline Engine". *SAE International Journal of Engines* 6.(2) (2013), pp. 941–952. DOI: 10.4271/2013-01-1103. URL: https://www.sae.org/content/2013-01-1103/ (cit. on p. 16).

[49] P. Price, R. Stone, D. OudeNijeweme, and X. Chen. "Cold Start Particulate Emissions from a Second Generation DI Gasoline Engine". *SAE Technical Paper 2007-01-1931* (2007). DOI: 10.4271/2007-01-1931. URL: https://www.sae.org/content/2007-01-1931/ (cit. on p. 16).

[50] M. Braisher, R. Stone, and P. Price. "Particle Number Emissions from a Range of European Vehicles". *SAE Technical Paper 2010-01-0786* (2010). DOI: 10.4271/2010-01-0786. URL: https://www.sae.org/content/2010-01-0786/ (cit. on p. 16).

[51] G. Saliba et al. "Comparison of Gasoline Direct-Injection (GDI) and Port Fuel Injection (PFI) Vehicle Emissions: Emission Certification Standards, Cold-Start, Secondary Organic Aerosol Formation Potential, and Potential Climate Impacts". *Environmental Science and Technology* 51.(11) (2017), pp. 6542–6552. DOI: 10.1021/acs.est.6b06509. URL: https://pubs.acs.org/doi/10.1021/acs.est.6b06509 (cit. on p. 16).

[52] H. Mansouri and F. Ommi. "Performance prediction of aircraft gasoline turbocharged engine at high-altitudes". *Applied Thermal Engineering* 156 (2019), pp. 587–596. DOI: 10.1016/j.applthermaleng.2019.04.116. URL: https://linkinghub.elsevier.com/retrieve/pii/S1359431118380268 (cit. on p. 16).

[53] T. Alger, T. Chauvet, and Z. Dimitrova. "Synergies between high EGR operation and GDI systems". *SAE International Journal of Engines* 1.(1) (2009), pp. 101–114. DOI: 10.4271/2008-01-0134 (cit. on pp. 17, 24, 25, 74, 127).

[54] V. Macián, B. Tormos, V. Bermúdez, and L. Ramírez. "Assessment of the effect of low viscosity oils usage on a light duty diesel engine fuel consumption in stationary and transient conditions". *Tribology International* 79 (2014), pp. 132–139. DOI: 10.1016/j.triboint.2014.06.003. URL: https://linkinghub.elsevier.com/retrieve/pii/S0301679X14002199 (cit. on p. 17).

[55] D. Zeppei, S. Koch, and A. Rohi. "Ball Bearing Technology for Passenger Car Turbochargers". *MTZ worldwide* 77.(11) (2016), pp. 26–31. DOI: 10.1007/s38313-016-0109-z. URL: http://link.springer.com/10.1007/s38313-016-0109-z (cit. on p. 17).

[56] B. Hu, S. Akehurst, A. Lewis, P. Lu, D. Millwood, C. Copeland, E. Chappell, A. De Freitas, J. Shawe, and D. Burtt. "Experimental analysis of the V-Charge variable drive supercharger system on a 1.0 L GTDI engine". *Proceedings of the Institution of Mechanical Engineers, Part D: Journal of Automobile Engineering* 232.(4) (2018), pp. 449–465. DOI: 10.1177/0954407017730464 (cit. on p. 17).

[57] J. R. Serrano, H. Climent, J. De la Morena, and A. Gómez-Vilanova. "On the impact of turbocharger thermo-mechanical limitations on new generation gasoline engines". *Applied Thermal Engineering* 222 (2023), p. 119934. DOI: 10.1016/j.applthermaleng.2022.119934. URL: https://linkinghub.elsevier.com/retrieve/pii/S1359431122018646 (cit. on pp. 17, 19, 25).

[58] R. Kurz and R. White. "Surge avoidance in gas compression systems". *Journal of Turbomachinery* 126.(4) (2004), pp. 501–506. DOI: 10.1115/1.1777577 (cit. on p. 17).

[59] J. Andersen, F. Lindström, and F. Westin. "Surge definitions for radial compressors in automotive turbochargers". *SAE International Journal of Engines* 1.(1) (2009), pp. 218–231. DOI: 10.4271/2008-01-0296 (cit. on p. 17).

[60] W. Oakes, P. Lawless, J. Fagan, and S. Fleeter. "High-speed centrifugal compressor surge initiation characterization". *Journal of Propulsion and Power* 18.(5) (2002), pp. 1012–1018. DOI: 10.2514/2.6049 (cit. on p. 17).

[61] A. Engeda, Y. Kim, R. Aungier, and G. Direnzi. "The Inlet Flow Structure of a Centrifugal Compressor Stage and Its Influence on the Compressor Performance". *ASME Journal of Fluids Engineering* 125.(5) (2003), pp. 779–785. DOI: 10.1115/1.1601255 (cit. on pp. 17, 113).

[62] J. Galindo, H. Climent, C. Guardiola, and A. Tiseira. "On the effect of pulsating flow on surge margin of small centrifugal compressors for automotive engines". *Experimental Thermal and Fluid Science* 33.(8) (2009), pp. 1163–1171. DOI: 10.1016/j.expthermflusci.2009.07.006 (cit. on pp. 17, 113).

[63] P. Podevin, A. Danlos, M. Deligant, P. Punov, A. Clenci, and G. De La Bourdonnaye. "Automotive compressor: Effect of an electric throttle in the upstream circuit on the surge limit". In: *MATEC Web of Conferences*. Vol. 234. 2018. DOI: 10.1051/matecconf/201823403006 (cit. on pp. 17, 113).

[64] J. Galindo, J. Serrano, H. Climent, and A. Tiseira. "Experiments and modelling of surge in small centrifugal compressor for automotive engines". *Experimental Thermal and Fluid Science* 32.(3) (2008), pp. 818–826. DOI: 10.1016/j.expthermflusci.2007.10.001 (cit. on pp. 17, 114).

[65] J. Galindo, A. Tiseira, R. Navarro, D. Tarí, and C. Meano. "Effect of the inlet geometry on performance, surge margin and noise emission of an automotive turbocharger compressor". *Applied Thermal Engineering* 110 (2017), pp. 875–882. DOI: 10.1016/j.applthermaleng.2016.08.099 (cit. on p. 17).

[66] J. Galindo, J. Serrano, X. Margot, A. Tiseira, N. Schorn, and H. Kindl. "Potential of flow pre-whirl at the compressor inlet of automotive engine turbochargers to enlarge surge margin and overcome packaging limitations". *International Journal of Heat and Fluid Flow* 28.(3) (2007), pp. 374–387. DOI: 10.1016/j.ijheatfluidflow.2006.06.002 (cit. on p. 17).

[67] J. Lujan, J. Pastor, H. Climent, and M. Rivas. "Experimental Characterization and Modelling of a Turbocharger Gasoline Engine Compressor By-Pass Valve in Transient Operation". *SAE Technical Paper 2015-24-2524* (2015). DOI: 10.4271/2015-24-2524 (cit. on pp. 17, 89).

[68] Z. Lou and G. Zhu. "Review of Advancement in Variable Valve Actuation of Internal Combustion Engines". *Applied Sciences* 10.(4) (2020), p. 1216. DOI: 10.3390/app10041216. URL: https://www.mdpi.com/2076-3417/10/4/1216 (cit. on p. 18).

[69] F. Bonatesta, G. Altamore, J. Kalsi, and M. Cary. "Fuel economy analysis of part-load variable camshaft timing strategies in two modern small-capacity spark ignition engines". *Applied Energy* 164 (2016), pp. 475–491. DOI: 10.1016/j.apenergy.2015.11.057. URL: https://linkinghub.elsevier.com/retrieve/pii/S030626191501507X (cit. on p. 19).

[70] P. Piqueras, J. D. la Morena, E. J. Sanchis, and R. Pitarch. "Impact of Exhaust Gas Recirculation on Gaseous Emissions of Turbocharged Spark-Ignition Engines". *Applied Sciences* 10.(21) (2020), p. 7634. DOI: 10.3390/app10217634. URL: https://www.mdpi.com/2076-3417/10/21/7634 (cit. on pp. 19, 25).

[71] M. Sellnau and E. Rask. "Two-Step Variable Valve Actuation for Fuel Economy, Emissions, and Performance". *SAE Technical Paper 2003-01-0029* (2003). DOI: 10.4271/2003-01-0029. URL: https://www.sae.org/content/2003-01-0029/ (cit. on p. 20).

[72] S. Hara, S. Suga, S. Watanabe, and M. Nakamura. "Variable valve actuation systems for environmentally friendly engines". *Hitachi Review* 58.(7) (2009), pp. 319–324 (cit. on p. 20).

[73] Q. Li, J. Liu, J. Fu, X. Zhou, and C. Liao. "Comparative study on the pumping losses between continuous variable valve lift (CVVL) engine and variable valve timing (VVT) engine". *Applied Thermal Engineering* 137 (2018), pp. 710–720. DOI: 10.1016/j.applthermaleng.2018.04.017. URL: https://linkinghub.elsevier.com/retrieve/pii/S1359431117351918 (cit. on p. 20).

[74] W. Shin, M. Kim, S. Oh, C. Lee, H. Hwang, H. H. Song, H. W. Kim, B. S. Kim, and K. P. Ha. "An Experimental Study on a Six-Stroke Gasoline Homogeneous Charge Compression Ignition (HCCI) Engine with Continuously Variable Valve Duration (CVVD)". *SAE Technical Paper 2021-01-0512* (2021). DOI: 10.4271/2021-01-0512. URL: https://www.sae.org/content/2021-01-0512/ (cit. on p. 20).

[75] K. Akima, K. Seko, W. Taga, K. Torii, and S. Nakamura. "Development of New Low Fuel Consumption 1.8L i-VTEC Gasoline Engine with Delayed Intake Valve Closing". *SAE Technical Paper 2006-01-0192* (2006). DOI: 10.4271/2006-01-0192. URL: https://www.sae.org/content/2006-01-0192/ (cit. on p. 20).

[76] J. B. Heywood. "Ideal Models of Engine Cycles". In: *Internal Combustion Engine Fundamentals*. 2nd. New York: McGraw-Hill Education, 2018. URL: https://www.accessengineeringlibrary.com/content/book/9781260116106 (cit. on p. 20).

[77] M. Roberts. "Benefits and Challenges of Variable Compression Ratio (VCR)". *SAE Technical Paper 2003-01-0398* (2003). DOI: 10.4271/2003-01-0398. URL: https://www.sae.org/content/2003-01-0398/ (cit. on p. 21).

[78] K. Wittek, F. Geiger, J. Andert, M. Martins, V. Cogo, and T. Lanzanova. "Experimental investigation of a variable compression ratio system applied to a gasoline passenger car engine". *Energy Conversion and Management* 183 (2019), pp. 753–763. DOI: 10.1016/j.enconman.2019.01.037. URL: https://linkinghub.elsevier.com/retrieve/pii/S0196890419300834 (cit. on p. 21).

[79] K. Fridrichová, L. Drápal, J. Vopařil, and J. Dlugoš. "Overview of the potential and limitations of cylinder deactivation". *Renewable and Sustainable Energy Reviews* 146 (2021), p. 111196. DOI: 10.1016/j.rser.2021.111196. URL: https://linkinghub.elsevier.com/retrieve/pii/S1364032121004846 (cit. on p. 21).

[80] A. Kouba, B. Hnilicka, and J. Navratil. "Downsized Gasoline Engine Cylinder Deactivation MiL Development and Validation Using Real-Time 1-D Gas Code". *SAE Technical Paper 2018-01-1244* (2018). DOI: 10.4271/2018-01-1244. URL: https://www.sae.org/content/2018-01-1244/ (cit. on p. 21).

[81] R. Golzari, H. Zhao, J. Hall, M. Bassett, J. Williams, and R. Pearson. "Impact of intake port injection of water on boosted downsized gasoline direct injection engine combustion, efficiency and emissions". *International Journal of Engine Research* 22.(1) (2021), pp. 295–315. DOI: 10.1177/1468087419832791 (cit. on p. 21).

[82] C. Tornatore, D. Siano, L. Marchitto, A. Iacobacci, G. Valentino, and F. Bozza. "Water Injection: a Technology to Improve Performance and Emissions of Downsized Turbocharged Spark Ignited Engines". *SAE International Journal of Engines* 10.(5) (2017), pp. 2319–2329. DOI: 10.4271/2017-24-0062. URL: https://www.sae.org/content/2017-24-0062/ (cit. on p. 21).

[83] M. Fratita, F. Popescu, J. Martins, F. Brito, and T. Costa. "Direct water injection and combustion time in SI engines". *Energy Reports* 7 (2021), pp. 798–803. DOI: 10.1016/j.egyr.2021.07.061. URL: https://linkinghub.elsevier.com/retrieve/pii/S2352484721005266 (cit. on p. 21).

[84] B. Ashok, A. N. Kumar, A. Jacob, and R. Vignesh. "Emission formation in IC engines". In: *NOx Emission Control Technologies in Stationary and Automotive Internal Combustion Engines*. Elsevier, 2022, pp. 1–38. DOI: 10.1016/B978-0-12-823955-1.00001-2. URL: https://linkinghub.elsevier.com/retrieve/pii/B9780128239551000012 (cit. on p. 22).

[85] S. Rood, S. Eslava, A. Manigrasso, and C. Bannister. "Recent advances in gasoline three-way catalyst formulation: A review". *Proceedings of the Institution of Mechanical Engineers, Part D: Journal of Automobile Engineering* 234.(4) (2020), pp. 936–949. DOI: 10.1177/0954407019859822. URL: http://journals.sagepub.com/doi/10.1177/0954407019859822 (cit. on p. 22).

[86] W. B. Ribbens. "The Basics of Electronic Engine Control". In: *Understanding Automotive Electronics*. Elsevier, 2017, pp. 135–182. DOI: 10.1016/B978-0-12-810434-7.00004-1. URL: https://linkinghub.elsevier.com/retrieve/pii/B9780128104347000041 (cit. on p. 22).

[87] S. Kafle, H. Valera, and A. K. Agarwal. "Evolution of Catalytic Converters for Spark Ignition Engines to Control Emissions". In: *Novel Internal Combustion Engine Technologies for Performance Improvement and Emission Reduction*. Springer, 2021, pp. 175–196. DOI: 10.1007/978-981-16-1582-5_7. URL: https://link.springer.com/10.1007/978-981-16-1582-5_7 (cit. on p. 22).

[88] A. Joshi and T. V. Johnson. "Gasoline Particulate Filters—a Review". *Emission Control Science and Technology* 4 (2018), pp. 219–239. DOI: 10.1007/s40825-018-0101-y. URL: http://link.springer.com/10.1007/s40825-018-0101-y (cit. on p. 23).

[89] K. Nam, J. Yu, and S. Cho. "Improvement of Fuel Economy and Transient Control in a Passenger Diesel Engine Using LP(Low Pressure)-EGR". *SAE Technical Paper 2011-01-0400* (2011). DOI: 10.4271/2011-01-0400. URL: https://www.sae.org/content/2011-01-0400/ (cit. on p. 23).

[90] Y. Kawabata, T. Sakonji, and T. Amano. "The Effect of NOx on Knock in Spark-ignition Engines". *SAE Technical Paper 1999-01-0572* (1999). DOI: 10.4271/1999-01-0572. URL: https://www.sae.org/content/1999-01-0572/ (cit. on p. 23).

[91] V. Macián, J. Luján, H. Climent, J. Miguel-García, S. Guilain, and R. Boubennec. "Cylinder-to-cylinder high-pressure exhaust gas recirculation dispersion effect on opacity and NOx emissions in a diesel automotive engine". *International Journal of Engine Research* 22.(4) (2021), pp. 1154–1165. DOI: 10.1177/1468087419895401 (cit. on p. 23).

[92] L. Zhong, M. Musial, R. Reese, and G. Black. "EGR Systems Evaluation in Turbocharged Engines". *SAE Technical Paper 2013-01-0936* (2013). DOI: 10.4271/2013-01-0936. URL: https://www.sae.org/content/2013-01-0936/ (cit. on pp. 23, 24).

[93] J. Luján, H. Climent, F. Arnau, and J. Miguel-García. "Analysis of low-pressure exhaust gases recirculation transport and control in transient operation of automotive diesel engines". *Applied Thermal Engineering* 137 (2018), pp. 184–192. DOI: 10.1016/j.applthermaleng.2018.03.085 (cit. on p. 24).

[94] M. E. Rivas Perea. "Assessment of fuel consumption reduction strategies on a gasoline turbocharged direct injection engine with a cooled EGR system". PhD thesis. Valencia (Spain): Universitat Politècnica de València, 2016. DOI: 10.4995/Thesis/10251/68497. URL: https://riunet.upv.es/handle/10251/68497 (cit. on p. 24).

[95] K. Kumano and S. Yamaoka. "Analysis of Knocking Suppression Effect of Cooled EGR in Turbo-Charged Gasoline Engine". *SAE Technical Paper 2014-01-1217* (2014). DOI: 10.4271/2014-01-1217. URL: https://www.sae.org/content/2014-01-1217/ (cit. on p. 24).

[96] K. Siokos, R. Koli, R. Prucka, J. Schwanke, and J. Miersch. "Assessment of Cooled Low Pressure EGR in a Turbocharged Direct Injection Gasoline Engine". *SAE International Journal of Engines* 8.(4) (2015), pp. 1535–1543. DOI: 10.4271/2015-01-1253 (cit. on pp. 25, 74, 127).

[97] R. Shimura, H. Zhao, and X. Wang. "Expansion of external EGR effective region and influence of dilution on boosted operation of a downsized turbocharged GDI engine". *SAE Technical Paper 2019-01-2252* (2019). DOI: 10.4271/2019-01-2252 (cit. on p. 25).

[98] G. Pilla and L. Francqueville. "Stabilization of Highly Diluted Gasoline Direct Injection Engine using Innovative Ignition Systems". *SAE International Journal of Engines* 7.(4) (2014), pp. 1734–1743. DOI: 10.4271/2014-01-2598 (cit. on p. 25).

[99] K. Siokos and R. Prucka. "Transient Operation and Over-Dilution Mitigation for Low-Pressure EGR Systems in Spark-Ignition Engines". *SAE International Journal of Engines* 11.(5) (2018), pp. 525–538. DOI: 10.4271/03-11-05-0035 (cit. on p. 26).

[100] P. Davis and M. Peckham. "The Analysis of Gasoline Transient Emissions Behaviour Using Fast Response Gas Analysers". *SAE Technical Paper 2007-26-015* (2007). DOI: 10.4271/2007-26-015 (cit. on p. 26).

[101] J. Sarlashkar, S. Rengarajan, and R. Roecker. "Transient Control of a Dedicated EGR Engine". *SAE Technical Paper 2016-01-0616* (2016). DOI: 10.4271/2016-01-0616. URL: https://www.sae.org/content/2016-01-0616/ (cit. on p. 26).

[102] A. Wiese, A. Stefanopoulou, J. Buckland, and A. Y. Karnik. "Modelling and Control of Engine Torque for Short-Circuit Flow and EGR Evacuation". *SAE Technical Paper 2017-01-0606* (2017). DOI: 10.4271/2017-01-0606. URL: https://www.sae.org/content/2017-01-0606/ (cit. on p. 26).

[103] K. Shen, Z. Xu, Z. Zhu, and L. Yang. "Combined effects of electric supercharger and LP-EGR on performance of turbocharged engine". *Energy* 244 (2022), p. 123176. DOI: 10.1016/j.energy.2022.123176. URL: https://linkinghub.elsevier.com/retrieve/pii/S0360544222000792 (cit. on pp. 27, 80).

[104] F. Liu, J. M. Pfeiffer, R. Caudle, P. Marshall, and P. Olin. "Low Pressure Cooled EGR Transient Estimation and Measurement for an Turbocharged SI Engine". *SAE Technical Paper 2016-01-0618* (2016). DOI: 10.4271/2016-01-0618. URL: https://www.sae.org/content/2016-01-0618/ (cit. on p. 27).

Chapter 3

Experimental and theoretical tools

Contents

3.1 Introduction

The main tools employed in the present thesis are a 1D engine model and an engine test stand. The former was used to analyze fluid dynamics and transport phenomena in engine pipes and volumes; while the latter was utilized mainly to calibrate and validate the 1D model and to evaluate the engine combustion and exhaust emissions. More details about the use of these two tools will be given in **Chapter 4** and **Chapter 5**, where applicable. In addition, the 0D models of two vehicles, a hybrid electric sport utility vehicle (SUV) and its conventional counterpart, were developed to assess the impact of the EGR strategy on fuel economy under WLTP driving cycle conditions.

Therefore, this chapter is structured as set out below. The experimental setup is presented in Section 3.2, where the main characteristics of the gasoline engine and the control and measurement devices are provided, and the 1D engine model description is given in Section 3.3. Besides, three technical solutions, such as a secondary air path, a pressurized air tank, and an electric supercharger, were investigated to improve air management and engine performance during transient maneuvers. The modeling of the three systems mentioned is also explained in Section 3.3. Finally, Section 3.4 is devoted to describing the 0D SUV models and the energy management strategy used for the hybrid powertrain.

3.2 Experimental setup

3.2.1 The gasoline engine

In the present thesis, a 4-stroke 4-cylinder downsized (1.3 l) turbocharged direct injection SI gasoline engine with VVT and VGT technologies is employed. Table 3.1 shows the main engine's attributes. The VVT system enables the variation of the intake and exhaust camshaft timings in a range of 40 crank-angle degrees (CAD) without modifying the valve lift or opening duration. And the VGT turbocharger allows for a maximum boost pressure of 2.5 bar. Besides, the original engine is equipped with a Euro 6 after-treatment system, consisting of a conventional three-way catalyst followed by a gasoline particulate filter, and a compact water charge air cooler (WCAC) integrated into the intake manifold.

Table 3.1: Engine's attributes.

Attribute	**Description**
Technology	Euro 6 GTDI
Displacement	1300 cc
Compression ratio	10:1
Number of cylinders	4
Bore / Stroke	72.20 / 81.35 mm
Camshaft system	Variable valve timing
Total number of valves (intake / exhaust)	8 / 8
Type of injection	Direct injection
Turbocharger	Water-cooled with VGT
After-treatment system	TWC + GPF

A low-pressure EGR system was added to the original engine. It is composed of an EGR valve, a water-to-air intercooler, and a T-shape flow splitter to extract the exhaust gases downstream of the GPF. A choke valve, named "intake flap", was also placed in the intake line, just upstream of the EGR joint, to increase the pressure difference between the intake and exhaust lines if required. In addition, a secondary air path (SAP) was installed to bypass the main intake path, connecting the air filter outlet to the intake ports. This bypass allows fresh air to be rapidly supplied to the cylinders to prevent combustion instabilities during aggressive tip-out maneuvers. The SAP system consists of a flowmeter, a check valve (DN20), and a pipe linked to a secondary entry to the intake manifold, from where the fresh air is carried by four rails to the intake ports. All these systems, along with the control and measurement devices described in the following subsection, are represented in the schematic engine's layout provided in Figure 3.1.

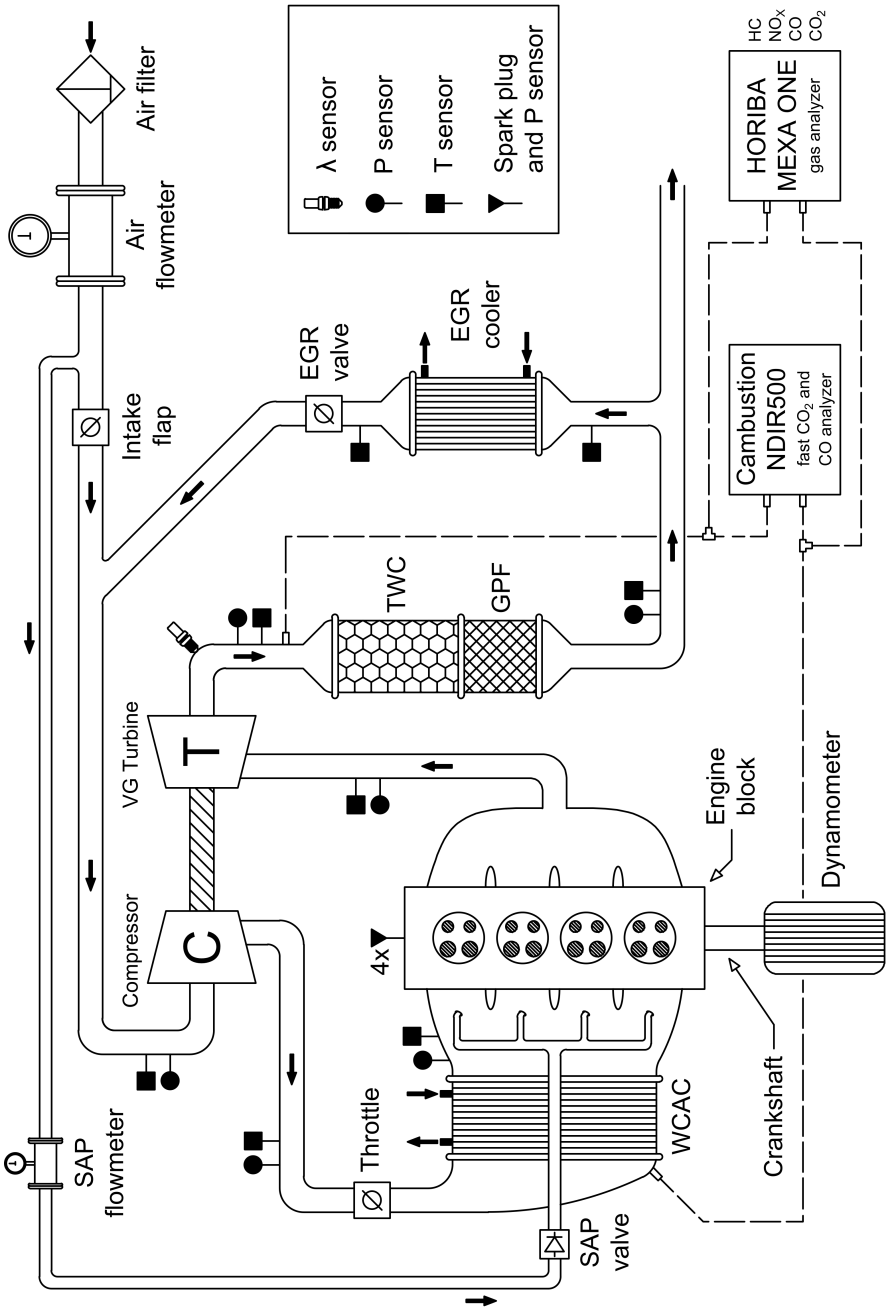

Figure 3.1: Schematic engine's layout.

3.2.2 Test bench and instrumentation

The engine was installed and fully instrumented in a dynamic test rig with the AVL AFA 200/4-8EU brake dynamometer, whose torque and rotational speed were controlled by means of the AVL PUMA software. This software was also used to acquire the pressure and temperature values in the most relevant engine parts, air and fuel mass flows, turbocharger speed, and engine raw emissions, all with a sampling frequency of 20 Hz. The location of the temperature (K-type thermocouples) and pressure (Kistler 4260A piezoresistive type transmitters) sensors is shown in Figure 3.1. The total and secondary air mass flows, the fuel mass flow, and the turbocharger speed were registered using the AVL FLOWSONIX, ABB Sensyflow FMT700-P, AVL 733S, and MICRO-EPSILON DZ140 devices, respectively. Besides, two gas analyzers were employed: the HORIBA MEXA-ONE to measure raw NOx, CO_2, CO, and HC emissions, and the Cambustion NDIR500 to provide the concentrations of CO and CO_2 in both the intake and exhaust gases under transient operating conditions. The EGR rate was estimated by applying Equation 3.1 according to [105]:

$$EGR\,[\%] = \frac{[CO_2]_{intake} - [CO_2]_{ambient}}{[CO_2]_{exhaust} - [CO_2]_{ambient}} \cdot 100 \tag{3.1}$$

where the intake ($[CO_2]_{intake}$) and exhaust ($[CO_2]_{exhaust}$) mole fractions of CO_2 are measured at the intake manifold and turbine outlet, respectively. The $[CO_2]_{ambient}$ represents the ambient mole fraction of CO_2.

Crank-angle resolved pressure traces were measured in the four cylinders with pressure sensors integrated into the spark plugs (AVL Z133), and in the manifolds with Kitsler 601CAA piezoelectric type sensors. These instantaneous pressure signals, along with the CO and CO_2 measurements from the Cambustion NDIR500 device, are registered with a frequency of 5 samples per CAD through the PXI 6123 and PXI 6251 acquisition modules, both programmed with Labview by National Instruments TM [106]. In addition, the engine control unit (ECU), designed for the original engine without EGR, was partially bypassed with the ETAS ES910 prototyping and interface module, enabling any modification of the VVT system, spark timing, injected fuel, and throttle position. The ECU was also equipped with an air flowmeter, placed at the air filter outlet, to guarantee proper lambda control when operating with EGR. The PXI 7813R and NI 9759 control modules were used to man-

age the EGR valve, intake flap, SAP valve, and VGT position in open-loop configuration [107].

Furthermore, the instantaneous in-cylinder pressure signals were processed, in real time, to display the values of COV (coefficient of variation), MAPO (maximum amplitude of pressure oscillations), and combustion phase and duration for every engine cycle, as explained in [106, 107]. These variables were used as real-time references to set spark timing in the tests with EGR. The COV is a measurement of the cycle-to-cycle combustion variability [107], and the MAPO is one of the most extended methods for knock detection [106]. The combustion parameters were calculated by means of the apparent heat release (AHR). The AHR is an estimation of the heat released by the fuel by ignoring heat transfer from the combustion chamber to the walls and by replacing the ratio of specific heats with a constant parameter (κ, usually around 1.3). Equation 3.2 presents the first law of thermodynamics for the combustion chamber assuming ideal gas behavior, and Equation 3.3 provides the apparent heat release rate (AHRR). As observed in the latter, the AHRR is only a function of the in-cylinder pressure and volume.

$$\frac{dQ_f}{dt} = \frac{c_p}{c_p - c_v} \cdot p_{cc} \frac{dV_{cc}}{dt} + \frac{c_v}{c_p - c_v} \cdot V_{cc} \frac{dp_{cc}}{dt} + \frac{dQ_w}{dt} \tag{3.2}$$

$$AHRR = \frac{\kappa}{\kappa - 1} \cdot p_{cc} \frac{dV_{cc}}{dt} + \frac{1}{\kappa - 1} \cdot V_{cc} \frac{dp_{cc}}{dt} \tag{3.3}$$

where p_{cc} and V_{cc} are the instantaneous pressure and volume at the combustion chamber, Q_f is the heat released by the fuel, Q_w is the heat transfer from the combustion chamber to the walls, and the terms c_p and c_v represent the specific heat capacities of the in-cylinder gases at constant pressure and volume, respectively.

3.3 1D engine model

3.3.1 Model description

The 1D model of the whole gasoline engine described in Section 3.2, including the EGR, VVT, and VGT technologies, was developed using GT-POWER software. The air filter, TWC, and GPF were also modeled to replicate the

gas flow pressure drop in these devices. The convective heat transfer in GT-POWER flow components is estimated by applying the Colburn analogy in ducts and volumes and the classic Woschni correlation in the cylinders [108]. Regarding the pressure losses, the Fanning factor is used to calculate friction between the working fluid and the pipe walls as a function of the surface roughness and Reynolds number [108]. Besides, in this particular case, a single-Wiebe function model was selected for combustion simulation due to its simplicity and low computational cost [109]. The single-Wiebe function is presented in Equation 3.4:

$$X_{fb} = 1 - \exp\left(-C\left(\frac{\alpha - \alpha_0}{\Delta\alpha}\right)^{m+1}\right) \tag{3.4}$$

where X_{fb}, α, α_0, and $\Delta\alpha$ are the mass fraction of fuel burned, the instantaneous crank angle, the crank angle at which the combustion starts, and the combustion duration. The adjustable parameters C and m define the combustion efficiency and the shape of the heat release rate curve. The m value is usually around 2 for SI engines, and C is set to 6.908 if assuming that 99.9% of the fuel injected is burnt at the end of combustion.

In order to perform accurate and predictive engine simulations, a series of empirical correlations were introduced into the model to adjust the heat transfer and pressure drop phenomena in all engine parts; and an artificial neural network (ANN) was trained to predict the Wiebe function parameters. This way, the Wiebe parameters are sensitive to changes in operating conditions. The empirical correlations and ANN are the main outputs of the model calibration procedure described in **Chapter 4**.

The turbocharger submodel was fed with hot-exposed compressor and turbine maps that were formerly extrapolated and adiabatized, as explained in [110], to enhance the limited data given by the manufacturers. Because of the use of adiabatized maps, the heat transfer through the turbine volute wall was considered accordingly. In addition, the following data provided by the engine manufacturer was introduced into the model in 1D and 2D lookup table formats: characteristic curves of all valves (discharge coefficient versus valve opening), intake and exhaust valve lift profiles (lift versus crank angle), and thermal efficiencies of the WCAC and EGR cooler (as a function of the gas and coolant mass flows).

3.3.2 Air management solutions

In the present thesis, a series of air management solutions have been proposed to improve engine operation with EGR during transient maneuvers. Some of these solutions simply consist in optimizing the opening or closing of the throttle, EGR valve, and intake flap; while others are more complex and require the use of auxiliary air supply systems, such as a secondary air path (SAP), a pressurized air tank (PAT), and an electric supercharger. These systems were exclusively investigated via 1D modeling, except the SAP solution, which was also tested. Figure 3.2 shows the GT-POWER schematic diagram of the whole engine intake path, from the environment to the intake ports, including the low-pressure EGR, SAP, PAT, and electric supercharger systems.

The SAP submodel was built with a check valve and round pipes, connecting the air filter outlet to the intake manifold secondary entry. The PAT system was recreated using a zero-dimensional air reservoir with a constant volume and a check valve. Two PAT configurations, named "upstream" and "downstream" due to the tank location regarding the compressor, were studied. The downstream tank is also connected to the intake manifold secondary entry, while the upstream tank pressurizes the volume between the EGR joint and the compressor inlet. When using the upstream PAT, the intake flap and EGR valve were modeled as check valves to avoid reverse flow. Besides, the tank was equipped with an anti-vacuum valve to not operate below the ambient pressure. This scenario might happen with the upstream configuration when the intake flap is partially closed to achieve high EGR rates.

The electric supercharger was modeled with three elements: a basic electric motor (EM) that requires a single input, the output power; a shaft with a simple model of mechanical losses (1D lookup table with the shaft speed as the input variable) that also includes the losses in the electric motor; and a compressor fed with hot-exposed maps previously extrapolated and adiabatized [110]. This system, along with a bypass valve, was installed downstream of the main compressor in series. In addition, a proportional controller was configured to regulate the EM output power based on the desired intake manifold pressure. The electric supercharger employed in this thesis is the same as the one researched in [111], and its main attributes are provided in Table 3.2.

The SAP system was only used for tip-outs, the electric supercharger for tip-ins, and the PAT for both maneuvers, as will be stated in **Chapter 5**.

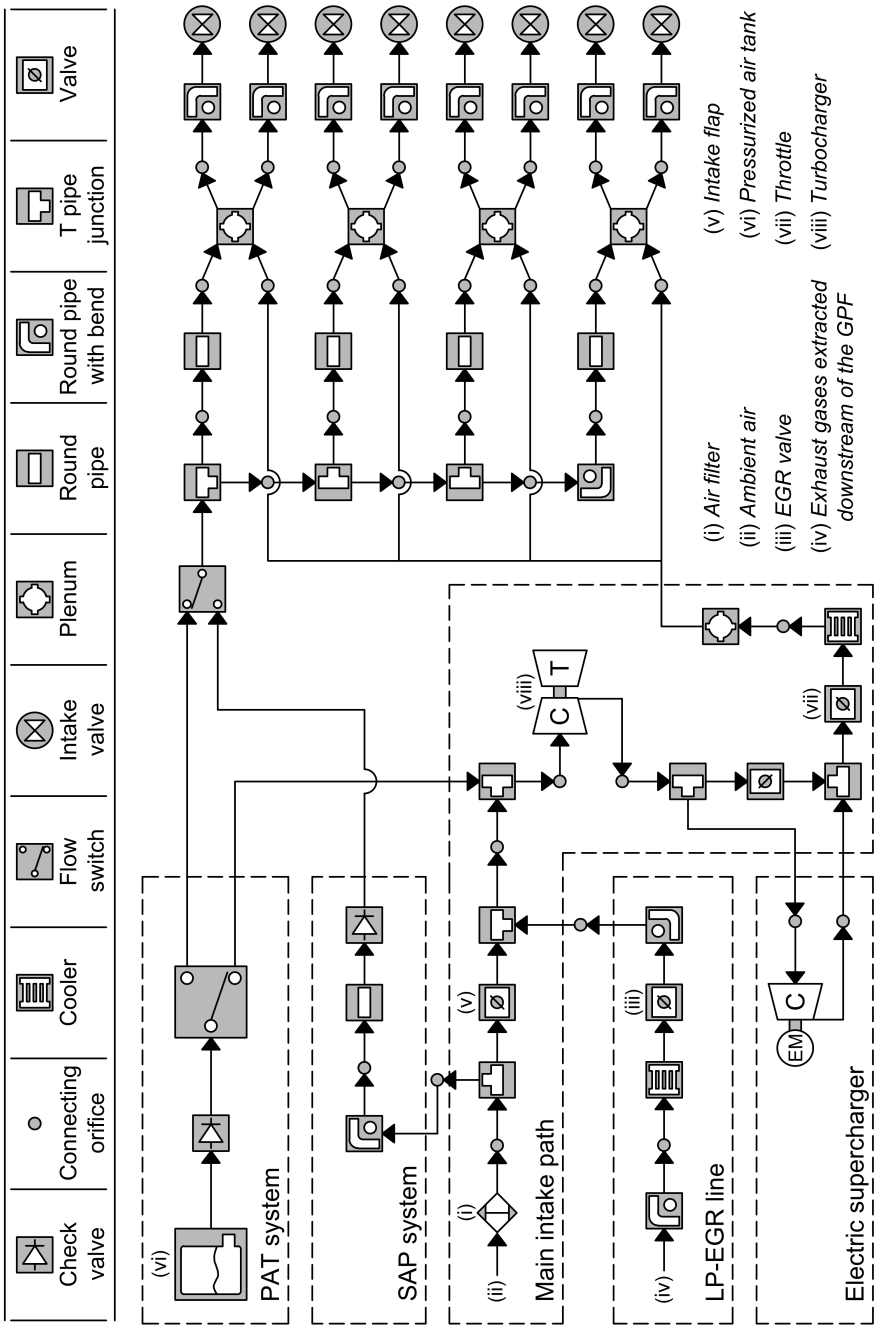

Figure 3.2: GT-POWER schematic diagram of the whole engine intake path, including the low-pressure EGR, SAP, PAT, and electric supercharger systems.

Table 3.2: Electric supercharger's attributes.

Attribute	**Description**
Moment of inertia	$2.4 \cdot 10^{-6}$ kg $\cdot$ m^2
Maximum compression ratio	1.5
Maximum compressor efficiency	0.85
Maximum electrical power	2 kW
Maximum speed	70000 rpm

3.4 0D vehicle models

3.4.1 Conventional vehicle

The passenger car selected to perform WLTP driving cycle simulations is a real conventional sport utility vehicle (SUV) of 2018, equipped with the SI gasoline engine described in Section 3.2. A 0D model of this SUV was developed using GT-SUITE software by Gamma Technologies LLC. The conventional SUV model consists of five subassemblies, named as 'ICE', 'ECU', 'Driver controller', 'Gearbox' and 'Vehicle', as illustrated in the schematic layout of the said model in Figure 3.3. The part 'ICE' is a map-based engine fuel consumption model that requires the following inputs: engine geometry, fuel properties, engine maps of fuel consumption and exhaust emissions, power demand and fuel injection shut-off strategy. The subassembly 'ECU' is a basic finite-state machine where the fuel shut-off strategy is defined. In particular, the fuel is shut off during braking events, as long as the engine torque demand is negative and lower than the negative of the engine friction torque, and during gear shifts.

The part 'Driver controller' is a model-based controller used to regulate the vehicle speed in dynamic simulations. This controller estimates the vehicle acceleration demand as the acceleration necessary to reach the desired speed in a second multiplied by an aggressiveness factor [112]. Based on the acceleration demand, the torque requested (τ_{req}) from the power sources (the internal combustion engine in conventional vehicles) is calculated as the sum of the external forces (aerodynamics, rolling resistance and gravity), the torque

required to accelerate the effective inertia of the entire drivetrain, and the load induced by a transient gear ratio [112], as shown in Equation 3.5:

$$\tau_{req} = \left[\frac{F_{ae} + F_{rr} + F_g}{R_d R_t}\right] r_w + \left[I_{it} + \frac{I_{ot}}{R_t^2} + \frac{I_d}{R_t^2} + \frac{I_a}{R_d^2 R_t^2} + \frac{M_v r_w^2}{R_d^2 R_t^2}\right] \dot{\omega}_d + \left[\frac{I_{ot}}{R_t^3} + \frac{I_d}{R_t^3} + \frac{I_a}{R_d^2 R_t^3} + \frac{M_v r_w^2}{R_d^2 R_t^3}\right] \omega_d \dot{R}_t \tag{3.5}$$

where F_{ae}, F_{rr}, and F_g are referred to the aerodynamic, rolling resistance and gravity forces. The differential ratio, transmission ratio and wheel radius are represented by the terms R_d, R_t, and r_w, respectively. The moments of inertia of the transmission input and output sides, driveshaft and axles are symbolized by I_{it}, I_{ot}, I_d, and I_a; while M_v and ω_d are the vehicle mass and the driveline speed at the clutch output. Besides, a gear shift strategy based on engine speed is specified in the 'Driver controller' to manage the gearbox.

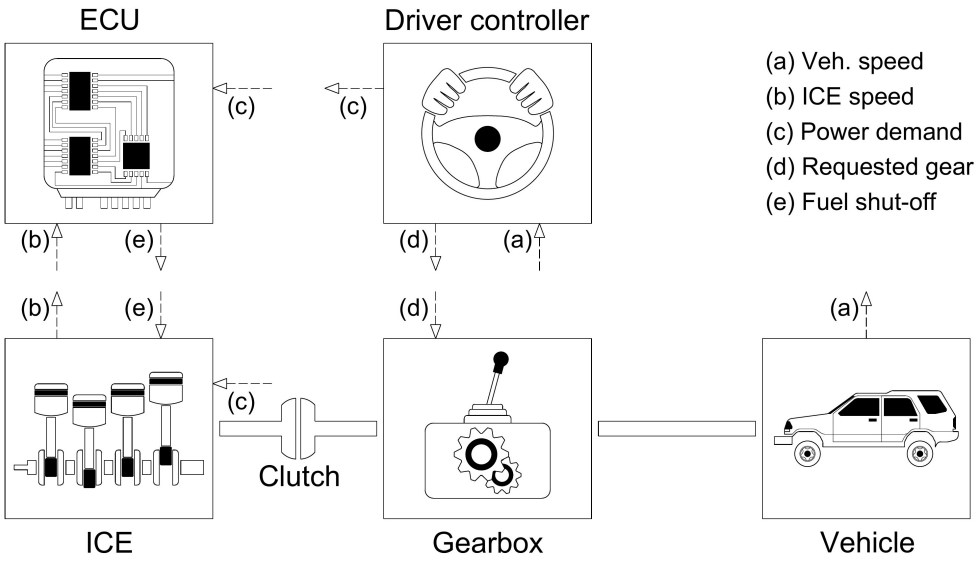

Figure 3.3: Schematic layout of the conventional vehicle model.

Finally, the vehicle aerodynamics and geometry, together with the transmission characteristics, were defined in the subassemblies 'Vehicle' and 'Gearbox'. The main specifications of the selected conventional SUV, provided in the manufacturer's website, are shown in Table 3.3.

Table 3.3: Main specifications of the selected conventional SUV.

Attribute	**Description**
Vehicle, passenger and cargo mass	1500 kg
Vehicle drag coefficient	0.33
Frontal area	2.38 m^2
Tires	215/60 R17
Gearbox	6-speed manual
Gear ratios	4.35, 2.48, 1.55, 1.14, 0.89, and 0.75
Differential ratio	3.6

3.4.2 Hybrid electric vehicle

The parallel in-line full hybrid version of the SUV presented in the previous subsection with a 2-kWh battery package was also modeled with GT-SUITE. The schematic layout of the hybrid electric vehicle (HEV) model is provided in Figure 3.4. The hybrid SUV model consists of seven parts: four of the five subassemblies included in the conventional SUV model ('ICE', 'Driver controller', 'Gearbox', and 'Vehicle'); the submodels of the electric motor (EM) of 50 kW and the battery; and the object 'EMS' where the energy management strategy (EMS) is defined to determine the power split between the ICE and EM. It should be noted that the weight of electrical components was added to the vehicle mass assuming 10 kg per battery capacity unit (kWh), 0.7 kg per electric motor power unit (kW) and 20 kg for the additional control units and cabling [113]. Besides, a second clutch between the engine and the electric motor was included. In order to estimate the battery state of charge (SOC), a simplified SOC model based on Kirchhoff's voltage law (Equation 3.6) and Coulomb Counting method (Equation 3.7) was utilized:

$$\Omega_{int} \cdot i^2 + E_{oc} \cdot i + P_{bat} \cdot \eta_c = 0 \tag{3.6}$$

$$SOC\,(t + \Delta t) = SOC\,(t) - \frac{1}{BC} \int_t^{t+\Delta t} i\ dt \tag{3.7}$$

where the terms Ω_{int}, E_{oc}, i, P_{bat} and BC are referred to the following battery parameters: internal resistance, open circuit voltage, instantaneous current, power (negative sign during battery charging) and total capacity, in that order. The Coulomb efficiency is represented by the term η_c.

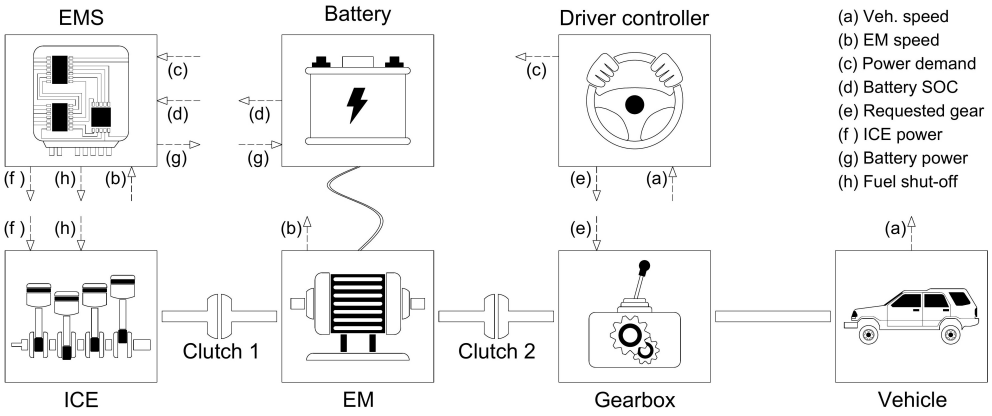

Figure 3.4: Schematic layout of the parallel in-line full HEV model.

Regarding the type of energy management strategy (EMS), a deterministic rule-based EMS was selected due to its simplicity and robustness [114]. This EMS was implemented into the HEV model by means of a GT-SUITE finite-state machine (FSM), which consists of states and transitions. The states are the hybrid powertrain operation modes, while the transitions are the logical conditions under which the FSM can change from one state to another [112]. Five main operation modes were defined according to the power split between the ICE and EM: pure electric, hybrid, conventional, regenerative braking, and conventional braking. Table 3.4 provides a summary of the information entered into the EMS, including, for every operating mode, the ICE torque request, the EM torque request, the state of the clutch between the ICE and the EM ('Clutch 1'), and the logical conditions to stay in that mode. As

observed in Table 3.4, operating in a specific mode depends on the battery SOC, driver power demand, and vehicle speed.

Table 3.4: Rule-based EMS: operation modes of the hybrid SUV.

Operation mode	**ICE torque request**	**EM torque request**	**Clutch 1**	**Conditions**
Pure electric	0	τ_d	open	$SOC > SOC_{min}$ **and** $v < v_{up}$
Hybrid	τ^*_{ICE}	$\tau_d - \tau^*_{ICE}$	closed	$\Big\{SOC > SOC_{min}$ **and** $v > v_{low}$ **and** $\Big[\{\tau^*_{ICE} \geq \tau_d \geq -F_{ICE}$ **and** $SOC < SOC_{max}\}$ **or** $\{\tau^*_{ICE} < \tau_d\}\Big]\Big\}$ **or** $\Big\{SOC < SOC_{min}$ **and** $\tau^*_{ICE} \geq \tau_d \geq -F_{ICE}\Big\}$
Conventional	τ_d	0	closed	$\Big\{SOC > SOC_{min}$ **and** $v > v_{low}$ **and** $\tau^*_{ICE} \geq \tau_d \geq -F_{ICE}$ **and** $SOC > SOC_{max}\Big\}$ **or** $\Big\{SOC < SOC_{min}$ **and** $\tau^*_{ICE} \geq \tau_d \geq -F_{ICE}\Big\}$
Regenerative braking	0	$\tau_d + F_{ICE}$	closed	$\tau_d < -F_{ICE}$ **and** $SOC < SOC_{max}$
Braking	0	0	closed	$\tau_d < -F_{ICE}$ **and** $SOC \geq SOC_{max}$

τ_d: driver torque demand; τ^*_{ICE}: ICE torque at which the BSFC is minimum for a given engine speed; F_{ICE}: engine friction torque; v: vehicle speed; v_{up}, v_{low}: upper and lower limit of the vehicle speed for the transitions between pure electric and hybrid modes.

The vehicle is initially launched in pure electric mode (unless the battery is low), that is, the EM supplies the whole driver power demand. Once either the battery is discharged or the vehicle speed is higher than a certain threshold, the ICE is started and the 'Clutch 1' is closed. While the hybrid mode is active, the engine constantly operates at its minimum BSFC (brake-specific fuel consumption) curve. Therefore, the battery is always charging when the

torque demand (τ_d) is lower than the engine torque value at which the BSFC is minimum for a given engine speed (τ^*_{ICE}), and vice versa (Table 3.4). With regard to the conventional mode, in which the vehicle is exclusively powered by the ICE, it is used under the following two scenarios: either if τ_d is lower than τ^*_{ICE} and the battery is totally charged, or if τ_d is higher than τ^*_{ICE} and the battery SOC reaches its minimum. The last two operation modes, regenerative and conventional braking, are activated when the driver torque demand is negative. During a regenerative braking, part of the vehicle kinetic energy is converted into electric energy and stored in the battery, as long as the SOC is lower than its maximum. Otherwise, a conventional braking takes place.

Chapter 3 references

[105] F. Payri, J. Luján, H. Climent, and B. Pla. "Effects of the intake charge distribution in HSDI engines". *SAE Technical Paper 2010-01-1119* (2010). DOI: 10.4271/2010-01-1119 (cit. on p. 43).

[106] B. Pla, J. De La Morena, P. Bares, and I. Jiménez. "Knock Analysis in the Crank Angle Domain for Low-Knocking Cycles Detection". *SAE Technical Paper 2020-01-0549* (2020). DOI: 10.4271/2020-01-0549 (cit. on pp. 43, 44).

[107] B. Pla, J. De la Morena, P. Bares, and I. Jiménez. "Cycle-to-cycle combustion variability modelling in spark ignited engines for control purposes". *International Journal of Engine Research* 21.(8) (2020), pp. 1398–1411. DOI: 10.1177/1468087419885754 (cit. on p. 44).

[108] Gamma Technologies LCC. *GT-Suite: Flow Theory Manual*. Westmont, IL (USA), 2018 (cit. on p. 45).

[109] J. Ghojel. "Review of the development and applications of the Wiebe function: A tribute to the contribution of Ivan Wiebe to engine research". *International Journal of Engine Research* 11.(4) (2010), pp. 297–312. DOI: 10.1243/14680874JER06510 (cit. on p. 45).

[110] J. R. Serrano, F. J. Arnau, L. M. Garciá-Cuevas, A. Gómez-Vilanova, S. Guilain, and S. Batard. "A methodology for measuring turbocharger adiabatic maps in a gas-stand and its usage for calibrating control oriented and one-dimensional models at early ICE design stages". *ASME Journal of Energy Resources Technology* 143.(4) (2021), p. 042303. DOI: 10.1115/1.4048229 (cit. on pp. 45, 46, 113).

[111] A. Broatch, M. Diez, J. R. Serrano, P. Olmeda, and A. Gómez-Vilanova. "An experimental methodology and model for characterizing radial centrifugal compressors of turbocharged engines from diathermal perspective". In: *IFToMM World Congress 2019: Advances in Mechanism and Machine Science*. Krakow (Poland), 2019, pp. 883–892. DOI: 10.1007/978-3-030-20131-9_88. URL: http://link.springer.com/10.1007/978-3-030-20131-9_88 (cit. on p. 46).

[112] Gamma Technologies LCC. *GT-Suite: Vehicle Driveline and HEV Application Manual*. Westmont, IL (USA), 2018 (cit. on pp. 48, 49, 51).

[113] J. M. Luján, A. García, J. Monsalve-Serrano, and S. Martínez-Boggio. "Effectiveness of hybrid powertrains to reduce the fuel consumption and NOx emissions of a Euro 6d-temp diesel engine under real-life driving conditions". *Energy Conversion and Management* 199 (2019), p. 111987. DOI: 10.1016/j.enconman.2019.111987 (cit. on p. 50).

[114] F. Zhang, L. Wang, S. Coskun, H. Pang, Y. Cui, and J. Xi. "Energy Management Strategies for Hybrid Electric Vehicles: Review, Classification, Comparison, and Outlook". *Energies* 13.(13) (2020), p. 3352. DOI: 10.3390/en13133352. URL: https://www.mdpi.com/1996-1073/13/13/3352 (cit. on p. 51).

Chapter 4

Optimization of the engine operation with EGR

Contents

4.1 Introduction

The optimization of the EGR and VVT strategies is addressed in this chapter. As stated in previous chapters, the gasoline engine researched in this thesis was originally conceived to operate without EGR. Therefore, before studying the engine behavior under transient conditions, an optimization process was carried out to find the EGR and VVT settings that minimize fuel consumption at specific steady-state operating points. These points were selected based on the engine operation during a WLTP driving cycle test.

This chapter is structured as stated below. Section 4.2 is devoted to the selection criterion of the steady-state engine operating points, and Section 4.3 details the optimization procedure. The fuel saving achieved with EGR at each operating point is quantified and analyzed in Section 4.4. Besides, conventional and hybrid vehicle simulations were performed to evaluate the impact of the EGR strategy on fuel economy under driving conditions. The results of these simulations are also presented in Section 4.4.

4.2 Selection of steady-state engine operating points

A WLTP class 3b driving cycle was carried out in the engine test cell at warm conditions, during which the EGR strategy was not used. The WLTP homologation cycle, with a total duration of 30 minutes, is divided into four parts (scenarios) with different average speeds: low (urban), medium (sub-urban), high (rural), and extra-high (highway). Figure 4.1 shows the WLTP speed profile for class 3b vehicles. In order to replicate the engine running conditions during the driving cycle in the test bench, the AVL PUMA software was fed with the speed profile in Figure 4.1 and the vehicle characteristics in Table 3.3.

Figure 4.2 illustrates the experimental engine running conditions, defined by the brake mean effective pressure (BMEP) and rotational speed, recorded with a sampling frequency of 10 Hz throughout the WLTP cycle test. Based on these data, 16 steady-state operating points, which cover the bulk of the engine operation, were selected to be optimized with EGR. These 16 points, along with the idle conditions at 900 rpm, are marked in Figure 4.2 with red crosses.

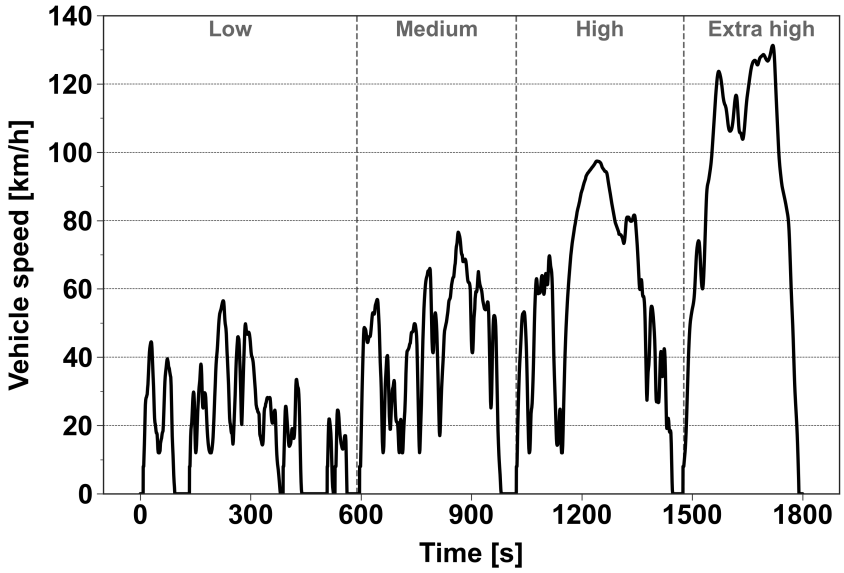

Figure 4.1: WLTP speed profile for class 3b vehicles

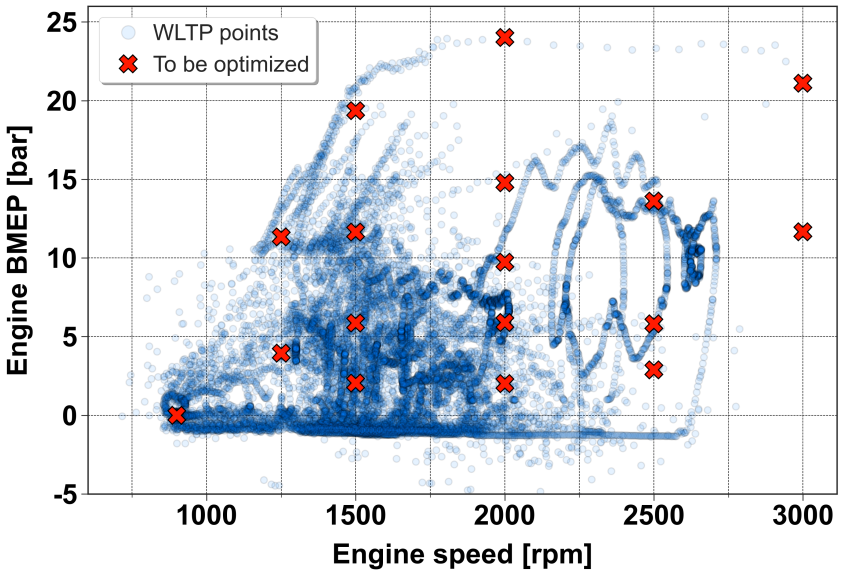

Figure 4.2: Experimental engine running conditions during the WLTP cycle performed in the test rig. The 16 operating points selected to be optimized with EGR, along with the idle conditions, are marked with red crosses.

4.3 Optimization of the VVT and EGR strategies

An optimization method mostly based on 1D simulations was used to reduce the costs associated with engine testing. The simulations were supported with only the experimental work needed to calibrate the engine model and validate the predicted results. This method consisted of four stages: experimental EGR sweeps for different valve overlap conditions at each operating point, 1D model calibration using these experimental data, parametric studies with the fitted model to find the optimum EGR rate and VVT settings, and a reduced design of experiments (DOE) to verify the trends observed with the model. Each stage is detailed below.

4.3.1 Experimental EGR sweeps

Around 300 steady-state engine tests distributed into the 16 selected operating points were performed by varying the EGR rate and VVT settings, in order to adjust the 1D model for a wide range of in-cylinder gas pressures, temperatures, and compositions. In particular, six EGR rates (0, 5, 10, 15, 20, and 25%) for three pairs of VVT settings (minimum, intermediate, and maximum valve overlaps) were tested for every operating point. In each of these 300 tests, the injection timing was set to 82 CAD after the start of the intake stroke (early DI strategy). And the spark timing was fixed in real time by assuming that the optimal combustion start in SI engines generally leads to a value of CA50 (the crank angle at which 50% of the heat is released) between 5 and 10 CAD after top dead center [115]. In the event of knocking, the spark timing was delayed as much as necessary. In addition, a COV limit of 3% was considered to guarantee combustion stability, so those experiments in which the COV of the indicated mean effective pressure was higher than 3% were excluded.

4.3.2 1D model calibration

The 1D engine model calibration was carried out following the methodology developed by Serrano et al. [1], which consists of three steps: tuning of fitting parameters, model validation, and obtention of empirical correlations.

In the first step, the experimental EGR sweeps were reproduced with the model to adjust heat transfer and pressure drop phenomena in pipes and volumes by modifying heat transfer and friction multipliers (fitting parameters). Tuning the fitting parameters was automatized using a series of proportional-integral (PI) controllers, which were configured to replicate the experimental cycle-averaged temperature and pressure values around the turbocharger and at the intake and exhaust manifolds. The way that these variables were fitted in the 1D model is explained below:

- The compressor inlet pressure (p_1) was adjusted with the friction multiplier (FM) of the air filter, while the temperature (T_1) was not controlled. So, achieving the experimental T_1 values depended on how accurately the air mass flow, EGR rate, and EGR cooler outlet temperature were reproduced.
- The compressor outlet temperature (T_2) was artificially fitted by imposing a wall temperature equal to the experimental T_2 value in the pipe downstream of the compressor and by setting the heat transfer multiplier (HTM) of this pipe to 1000. Fitting T_2 is important to correctly predict the heat transferred in the WCAC. The compressor outlet pressure (p_2) was regulated by varying turbocharger speed.
- The intake manifold pressure (p_{int}) was controlled with the throttle opening, and the temperature (T_{int}) with the WCAC coolant mass flow.
- In order to adjust p_{int} and the exhaust manifold pressure (p_{exh}) simultaneously, the turbocharger was decoupled by unlinking the compressor and turbine powers [1]. This way, p_{exh} could be regulated by changing the VGT position without affecting turbocharger speed. The turbine inlet temperature (T_{exh}) was fitted by tuning the exhaust manifold HTM.
- The pressure drop along the exhaust line was calibrated using two friction multipliers. The FM of the after-treatment system was used to adjust the turbine outlet pressure, and the GPF outlet pressure was fitted by tuning the FM in the pipes and volumes located downstream of the GPF.
- The EGR rate was regulated by varying the opening of the EGR valve and intake flap, and the EGR cooler outlet temperature was controlled with the coolant mass flow.

In the second step, the results of the engine simulations performed in the first step were validated. The predicted values of air mass flow (AMF) and indicated mean effective pressure (IMEP) were compared with their respective experimental ones, and the instantaneous pressure traces in the manifolds and cylinders were also checked. Regarding those variables regulated with PI controllers in the first step, their validation was not required because they were perfectly replicated (errors around 0%). An error threshold of 5% was considered for both AMF and IMEP variables in the interest of reliability. In other words, the fitting parameters of each simulation were employed as inputs to obtain the empirical correlations only if the corresponding AMF and IMEP relative errors were lower than 5%.

Figure 4.3 and Figure 4.4 illustrate the modeling AMF and IMEP errors related to the 300 engine tests simulated in the first step. In particular, two types of errors were calculated for each variable per operating point: the mean absolute percentage error (MAPE) and maximum error (in absolute valve). These figures demonstrate that no error in AMF and IMEP exceeds the 5% threshold.

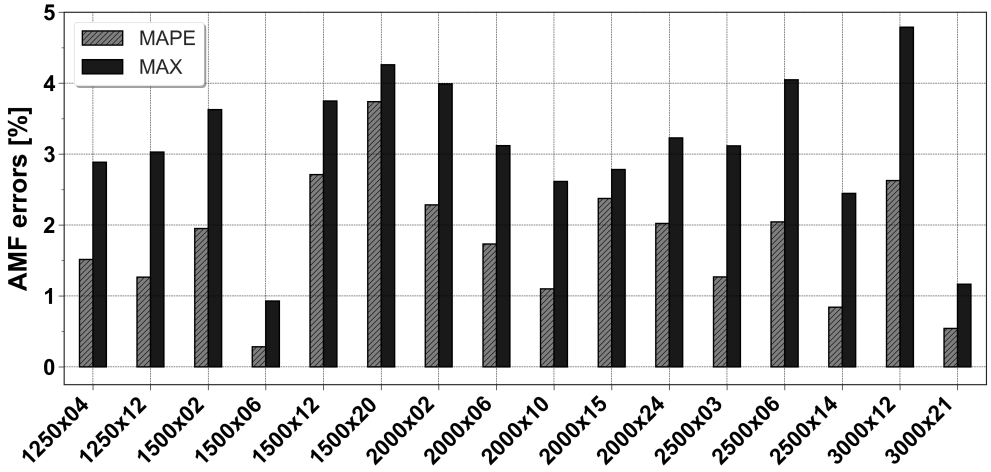

Figure 4.3: Modeling AMF errors related to the 16 operating points used for the model calibration. In the x-axis labels, the first value is referred to the engine speed (rpm) and the second one to the engine BMEP (bar).

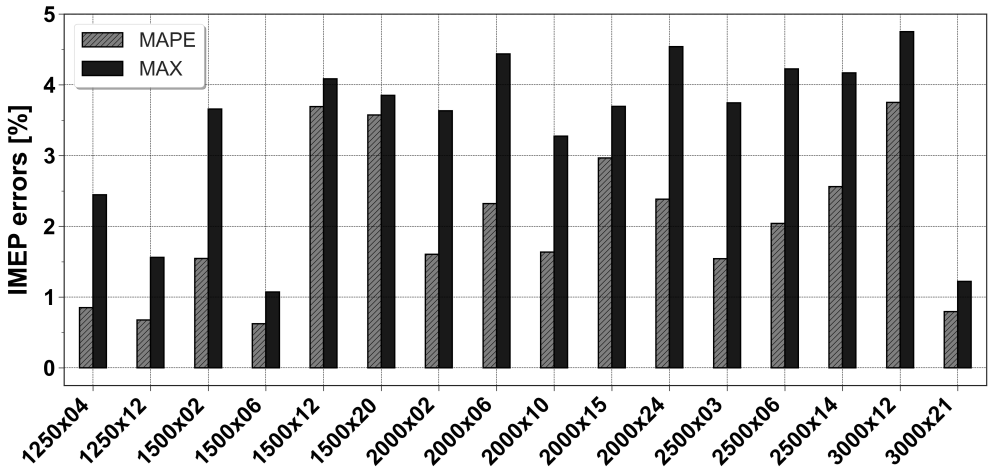

Figure 4.4: Modeling IMEP errors related to the 16 operating points used for the model calibration. In the x-axis labels, the first value is referred to the engine speed (rpm) and the second one to the engine BMEP (bar).

Figure 4.5 and Figure 4.6 show the experimental and modeling p-V diagrams (in a logarithmic scale) at two steady-state engine operating points: 6 bar BMEP at 1500 rpm and 12 bar BMEP at 3000 rpm. As seen in both figures, the 1D engine model reproduces the gas exchange process with remarkable accuracy, but also the in-cylinder heat transfer phenomenon and the combustion process.

In the third and final step, empirical correlations were determined from the validated fitting parameters, and an artificial neural network (ANN) was trained with experimental and modeling data, as detailed in [1], to predict Wiebe function parameters for combustion simulation. Table 4.1 provides the following attributes of the correlations and ANN introduced into the model: (i) the involved variable; (ii) the fitting parameter or correlation output; (iii) the independent variables or inputs; (iv) the type of correlation; and (v) the coefficient of determination (R^2).

The model calibration was completed with the implementation of these empirical correlations. Then, the turbocharger was recoupled, and all the PI controllers, except the one that regulates the engine load (by means of the throttle or VGT position), were removed. This way, the 1D model was ready to perform predictive engine simulations.

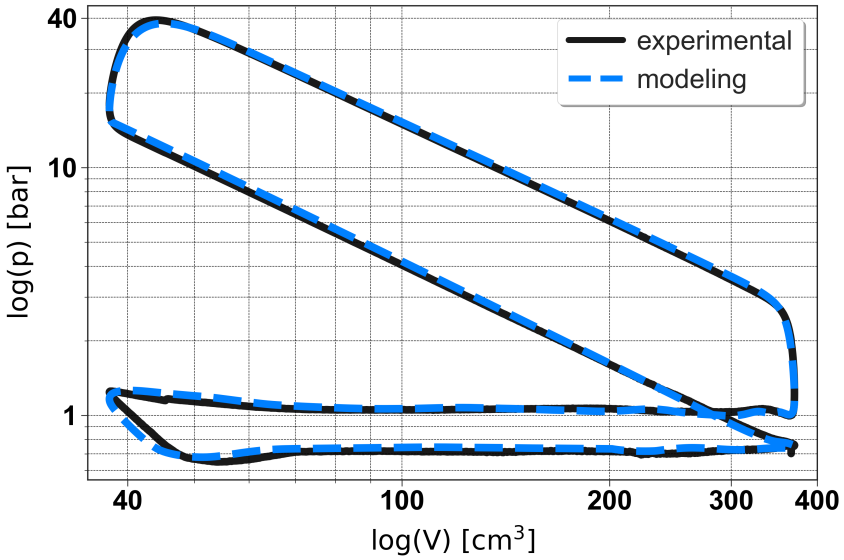

Figure 4.5: Experimental (solid line) and modeled (dashed) p-V diagrams (log scale) at 1500 rpm and 6 bar BMEP.

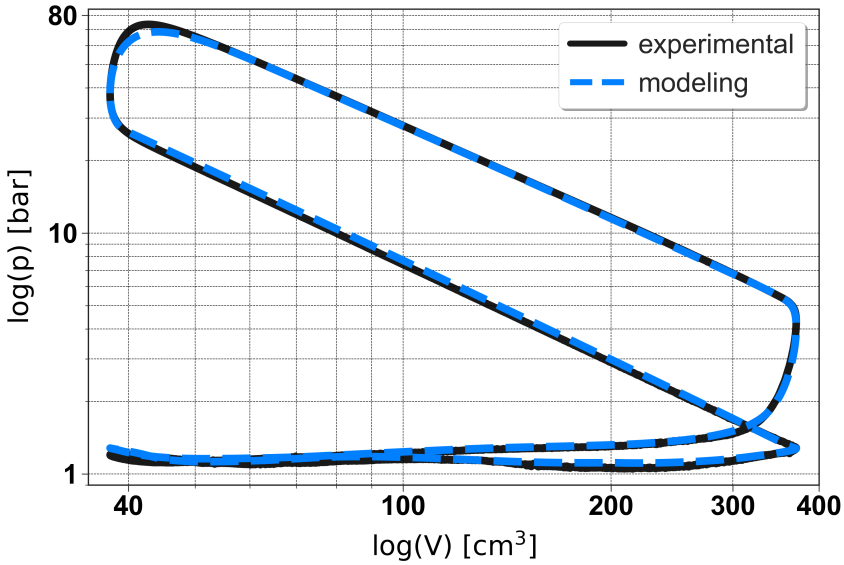

Figure 4.6: Experimental (solid line) and modeled (dashed) p-V diagrams (log scale) at 3000 rpm and 12 bar BMEP.

Table 4.1: Attributes of the empirical correlations and ANN implemented into the 1D engine model. (*) R^2 related to the ANN training data set.

Involved variable	**Fitting parameter**	**Independent variables**	**Correlation type**	R^2
p_1	FM of the air filter	Air volume flow	Quadratic polynomial equation	0.98
T_{int}	WCAC coolant flow	Engine speed and IMEP	3D map from scattered data	-
T_{exh}	HTM of the exhaust manifold	Gas temperature at the exhaust ports and gas mass flow through the turbine	Linear polynomial equation	0.81
Turbine outlet pressure	FM of the TWC and GPF	Gas volume flow at the GPF inlet	Quadratic polynomial equation	0.97
GPF outlet pressure	FM of the exhaust line	Gas volume flow through the exhaust line	Quadratic polynomial equation	0.98
EGR cooler inlet temperature	HTM of the EGR line	Gas temperature at the GPF outlet and EGR mass flow	Linear polynomial equation	0.75
EGR cooler outlet temperature	Coolant flow in the EGR cooler	Engine speed and IMEP	3D map from scattered data	-
Comb. phasing (Wiebe function)	CA50	Spark timing, λ, engine speed and in-cylinder temperature, pressure, trapped mass and residual gas fraction at IVC.	Quadratic polynomial neural network	0.98*
Comb. duration (Wiebe function)	CA1090	Spark timing, λ, engine speed and in-cylinder temperature, pressure, trapped mass and residual gas fraction at IVC.	Quadratic polynomial neural network	0.96*
Engine friction losses	FMEP	Engine speed and maximum cylinder pressure	Chen-Flynn model	0.81

4.3.3 Parametric engine simulations

A parametric study per operating point was performed with the fitted model. Each parametric study consists of 150 engine simulations, in which 25 pairs of IVO (intake valve opening) and EVC (exhaust valve closing) values were modeled for each of the six EGR rates (0, 5, 10, 15, 20 and 25%). For all these simulations, the ambient pressure and temperature were set to 1 bar and 25°C (standard ambient conditions) and a λ value of 1 was used. Figure 4.7 shows an example of the modeling results obtained at 1500 rpm and 6 bar BMEP: (a) the indicated efficiency contour map as a function of IVO and EVC for

10% EGR, and (b) the evolution of indicated efficiency for different EGR rates under minimum and maximum valve overlap conditions. In Figure 4.7**a**, the combinations of IVO (x-axis) and EVC (y-axis) equal to 0–0 CAD and 40–40 CAD provide the minimum and maximum valve overlap, respectively. These modeling results demonstrated that fuel consumption at 1500 rpm and 6 bar might be minimized with a high EGR rate and long valve overlap.

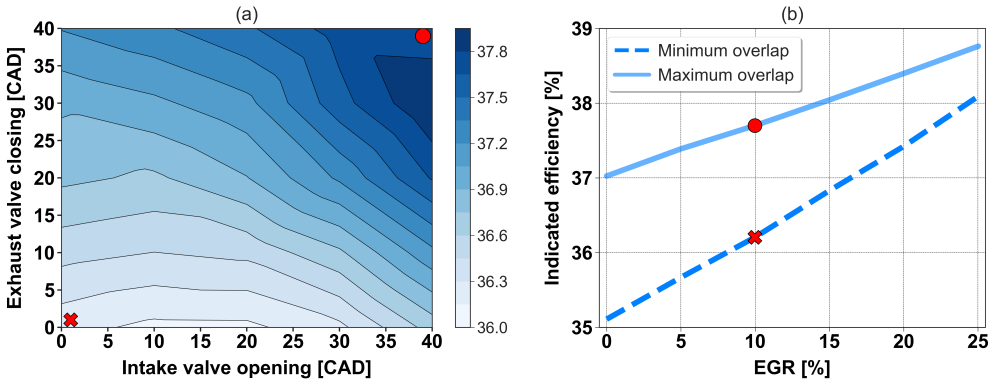

Figure 4.7: Contour map of the modeled indicated efficiency (in % in the colorbar) as a function of IVO and EVC for 10% EGR at 1500 rpm and 6 bar BMEP (a), and the evolution of the modeled indicated efficiency for different EGR rates under minimum and maximum valve overlap conditions at the same operating point (b).

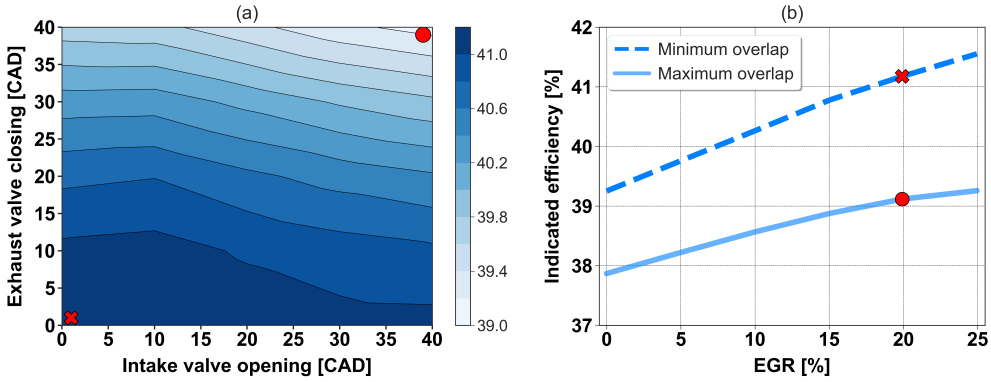

Figure 4.8: Contour map of the modeled indicated efficiency (in % in the colorbar) as a function of IVO and EVC for 20% EGR at 3000 rpm and 12 bar BMEP (a), and the evolution of the modeled indicated efficiency for different EGR rates under minimum and maximum valve overlap conditions at the same operating point (b).

Figure 4.8 illustrates (a) the indicated efficiency contour map as a function of IVO and EVC for 20% EGR at 3000 rpm and 12 bar BMEP, and (b) the evolution of indicated efficiency for different EGR rates under minimum and maximum valve overlap conditions at the same operating point. In this case, fuel economy was maximized with 25% EGR and a short valve overlap period.

4.3.4 Reduced DOE

As the last stage of the engine performance optimization with EGR, a DOE with around 10 experiments per operating point was performed, in which the best combinations of EGR and VVT settings found via modeling were tested. This final stage is critical to verify the absence of knocking or combustion instabilities, given that these phenomena are not reproduced with the model. For example, at 1500 rpm and 6 bar BMEP, a substantial deterioration in combustion stability was detected from 20% EGR with maximum valve overlap. This can be seen in Figure 4.9, which shows the IMEP COV values for the experimental EGR sweeps performed at 1500 rpm and 6 bar BMEP under minimum and maximum valve overlap conditions.

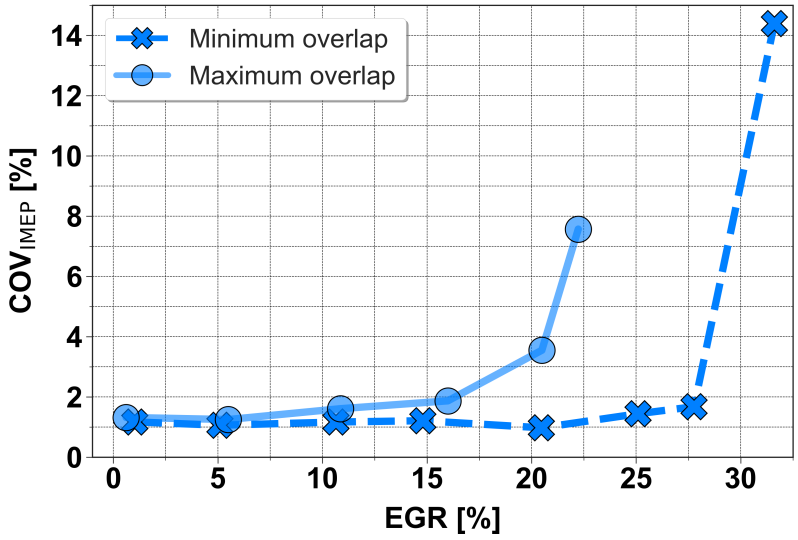

Figure 4.9: Evolution of the experimental COV of the IMEP for different EGR rates under minimum (crosses) and maximum (circles) valve overlap conditions at 1500 rpm and 6 bar BMEP.

The increase in COV from 20% EGR with maximum valve overlap leads to worse indicated efficiency values than the ones predicted by the model for the same EGR and VVT settings. In fact, the lowest fuel consumption at 1500 rpm and 6 bar BMEP is obtained with the minimum valve overlap, unlike the conclusions drawn by simulation (Figure 4.7), and 28% EGR. Nevertheless, the combination of a long valve overlap period of 60 CAD and 22% EGR also provides a very similar BSFC value. Given that the difference in BSFC between these two calibrations is lower than 0.5%, both have been taken into consideration for the studies presented in **Chapter 5** about the transient engine performance with EGR. One of the two calibrations will be selected for each study, particularly the one that creates the most challenging conditions.

4.4 Fuel economy improvement with EGR

In order to point out the value of the EGR strategy, this section presents and analyzes the fuel economy improvement from using EGR at each operating point considered for the engine calibration and under WLTP driving conditions.

4.4.1 Steady-state operating points

Figure 4.10 shows the EGR rates that minimize fuel consumption at the 16 steady-state engine operating conditions studied, and Figure 4.11 illustrates the fuel savings achieved with these EGR rates.

The fuel saving values in Figure 4.11 were calculated as the difference between the brake-specific fuel consumed by the engine with and without EGR at each working point, normalized by the latter. To obtain the BSFC values without EGR, the engine was tested using the original ECU calibration to define the spark timing and VVT settings.

4.4.2 Conventional vehicle simulations

The 0D conventional SUV model was fed with the experimental fuel consumption data of the 16 selected operating points with and without EGR.

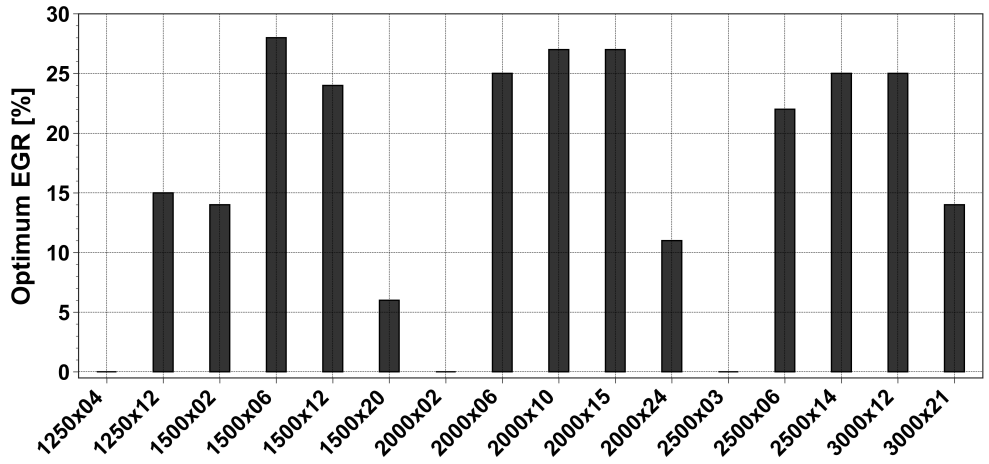

Figure 4.10: Optimum EGR rate at the 16 operating points studied. In the x-axis labels, the first value is referred to the engine speed (rpm) and the second one to the engine BMEP (bar).

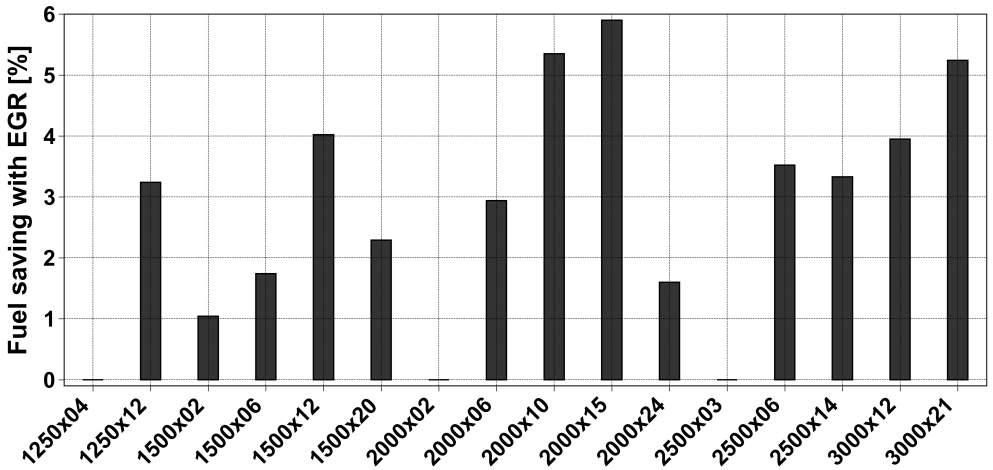

Figure 4.11: BSFC improvement achieved with EGR at the 16 operating points studied. In the x-axis labels, the first value is referred to the engine speed (rpm) and the second one to the engine BMEP (bar).

GT-SUITE utilizes these data to generate by interpolation the fuel consumption maps later used to predict engine performance during the vehicle simulation. Figure 4.12 provides two contour maps with the following information: (a) the fuel consumption of the SI engine operating without EGR, and (b) the improvement in fuel economy using EGR. The dashed black line on both maps represents the minimum BSFC curve for each engine speed. It should be noted that the highest fuel savings from the EGR strategy are achieved when operating at medium engine loads.

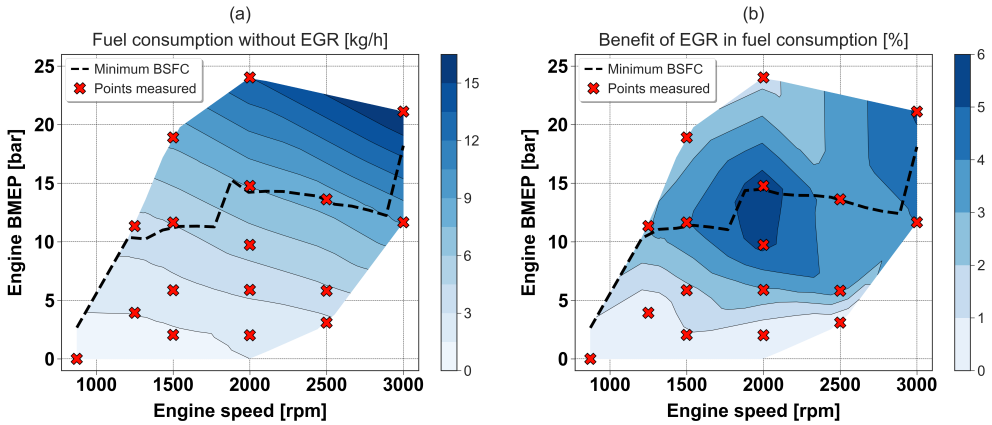

Figure 4.12: Contour map of engine fuel consumption (kg/h) without EGR (a), and contour map of EGR benefit (%) in fuel economy (b). The minimum BSFC curve is represented with the dashed black line.

By taking advantage of the WLTP cycle test previously presented in Section 4.2, the transient behavior of the conventional SUV model in terms of fuel consumption was validated. To this end, a first WLTP driving cycle simulation was performed using the data of engine fuel consumption without EGR. In this simulation, the model replicated the WLTP vehicle speed demand with a root-mean-square error of 1.79% (normalized by the average speed). Figure 4.13**a** shows the actual and predicted values of cumulative fuel consumption for the conventional powertrain without EGR during the WLTP driving cycle. And Figure 4.13**b** provides the corresponding modeling error, calculated as the difference between the actual and predicted values divided by the total fuel consumed.

Comparing the modeled total fuel consumed at the end of the WLTP cycle (1052 g) with the experimental value (1064 g), it can be stated that the GT-

SUITE vehicle model performance is highly accurate (accumulated error equal to around -1.14%).

In order to quantify the improvement in fuel economy from EGR under driving conditions, a second WLTP cycle was simulated using, in this case, the data of engine fuel consumption with EGR. The SI gasoline engine consumed 1025 g of fuel in this second simulation, 27 g less than without EGR (1052 g).

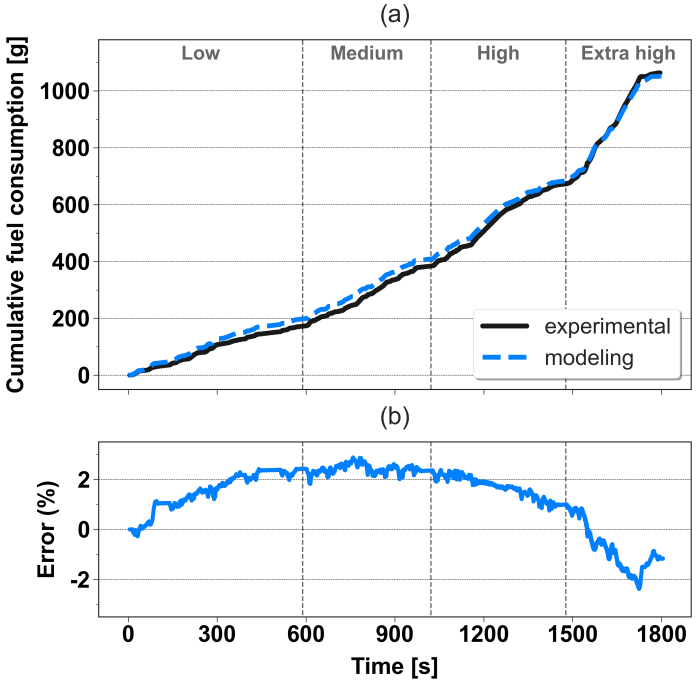

Figure 4.13: Actual (solid line) and predicted (dashed) values of cumulative fuel consumption for the conventional powertrain without EGR during the WLTP driving cycle (a), and the corresponding modeling error (b).

4.4.3 Hybrid electric vehicle simulations

As explained in Section 3.4, a series of deterministic rules were defined for the transitions between the different parallel full HEV operation modes, based on the driver power demand, battery SOC, and vehicle speed (Table 3.4). The logical conditions related to the SOC and vehicle speed were optimized, from the perspective of fuel economy, by performing two DOE procedures with 60

WLTP cycle simulations each: one considering the engine operating without EGR and the other with EGR. In particular, the variables to be optimized (DOE factors) were the upper and lower limits of the vehicle speed (v_{up}, v_{low}) and the maximum and minimum SOC (SOC_{max}, SOC_{min}).

A hysteresis loop was applied to the vehicle speed limit criterion to avoid successive engine starts and shutdowns. Therefore, an upper speed limit was considered to shift from the pure electric to hybrid mode, and a lower speed limit for the opposite transition. The difference between the upper and lower limits is the hysteresis width (w_h). For its part, the difference between the maximum and minimum SOC is the width of the SOC interval (w_i). Table 4.2 provides the levels of the DOE factors considered along with their respective optimum values with and without EGR. Some combinations of SOC_{max} and w_i levels were excluded to guarantee that the battery always operates within the usable SOC window; that is, between 30 and 70% SOC [116, 117]. Besides, it was assumed for every simulation that the battery was fully charged at the beginning.

Table 4.2: DOE by simulation for calibrating the rule-based EMS of the hybrid powertrain: factors, levels and optimum values.

DOE factor	**Levels**	**Optimum values without EGR**	**Optimum values with EGR**
Upper speed limit (km/h)	70, 80 and 90	90	90
Hysteresis width (km/h)	5 and 10	5	5
Maximum SOC (-)	0.55, 0.60, 0.65 and 0.70	0.7	0.7
SOC interval width (-)	0.20, 0.25, 0.30 and 0.40	0.3	0.3

Figure 4.14 and Figure 4.15 present the modeled WLTP fuel consumption of the hybrid SUV without and with EGR, respectively, for all feasible combinations of the DOE factor levels. To ensure a fair fuel consumption comparison, only those simulations in which the final SOC was equal to its initial value were included. Focusing on (Figure 4.14**a**), the fuel consumption for a hysteresis width of 5 km/h is reduced as the upper speed limit is increased.

A similar tendency is also observed for a w_h of 10 km/h, but in this case, the minimum fuel consumption with a v_{up} of 80 km/h is higher than with a v_{up} of 70 km/h. In short, the fuel economy without EGR was maximized with an upper speed limit of 90 km/h and a hysteresis width of 5 km/h. Regarding the battery, it is found that increasing the maximum SOC leads to better fuel economy (Figure 4.14**b**). The optimum values of SOC_{max} and w_i are equal to 0.7 and 0.3. The same trends as without EGR were observed with EGR (Figure 4.15).

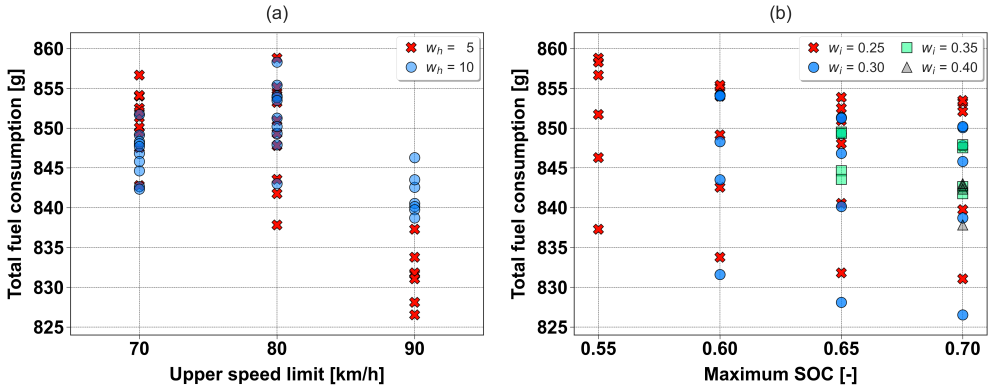

Figure 4.14: Predicted WLTP fuel consumption of the hybrid SUV without EGR versus: (a) upper speed limit for different hysteresis widths and (b) maximum SOC for different SOC interval widths.

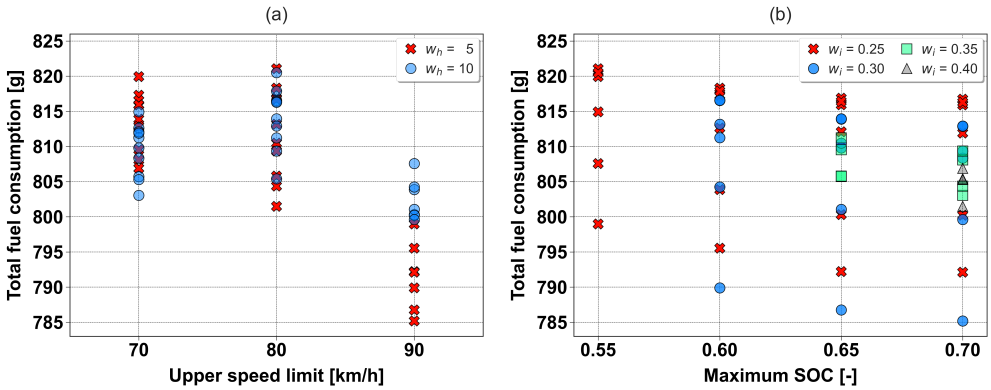

Figure 4.15: Predicted WLTP fuel consumption of the hybrid SUV with EGR versus: (a) upper speed limit for different hysteresis widths and (b) maximum SOC for different SOC interval widths.

Lastly, Figure 4.16 shows, on the contour map of EGR benefit in fuel consumption (previously provided in Figure 4.12**b**), the predicted engine operating points with EGR during the WLTP cycle for the optimum EMS calibration. As observed in this figure, the engine operation in the hybrid SUV is mostly concentrated on the minimum BSFC curve, just where the benefit of EGR in fuel economy is maximum.

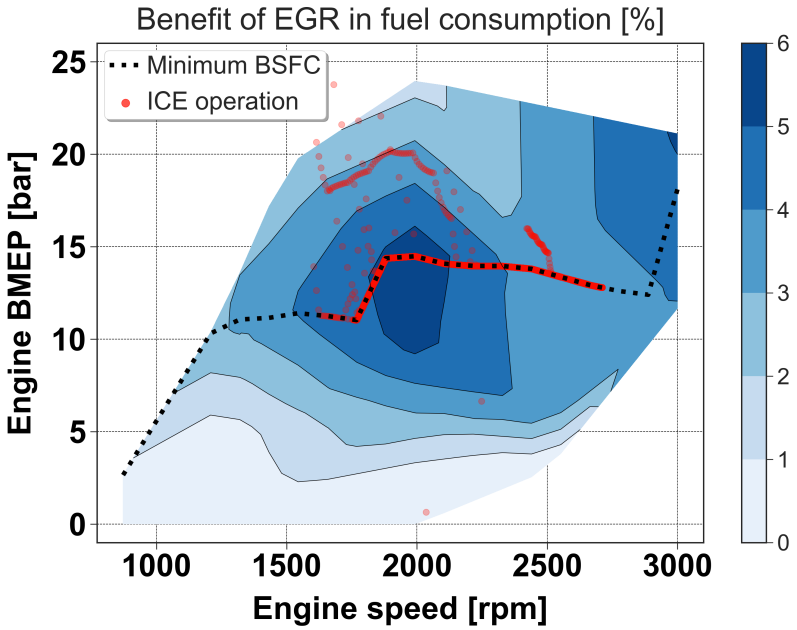

Figure 4.16: Predicted engine operating points with EGR during the WLTP cycle for the optimum calibration of the hybrid vehicle EMS, on the contour map of EGR benefit in fuel consumption.

4.4.4 Discussion

The impact of EGR on the fuel economy of SI engines is not uniform on the entire engine operating map, as shown in Figure 4.12**b**. Fuel savings above 3% are generally achieved at medium loads, between 8 and 16 bar BMEP, with EGR rates of around 25% at eight of the sixteen working points investigated (Figure 4.10). A peak EGR benefit of 5.9% is obtained at 2000 rpm and 15 bar BMEP. These results match the ones found in the research works of Alger et al. [53] and Siokos et al. [96], both previously reviewed in **Chapter 2**. In

addition, significant BSFC improvements are also achieved with EGR at high loads and 3000 rpm, while no (or very limited) benefits are obtained at low loads (Figure 4.11).

The bar chart in Figure 4.17 depicts the modeled WLTP fuel consumption of the conventional (labeled as "CONV.") and hybrid (with the optimum EMS calibration) vehicles with and without EGR. The fuel savings achieved with EGR in both powertrains, regarding the fuel consumed by their respective counterparts without EGR, are also included in this figure, above the corresponding bars. The EGR strategy improves the fuel consumption of the conventional SUV by 2.60% during the WLTP cycle. This improvement is similar to the arithmetic average (2.76%) of the fuel savings obtained for the 16 operating points (Figure 4.11).

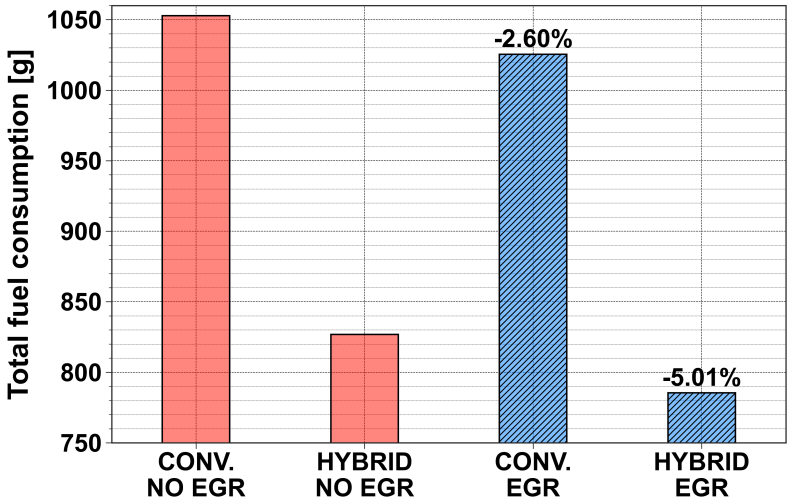

Figure 4.17: Modeled WLTP fuel consumption of the conventional and hybrid (with the optimum EMS calibration) vehicles with and without EGR.

As stated in the former subsection (Figure 4.16), the powertrain hybridization allows the ICE to mostly operate on its minimum BSFC curve, where the benefit of EGR is maximum (or comparatively high). This is clearly reflected in the fuel consumption of the hybrid SUV, leading to a saving of 5% (826 g of fuel without EGR versus 784 g with EGR), as noticed in Figure 4.17. This saving is almost twice the one obtained with EGR in the conventional SUV (2.6%). Therefore, it is concluded that hybridization notably increases

the benefit of EGR in fuel economy, thus justifying the application of this strategy in advanced SI gasoline engines working in complex hybrid-electric powertrains.

Chapter 4 references

[1] J. Serrano, H. Climent, R. Navarro, and D. González-Domínguez. "Methodology to Standardize and Improve the Calibration Process of a 1D Model of a GTDI Engine". *SAE Technical Paper 2020-01-1008* (2020). DOI: 10.4271/2020-01-1008. URL: https://www.sae.org/content/2020-01-1008/ (cit. on pp. xi, 60, 61, 63).

[53] T. Alger, T. Chauvet, and Z. Dimitrova. "Synergies between high EGR operation and GDI systems". *SAE International Journal of Engines* 1.(1) (2009), pp. 101–114. DOI: 10.4271/2008-01-0134 (cit. on pp. 17, 24, 25, 74, 127).

[96] K. Siokos, R. Koli, R. Prucka, J. Schwanke, and J. Miersch. "Assessment of Cooled Low Pressure EGR in a Turbocharged Direct Injection Gasoline Engine". *SAE International Journal of Engines* 8.(4) (2015), pp. 1535–1543. DOI: 10.4271/2015-01-1253 (cit. on pp. 25, 74, 127).

[115] G. Lavoie, E. Ortiz-Soto, A. Babajimopoulos, J. Martz, and D. Assanis. "Thermodynamic sweet spot for highefficiency, dilute, boosted gasoline engines". *International Journal of Engine Research* 14.(3) (2013), pp. 260–278. DOI: 10.1177/1468087412455372 (cit. on p. 60).

[116] J. Benajes, A. García, J. Monsalve-Serrano, and S. Martínez-Boggio. "Optimization of the parallel and mild hybrid vehicle platforms operating under conventional and advanced combustion modes". *Energy Conversion and Management* 190 (2019), pp. 73–90. DOI: 10.1016/j.enconman.2019.04.010 (cit. on p. 72).

[117] A. Pesaran. "Battery Requirements for Plug-In Hybrid Electric Vehicles: Analysis and Rationale". In: *23rd International Electric Vehicles Symposium and Exposition (EVS 23), Sustainability: The Future of Transportation*. Anaheim, California (USA), 2007. URL: https://www.osti.gov/biblio/923227 (cit. on p. 72).

Chapter 5

Transient engine operation under high EGR conditions

Contents

5.1 Introduction

The fuel consumption of the gasoline engine used in this thesis was maximized with LP-EGR rates of around 25% at half of the operating points studied in **Chapter 4**. However, as stated in Section 2.3, high EGR operation through low-pressure systems in downsized gasoline engines may penalize torque response during transient maneuvers. This chapter is therefore focused on analyzing how the EGR strategy affects the transient performance of the SI gasoline engine and evaluating the potential of different technical solutions to improve the said performance. Three studies are included in this chapter. Section 5.2 is devoted to analyzing the engine response time with EGR in tip-in maneuvers, while Section 5.3 is dedicated to studying combustion stability in tip-outs. Finally, for the sake of cost reduction, Section 5.4 proposes and evaluates an alternative method to manage compressor surge during aggressive tip-outs by taking advantage of the intake flap (Figure 3.1).

5.2 Engine response in tip-in maneuvers

In this section, three air management strategies (or solutions) are investigated to improve torque response during tip-in maneuvers under high EGR conditions. The three strategies are the following: reducing EGR dilution by rapidly closing the EGR valve simultaneously with the throttle opening; using a small tank of pressurized air that can be connected to either the intake manifold (downstream configuration) or the compressor inlet pipe (upstream); and installing an electric supercharger at the compressor outlet in series. The last two solutions have already been researched under different circumstances or from a distinct perspective [103, 118, 119], so the intention of the Ph.D. candidate is not to present these solutions as a groundbreaking technology. The contribution of this study lies in understanding the negative impact of EGR on the transient response of the gasoline engine and analyzing if the systems mentioned are useful for solving or minimizing this particular issue.

For that purpose, a series of tip-ins at 1500 rpm from 6 bar BMEP (62 Nm) to 12 bar BMEP (124 Nm) were tested and simulated. Tip-in tests were used to analyze the EGR influence on transient operation, validate the engine model performance, and assess the EGR reduction strategy. The pressurized air tank and electric supercharger systems were studied with 1D simulations.

The modeling of both systems was explained in Section 3.3 (Figure 3.2). It should be remarked that both torque response and fuel economy criteria were considered to evaluate the three air management strategies.

The tip-in operating conditions mentioned above were selected for two reasons. Firstly, the initial working point (6 bar BMEP and 1500 rpm) is quite relevant for conventional vehicles during the WLTP driving cycle (Figure 4.2). In particular, the engine works at around 1500 rpm between 4 and 8 bar BMEP during one sixth of the WLTP cycle. Secondly, there is a significant difference between operating with and without EGR at the final tip-in point. Turbocharging is almost not required with no EGR to reach 12 bar BMEP, while the VGT mechanism must be closed above 80% to achieve an EGR rate of 24%.

As stated in Section 4.3, at the initial tip-in point, the BSFC can be minimized through two combinations of EGR and VVT settings: either minimum valve overlap and 28% EGR or a valve overlap of 60 CAD and 22% EGR. Although both generate very similar fluid-dynamic conditions at all engine parts, the latter is chosen for this study because it leads to a slightly lower turbocharger speed, making the maneuver a bit more challenging.

The results of tip-in tests are provided in the first two subsections: (5.2.1) influence of EGR on torque response and (5.2.2) EGR reduction strategy. The tip-in simulations are presented in other three subsections: (5.2.3) validation of the transient model performance, (5.2.4) pressurized air tank, and (5.2.5) electric supercharger. Finally, all modeled and experimental data are analyzed together in Subsection 5.2.6 to compare the three air management solutions.

5.2.1 Influence of EGR on torque response

Two tip-in tests were performed, one without EGR (labeled "target") and the other with EGR ("baseline"), to determine the impact of high EGR operation on the transient engine response. Figure 5.1 depicts the time evolution of the valve setpoints in both tip-in tests. The setpoints of the throttle, VGT, intake flap, and spark timing were linearly changed from their initial to final values in two engine cycles. In the baseline case, the EGR valve was kept fully open during the whole maneuver, and the VVT system is configured to reduce the valve overlap from around 60 to 15 CAD also in two cycles. All the actuations were synchronized using the pedal signal. Figure 5.2 shows the time evolution

of the intake manifold pressure (a), air mass flow (b), turbocharger speed (c), and torque (d) in the target and baseline cases.

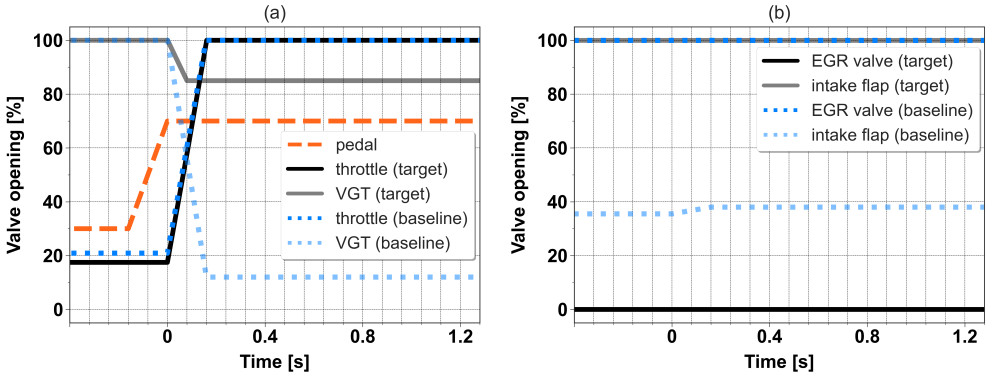

Figure 5.1: Time evolution of the throttle (a), VGT (a), EGR valve (b), and intake flap (b) setpoints in the target (case without EGR) and baseline (with EGR) tip-in tests.

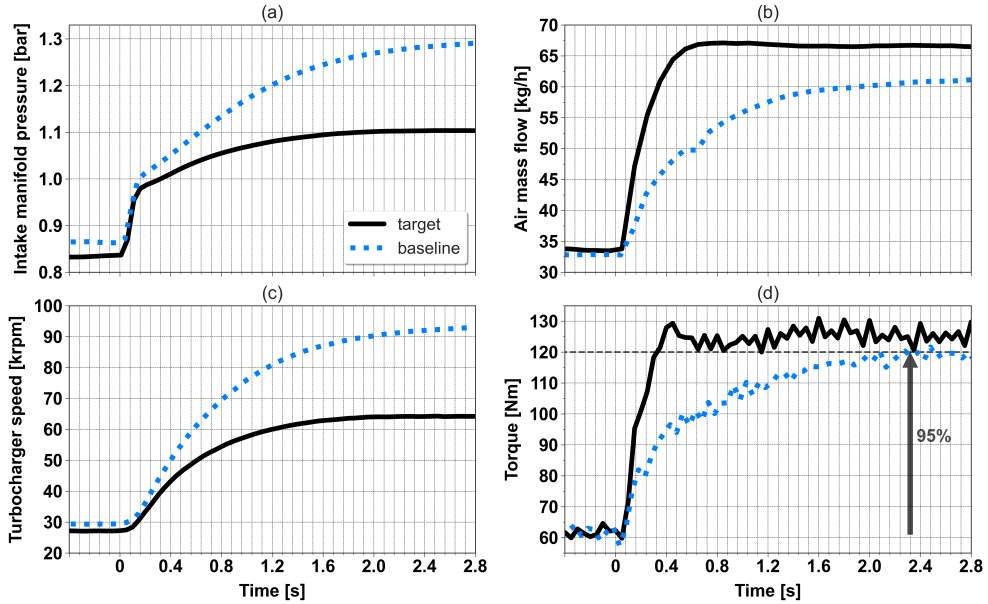

Figure 5.2: Time evolution of the intake manifold pressure (a), air mass flow (b), turbocharger speed (c), and torque (d) in the target (without EGR) and baseline (with EGR) tip-in tests.

A notably slower air mass flow increase is observed in the case with EGR (Figure 5.2**b**), leading to poor engine response. This behavior is because of the need for higher turbocharger acceleration, given that introducing 24% of EGR requires an additional pressure increment of around 0.20 bar in the intake manifold to reach the final torque (124 Nm). Comparing the torque evolution in both tip-ins reveals that the EGR strategy leads to a 2-s slower response time (Figure 5.2**d**). The response time is defined in this study as the time required to complete the 95% of the total load increase; that is, the time spent to achieve a torque value of 120 Nm.

5.2.2 EGR reduction strategy

Given the poor engine response with EGR, a first strategy, consisting in reducing the EGR dilution during the first engine cycles of the tip-in, was proposed to accelerate the torque increase. This strategy is carried out just by modifying the EGR valve actuation as explained below. Instead of keeping the EGR valve fully open as in the baseline tip-in, it is closed as fast as possible simultaneously with the throttle opening, kept closed for some engine cycles, and finally, reopened slowly. Twenty tip-in maneuvers divided into two stages were tested to determine the duration of the EGR valve closure and the slope of the reopening ramp. In the first stage, ten tip-in tests were performed with varying durations (3, 5, 7, 9, and 11 cycles) and slopes (40 and 80 units of opening per second). A conservative spark timing was used in these first tests to prevent knocking. In the second stage, the same ten tip-ins were repeated, but now adjusting the spark timing actuation based on the fast intake CO_2 measurements (registered using the Cambustion NDIR500 device) to enhance combustion. The best of these last tip-ins in terms of torque response (labeled "Case A") is the one that combines an EGR valve closure of 7 cycles with a reopening slope of 40.

Figure 5.3 shows the time evolution of the EGR valve (a) and spark timing (b) setpoints in the "baseline" and "Case A" tip-in tests. The rest of the valve actuations in Case A are the same as in the baseline tip-in (Figure 5.1). Figure 5.4 provides the time evolution of the intake manifold pressure (a), intake CO_2 volume fraction (b), air mass flow (c), engine torque (d), turbine inlet temperature (e), and turbocharger speed (f) in the "baseline" and "Case A" tip-in tests. Closing the EGR valve at the start of the maneuver improves torque response significantly, mainly due to a sharp increase in AMF before

0.4 s. In addition, higher enthalpy is provided to the turbine in Case A, leading to a better turbocharger acceleration (Figure 5.4**f**). The response time in Case A is around 0.57 s, only 0.25 s slower than in the target case without EGR and 1.75 s faster than in the baseline case. Finally, it should be stated that the torque overshoot observed from 0.8 s (Figure 5.4**d**) can be removed by adjusting the EGR valve actuation, as will be shown in Subsection **5.2.6**.

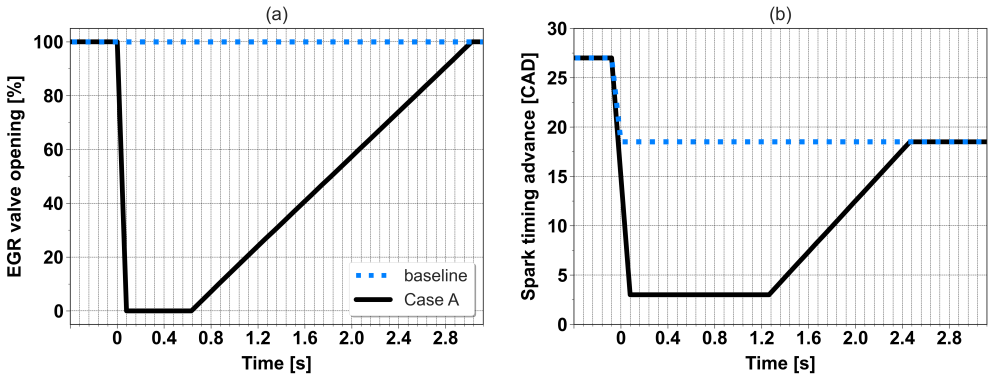

Figure 5.3: Time evolution of the EGR valve (a) and spark timing (b) setpoints in the "baseline" and "Case A" tip-in tests.

5.2.3 Validation of the transient 1D model response

The "Case A" tip-in test was simulated to validate the model performance under these particular transient conditions. The procedure followed to replicate the said tip-in is described below. The experimental throttle, EGR valve, and intake flap actuations were directly imposed into the model, and the VGT position was adjusted during the simulation to achieve the experimental pressure evolution in the intake manifold. This adjustment is explained in detail in [120] and mainly consists in applying a slight correction to the VGT position measurement using a PI controller. The experimental values of spark timing, air-to-fuel ratio, and VVT settings were also given to the model as inputs. In addition, some thermocouples were modeled to consider the thermal inertia of actual sensors in the main engine parts, such as the turbine inlet and outlet, compressor outlet, and intake manifold. Regarding the combustion, the Wiebe function parameters were predicted by means of the ANN.

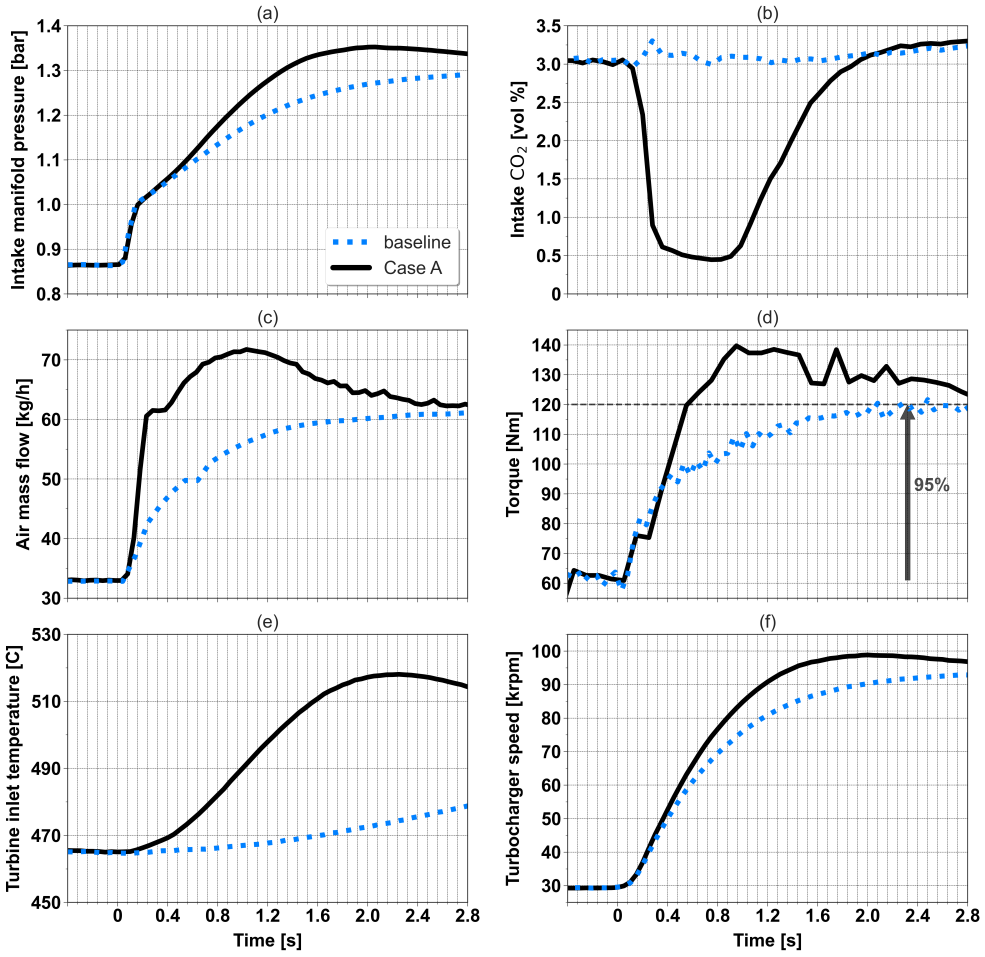

Figure 5.4: Time evolution of the intake manifold pressure (a), intake CO_2 volume fraction (b), air mass flow (c), engine torque (d), turbine inlet temperature (e), and turbocharger speed (f) in the "baseline" and "Case A" tip-in tests.

Figure 5.5 provides the experimental and modeled values of the following variables during the "Case A" tip-in: intake and exhaust manifold pressure (a), intake CO_2 volume fraction (b), air mass flow (c), IMEP and BMEP (d), turbocharger speed (e), and turbine inlet temperature (f).

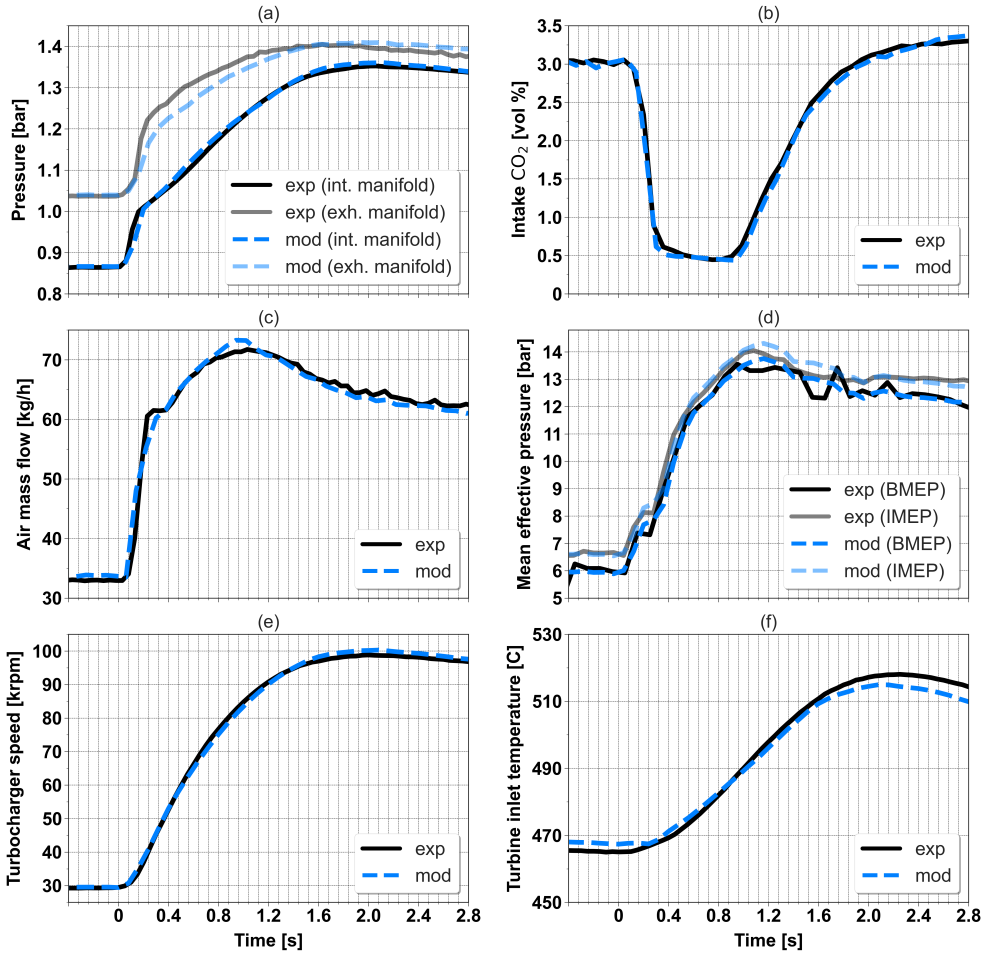

Figure 5.5: Actual (exp) and predicted (mod) values of the following variables during the "Case A" tip-in: pressure in the intake and exhaust manifolds (a), intake CO_2 volume fraction (b), air mass flow (c), IMEP and BMEP (d), turbocharger speed (e), and turbine inlet temperature (f).

The model prediction is quite accurate in general. The evolution of the intake manifold pressure is perfectly replicated by regulating the VGT position (errors lower than 1%). The gas pressure at the exhaust manifold is also well reproduced, but differences of up to 4% are detected at around 0.8 s. Such differences are probably because of a slight turbine efficiency overprediction. Besides, no noticeable errors are observed in the evolution of the intake CO_2

fraction and AMF, so the 1D model reproduces the gas exchange process precisely. If the intake flow and composition are achieved, the accurate modeling of the IMEP and BMEP demonstrates that the Wiebe parameters (ANN) and FMEP (Chen-Flynn model) are well estimated. Between 1.4 and 2.4 s, the model does not capture some BMEP fluctuations caused by combustion instabilities, given that the ANN was trained only under stable combustion conditions. The turbine inlet temperature is reproduced with errors lower than 5°C, so the heat transfer in the exhaust manifold is rightly corrected through the corresponding HTM correlation. Finally, the precise modeling of the turbocharger speed corroborates the high accuracy of the turbine and compressor maps.

5.2.4 Pressurized air tank (PAT)

A 2-L tank of fresh air, initially at 3 bar and 20°C, was employed for all simulations presented in this section. Firstly, it was assumed that larger tank volumes would not be feasible due to space restrictions. Secondly, after trying different values, it was found that an initial tank pressure of at least 3 bar is required to obtain the same torque response time as in the "target" tip-in without EGR. As mentioned before, two PAT configurations or locations were investigated: downstream and upstream. The downstream tank is directly linked to the intake manifold to increase the in-cylinder trapped air mass rapidly. Nevertheless, this strategy can lead to compressor surge and must be combined with a transient EGR valve closure, as in Case A, to prevent the torque drop once the tank empties. As an alternative, the upstream PAT is connected to the volume between the EGR joint and the compressor inlet (Figure 3.2). This way, the tank does not block the compressor, but its implementation involves using check valves to avoid reverse flow through the intake flap and EGR valve. Both downstream and upstream PAT strategies are detailed below. Lastly, it should be stated that the tank filling procedure is not addressed in this study.

5.2.4.1 Downstream PAT

Since the amount of pressurized air is limited (only 2 L), calibrating the opening timing of the tank valve (DN30) is essential for obtaining good results. Firstly, six tip-ins were simulated with the downstream PAT, in which three

PAT valve opening delays (0, 2, and 4 engine cycles regarding the throttle opening) and two EGR valve actuations (partially closed and fully open) were tried. Figure 5.6 shows the positions of the EGR and PAT valves during these six tip-in simulations. The rest of the valve actuations are the same as the ones utilized to replicate the "Case A" tip-in in Subsection **5.2.3**. In addition, the stoichiometric air-to-fuel ratio was imposed throughout the maneuver in all simulations, and the Wiebe function parameters were predicted using the ANN. Figure 5.7 illustrates the predicted values of the next variables during the six tip-ins presented in Figure 5.6: AMF through the PAT valve (a) and intake ports (b), EGR rate at the intake ports (c), and engine torque (d).

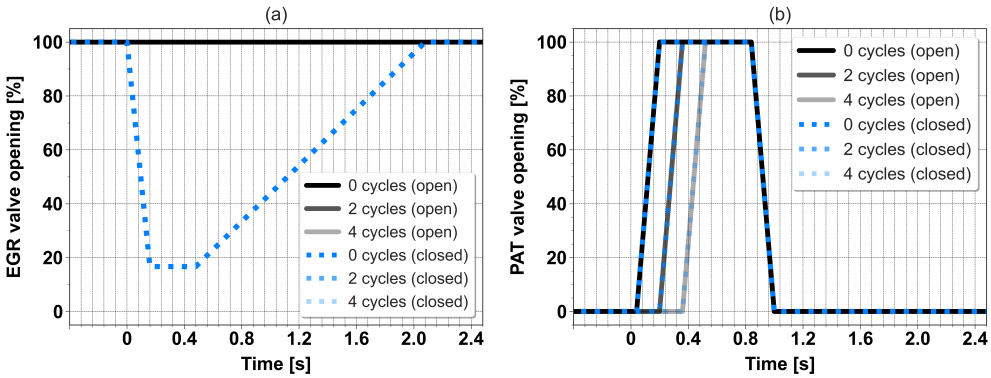

Figure 5.6: Opening percentage of the EGR (a) and PAT (b) valves during the six tip-in with the downstream PAT. In the legend, the first term refers to the PAT valve opening delay in cycles (regarding the throttle opening), and the second (in parentheses) is related to the EGR valve position.

The fastest torque response is achieved by combining a PAT valve opening delay of 2 cycles with the EGR reduction strategy (EGR valve partially closed during the first two seconds, as shown in Figure 5.6). The response time is not reduced when opening the PAT valve without any delay owing to the short-circuit of a portion of the pressurized air. As observed in Figure 5.7, the peak of AMF (through the intake ports) at 0.15 s does not result in a proportional torque increase. Though this short-circuit phenomenon happens in the six cases, it is more significant when the PAT valve opening is not delayed. This is because the abrupt pressure increase in the intake manifold takes place while the valve overlap is still quite long. It should be reminded that the VVT system was configured to provide a valve overlap period of around 60 and 15 CAD at the initial and final tip-in operating points, respectively. And the transition

between the initial and final VVT settings lasts 3 cycles. With regard to the EGR valve actuation, it is found that reducing the EGR dilution in the first 2 s is required to prevent a torque drop once the PAT becomes empty (Figure 5.7**d**).

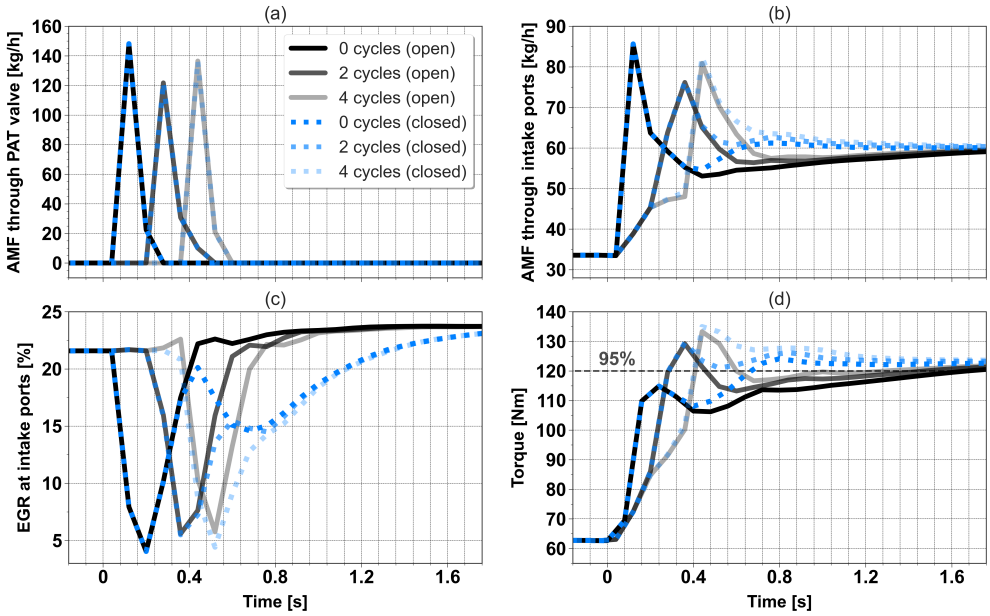

Figure 5.7: Modeled AMF through the PAT valve (a) and intake ports (b), EGR rate at the intake ports (c), and engine torque (d) during the six tip-in with the downstream PAT. In the legend, the first term refers to the PAT valve opening delay in cycles (regarding the throttle opening), and the second (in parentheses) is related to the EGR valve position.

As a disadvantage, the downstream PAT strategy leads to compressor surge because the air from PAT blocks the intake path. Surge appearance can be avoided, as in tip-out maneuvers [4, 67], using a by-pass (or anti-surge) valve that connects the inlet and outlet of the compressor when it approaches the surge limit. This by-pass valve was inserted into the 1D engine model, and the tip-in with the best torque response of the six cases in Figure 5.7 was re-simulated. The anti-surge valve was opened in this simulation when the compressor operating point exceeded the surge line, which was experimentally measured under steady-state non-pulsating flow conditions. Figure 5.8 illustrates the compressor operating path (a), engine torque (b), AMF through the

throttle and intake ports (c), and EGR rate at the intake ports (d) during two tip-in simulations: the case with a PAT valve opening delay of 2 cycles and with a transient EGR valve closure, formerly presented in Figure 5.7, and the same case but with compressor surge mitigation.

The flow recirculated through the by-pass valve gives rise to a negative mass flow rate in the throttle, slightly penalizing the torque increase. This was compensated by further closing the EGR valve, as seen in the time evolution of the EGR rate in the case with no surge in Figure 5.8**d**. After these simulations, it is concluded that combining the downstream PAT and EGR reduction strategies leads to a torque response time of 0.31 seconds.

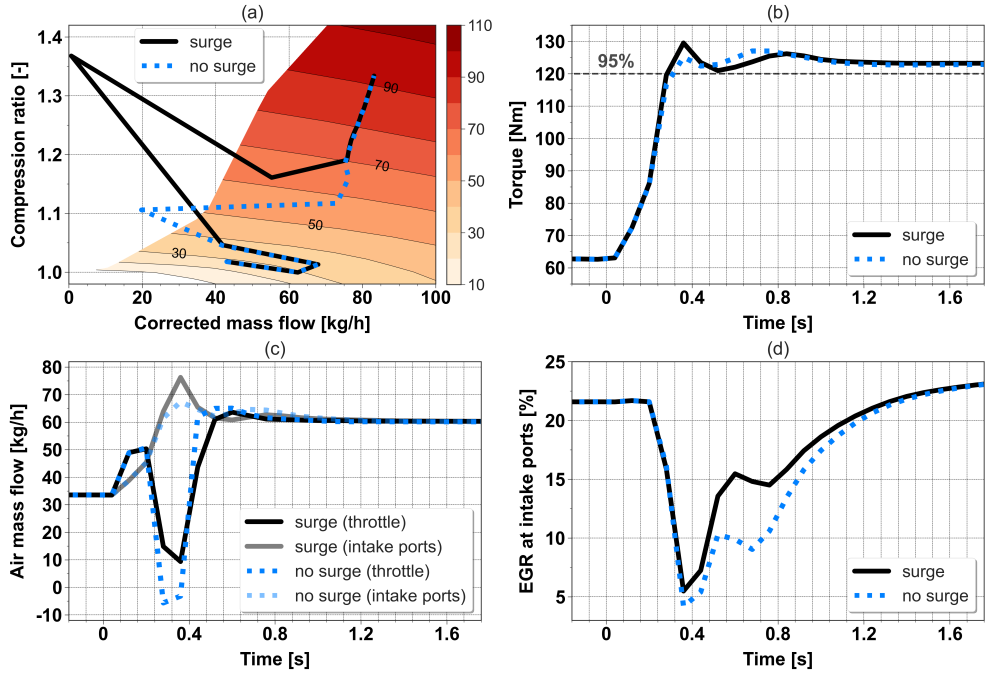

Figure 5.8: Predicted compressor operating path (a), engine torque (b), AMF through the throttle and intake ports (c), and EGR rate at the intake ports (d) during the best tip-in with the downstream PAT strategy with (dotted blue line) and without (solid black line) compressor surge mitigation. In the top-left plot (a), the corrected compressor speed values are given in the vertical colorbar in kRPM.

5.2.4.2 Upstream PAT

As with the downstream tank, tip-in simulations were carried out with the upstream PAT to optimize the opening of its valve (DN30). Due to the larger distance between the tank and cylinders, the fastest torque response is achieved by opening the PAT valve with no delay (simultaneously with the throttle). It should be stated that closing the EGR valve is not needed to avoid the torque drop after the tank emptying. The EGR dilution is reduced using the PAT even when depressurized, given that it is connected to the compressor inlet pipe where the pressure is slightly lower than the ambient. In relation to this, it should be reminded that the tank was equipped with an anti-vacuum valve, as explained in Section 3.3.

Figure 5.9 shows the time evolution of the AMF through the PAT valve (a) and intake ports (b), EGR rate at the intake ports (c), and engine torque (d) in the two following tip-in simulations: the best case with the downstream PAT without surge (labeled "Case B"), previously presented in Figure 5.8; and the best solution with the upstream PAT ("Case C") by opening the tank valve simultaneously with the throttle and keeping the EGR valve open. As noticed in Figure 5.9**a**, the tank valve opening in Case C is extended until the turbocharger provides the desired boost pressure, thus maintaining the EGR dilution below 20% during the first 1.3 s. Concerning the engine torque, the response time in Case C is around 0.43 s, 0.12 s slower than in Case B with the downstream tank.

5.2.5 Electric supercharger

A tip-in simulation was performed with the electric supercharger, which was actuated simultaneously with the throttle opening. The output power of the electric motor was regulated using a proportional controller to reach and maintain the intake manifold pressure target (1.3 bar). The peak power consumed by the electric supercharger (e-supercharger) was around 90% of its maximum capacity. The rest of the valve actuations were the same as in the baseline tip-in, so the valve positions were linearly changed in two engine cycles, and the EGR valve was kept open throughout the simulation. In addition, as in the tip-in simulations with the PAT, the ANN was used to estimate the Wiebe function parameters, and a constant air-to-fuel ratio equal to the stoichiometric was imposed.

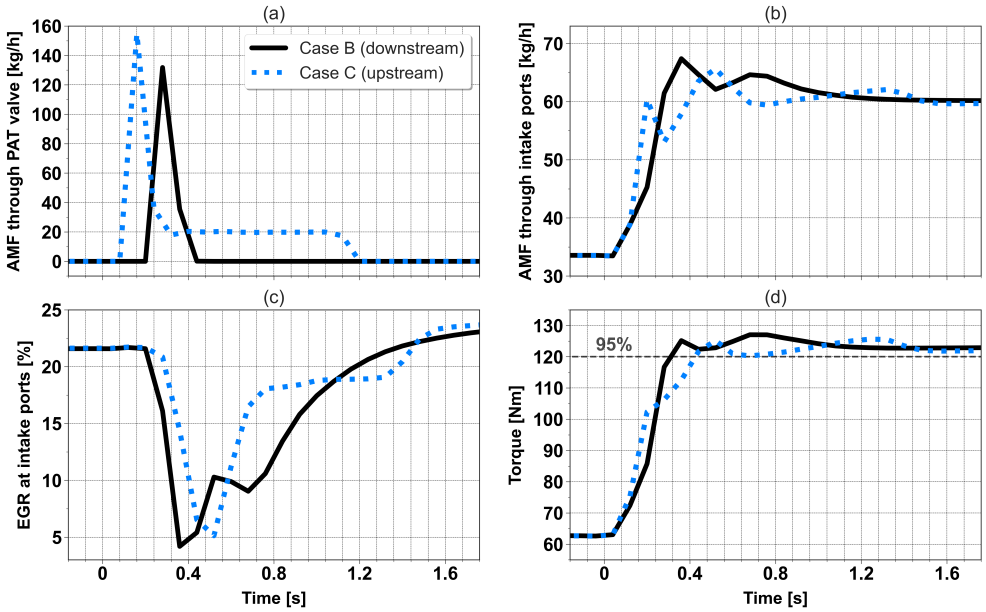

Figure 5.9: Modeled AMF through the PAT valve (a) and intake ports (b), EGR rate at the intake ports (c), and engine torque (d) during the "Case B" and "Case C" tip-in simulations.

Figure 5.10 illustrates the e-supercharger operating path (a), e-supercharger speed (b), intake manifold pressure (c), and engine torque (d) during the tip-in simulation with the electric supercharger (labeled "Case D"). The e-supercharger reached 48.000 rpm in 0.25 s, providing a maximum pressure ratio of 1.2. This resulted in a fast pressure increase in the intake manifold without the need to decrease the EGR dilution. Regarding the engine torque, it is concluded that the electric supercharger leads to a response time of 0.41 seconds.

5.2.6 Comparison of the solutions

This subsection provides a combined analysis of all the air management strategies, mostly based on the torque response and fuel economy. Other criteria, such as complexity and material costs, are also evaluated. To ensure a fair comparison, the EGR valve actuation in Case A was adjusted via modeling to remove the torque overshoot noticed in Figure 5.4**d**. The torque overshoot

was avoided by combining an EGR valve closure of 4 engine cycles (instead of 7) with a reopening slope of 35 units per second (instead of 40). The tip-in simulation with the adjusted EGR valve actuation was labeled "Case A+". In the interest of readability, Table 5.1 summarizes the main characteristics of the four solutions investigated in this study: EGR reduction (Case A+), downstream PAT with EGR reduction (Case B), upstream PAT (Case C), and electric supercharger (Case D).

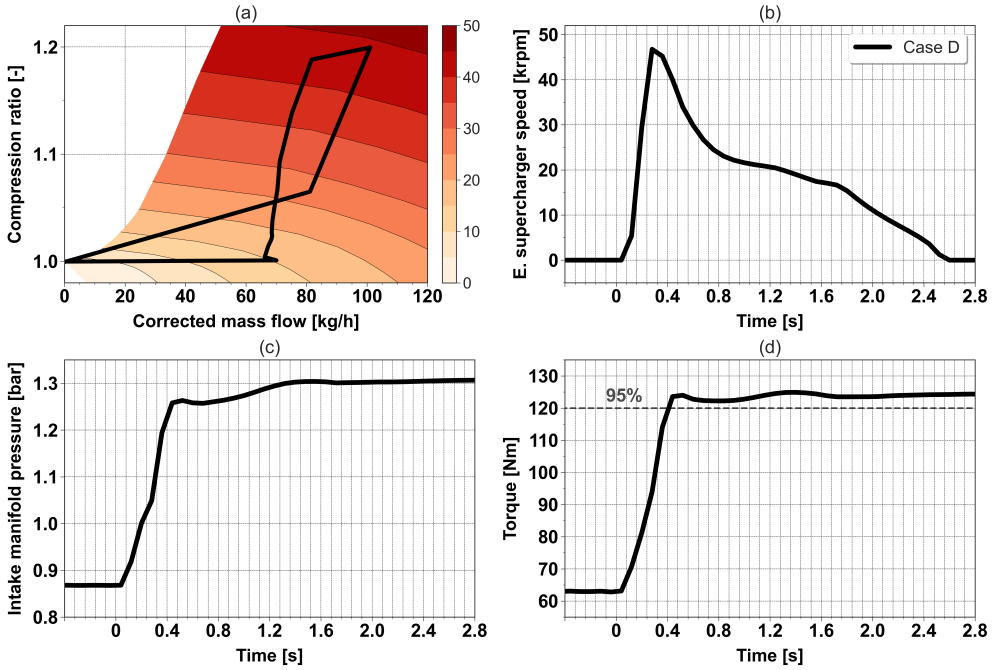

Figure 5.10: Electric supercharger operating path (a) and speed (b), intake manifold pressure (c), and engine torque (d) during the "Case D" tip-in simulation. In the top-left plot (a), the corrected e-supercharger speed values are given in the vertical colorbar in kRPM.

Figure 5.11 shows the time evolution of the modeled AMF through the intake ports (a), EGR rate at intake ports (b), engine torque (c), and corrected BSFC (d) in Cases A+, B, C, and D. The experimental torque values during the "target" and "baseline" tip-ins are also provided in Figure 5.11**c**. The corrected BSFC, calculated using Equation 5.1, includes a fuel penalty to take

into account the power delivered by the auxiliary boosting system (PAT or electric supercharger).

$$BSFC^*(j) = \frac{\dot{m}_f(j) + \overline{BSFC} \cdot \dot{W}_{sys}(j)}{\dot{W}_{eng}(j)} \tag{5.1}$$

where $BSFC^*(j)$ is the corrected BSFC in the engine cycle j, $\dot{m}_f$ the fuel mass flow rate (g/h), and $\dot{W}_{eng}$ the engine power (kW). The constant term $\overline{BSFC}$ refers to the average BSFC (290 g/kWh) of the SI engine working in the conventional SUV presented in Section 3.4 during the WLTP driving cycle (Figure 4.13). The power supplied by the auxiliary boosting system ($\dot{W}_{sys}$) is calculated using Equation 5.2:

$$\dot{W}_{sys}(j) = \begin{cases} V_{tank} \cdot \dfrac{p_{tank}(j-1) - p_{tank}(j)}{T_C}, \text{if } sys \text{ is the tank} \\ \\ \dot{W}_{e-s}(j), \text{if } sys \text{ is the electric supercharger} \end{cases} \tag{5.2}$$

where V_{tank} is the tank volume, p_{tank} the tank pressure, and T_C the duration of one engine cycle at 1500 rpm (0.08 s). The term $\dot{W}_{e-s}$ is the output power of the supercharger electric motor.

Figure 5.12 shows the average of the corrected BSFC (average $BSFC^*$) in the first 20 cycles (1.6 s) versus the torque response time for Cases A+, B, C, and D. A period of 20 cycles is selected for the average $BSFC^*$ because, after that time, the engine operating conditions (speed, load, and EGR) are practically stable in the four cases (Figure 5.11). The average $BSFC^*$ is estimated applying Equation 5.3:

$$average\ BSFC^* = \frac{\sum_{j=1}^{20}\left(\dot{m}_f(j) + \overline{BSFC} \cdot \dot{W}_{sys}(j)\right)}{\sum_{j=1}^{20} \dot{W}_{eng}(j)} \tag{5.3}$$

Table 5.1: Main characteristics of the four air management solutions used to improve the engine torque response during tip-in maneuvers: Case A+, B, C, and D. (+) The EGR valve actuation in Case A was corrected to prevent torque overshoot.

Case	**Strategy**	**EGR valve**	**Description**
A+	EGR reduction	Closed	The EGR valve is closed quickly, kept closed for 4 cycles, and reopened slowly in 35 cycles.
B	Downstream PAT combined with EGR reduction	Partially closed	A 2-L tank with air at 3 bar is linked to the intake manifold, and the tank valve is opened 2 cycles after the throttle opening. The EGR valve is closed until the 17% opening, kept in this position for 4 cycles, and reopened in 20 cycles. And the compressor by-pass valve is opened for a very short time.
C	Upstream PAT	Open	A 2-L tank with air at 3 bar is connected to the compressor inlet volume, and the tank valve is opened without any delay regarding the throttle opening.
D	Electric supercharger	Open	An electric supercharger is installed downstream of the compressor in series.

The EGR reduction strategy (Case A+) is the simplest and leads to an acceptable torque response time of 0.57 seconds with no additional equipment. By contrast, implementing this strategy is not easy. The EGR valve and spark plug actuations must be adapted according to the operating conditions of each tip-in maneuver to prevent torque overshoot and to ensure stable combustion. The best response time (0.31 s) is achieved with the downstream PAT (Case B), even being a bit better than in the target tip-in without EGR (Figure 5.11**c**). However, using the downstream PAT strategy involves higher fuel consumption (Figure 5.12), an added expense in materials, and a remarkable increase in complexity:

- Different initial tank pressure values may be demanded depending on the operating conditions.

- A tank filling procedure is required.
- If the PAT capacity is not enlarged, the downstream PAT must be combined with the EGR reduction strategy to avoid the torque drop once the PAT becomes empty.
- A dedicated PAT valve actuation is also required.
- The air flow from the downstream PAT blocks the intake path, leading to compressor surge.

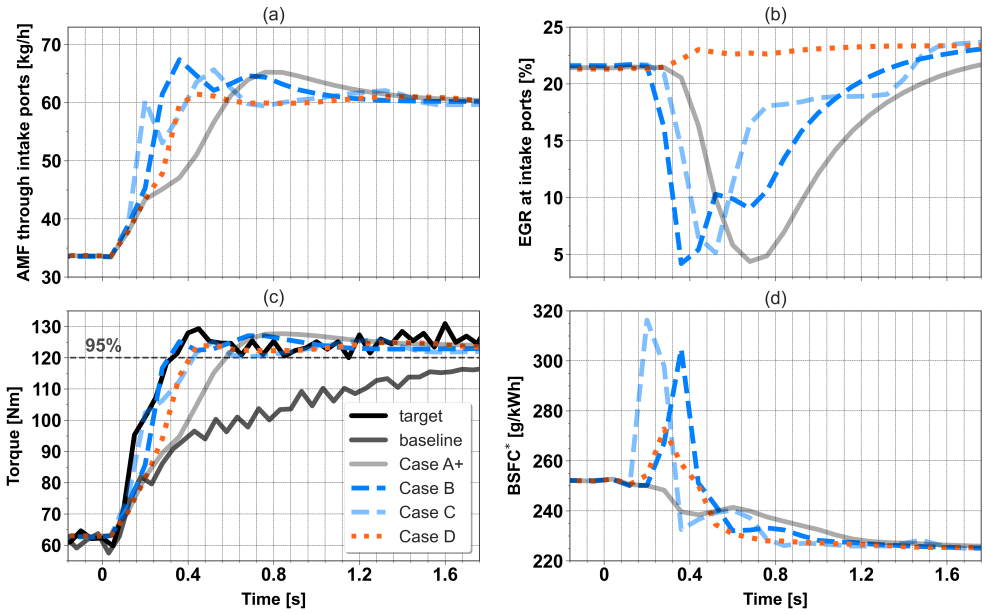

Figure 5.11: Time evolution of the following modeled variables in Cases A+, B, C, and D: AMF through the intake ports (a), EGR rate at intake ports (b), engine torque (c), and corrected BSFC (d). The experimental torque evolution in the "target" and "baseline" tip-ins is also included.

The upstream PAT solution (Case C) is a bit simpler, given that closing the EGR valve is not necessary and that the compressor is not blocked during the maneuver. It must be reminded that the EGR dilution in Case C is reduced using the tank itself thanks to its location. Nevertheless, the torque response with the upstream PAT is slower than with the downstream tank

(Figure 5.11**c**). In addition, installing the tank upstream of the compressor requires utilizing check valves to avoid reverse flow through the intake flap and EGR valve.

With the electric supercharger, a torque response time of 0.41 s is achieved while keeping the EGR rate over 22% (Figure 5.11**b**). High EGR operation throughout the tip-in makes a difference in fuel economy, causing the BSFC in Case D to be 1.6% lower than in Case B if considering the first 20 cycles (Figure 5.12). Concerning the BSFC evolution in Figure 5.11**d**, it should be noted that the peaks noticed in Cases B, C, and D before 0.4 s are because of two reasons: the short-circuit of a portion of the intake gases and, mainly, the fuel penalty related to the added boosting systems. It should also be stated that using the e-supercharger only requires the management of the electric motor to obtain the desired boost pressure, so the increase in complexity is minor.

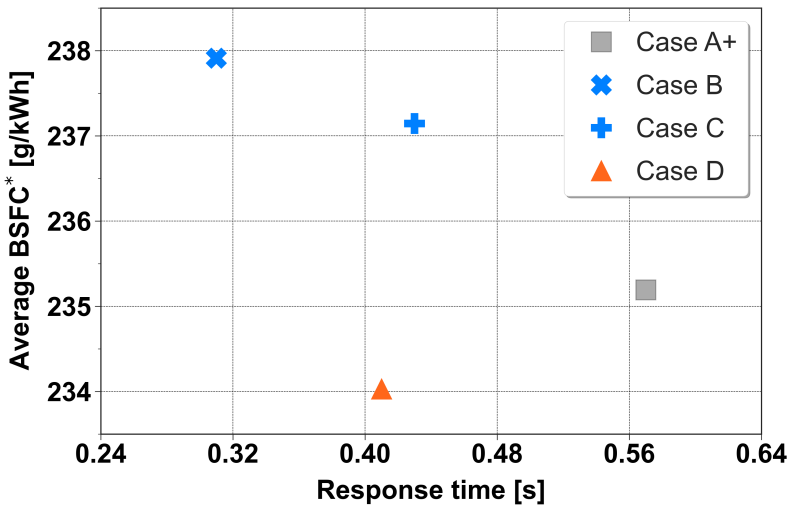

Figure 5.12: Average of the corrected BSFC in the first 20 cycles (1.6 s) versus torque response time for Cases A+, B, C, and D.

In summary, the EGR reduction strategy is the simplest solution and improves torque response notably regarding the baseline case. The best response time is achieved with the downstream PAT, but at the expense of a significant increase in complexity, costs, and fuel. And the electric supercharger system provides a good trade-off between fuel economy and torque response.

5.3 Engine response in tip-out maneuvers

In this section, three alternative solutions to fuel injection cutoff are investigated to avoid combustion instabilities during tip-out maneuvers under high EGR conditions. The three solutions are the following: optimizing the throttle actuation (based on delaying the throttle closure regarding the pedal demand), installing a secondary air-path which bypasses the main intake path (Figure 3.1), and connecting a small tank of pressurized air (as the one studied in the previous section, but with a different size) to the intake manifold. The idea behind applying these strategies is to reduce the EGR dilution as fast as possible, once the load reduction is demanded, without negatively affecting torque response.

To this end, tip-out maneuvers at 1500 rpm from 6 to 0.7 bar BMEP were tested and simulated. The potential of combining the two first strategies (delayed throttle closure and SAP) to improve combustion stability was analyzed with both experimental and modeling data. Separately, the third strategy (PAT) was only researched by simulation. The three air management solutions were evaluated based on two variables: the tip-out duration (related to engine response) and the number of misfire events (combustion stability).

A tip-out at 1500 rpm from 6 to 0.7 bar BMEP was selected due to the relevance of this maneuver for conventional cars during the WLTP driving cycle. Firstly, the gasoline engine operates at around 1500 rpm between 0 and 7 bar BMEP during one third of the WLTP cycle; and secondly, over 100 similar maneuvers to the chosen one were identified throughout the said cycle. The latter can be checked in Figure 5.13, which depicts the load-decrease maneuvers, at quasi-constant engine speed, whose initial operating point is close to 6 bar BMEP at 1500 rpm during the WLTP driving cycle shown in Figure 4.2. The size and color of the arrows in Figure 5.13 are related to the time derivative of the engine BMEP: values lower than 2 bar/s in black, lower than 4 bar/s in blue, and higher than 4 bar/s in red. Besides, it should be noted that 0.7 bar BMEP is the load provided by the engine when the pedal demand is zero at 1500 rpm.

Regarding the engine calibration at the initial tip-out operating point, fuel economy can be maximized using two combinations of EGR and VVT settings (as stated in Section 4.3): either minimum valve overlap and 28% EGR or a valve overlap of 60 CAD and 22% EGR. The former is chosen for

this study because, through it, the amount of exhaust gases accumulated along the intake path, from the EGR valve to the intake valves, is higher. This fact causes the maneuver to be more challenging. At the final tip-out point, the engine operates with no EGR.

The tip-out tests and simulations are presented in the next four subsections: (5.3.1) combustion stability issue, (5.3.2) validation of the transient model performance, (5.3.3) delayed throttle closure (DTC) and SAP strategies, and (5.3.4) pressurized air tank.

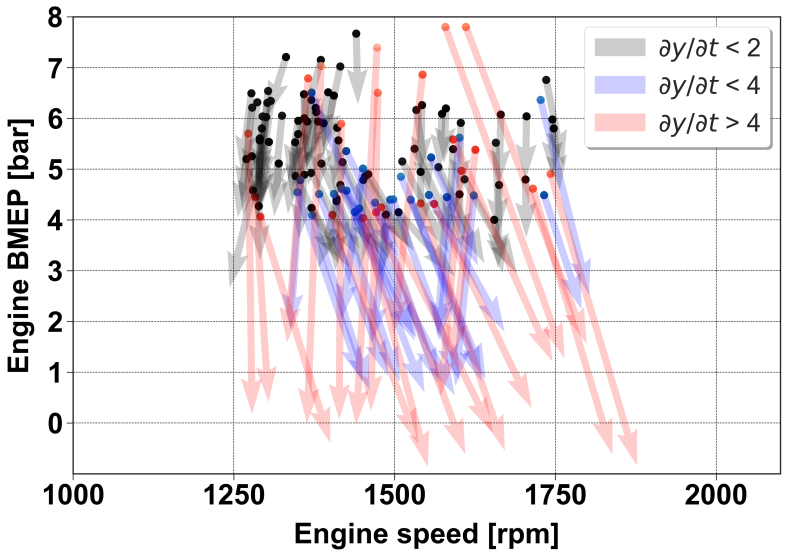

Figure 5.13: Load-decrease maneuvers at quasi-constant engine speed whose initial operating point is close to 6 bar BMEP at 1500 rpm during the WLTP driving cycle shown in Figure 4.2.

5.3.1 Combustion stability issue

A tip-out maneuver (labeled "baseline") was tested to assess combustion stability when using the default throttle actuation from the original ECU. In this tip-out, the SAP system valve was kept closed. Figure 5.14 illustrates the time evolution of the throttle (a), spark advance (a), EGR valve (b) and intake flap (b) setpoints in the baseline tip-out. The throttle closure was demanded with a ramp-down of one engine cycle (0.08 seconds at 1500 rpm), while the

EGR valve closing and intake flap opening were requested by means of 2-cycle ramps. The optimum spark advance is 34 CAD (before top dead center) at the initial tip-out point, to ensure stable combustion with 28% EGR, and 5 CAD at the final point, to prevent an excessive temperature decrease in the TWC. In order not to facilitate the occurrence of misfires, a slow linear transition of 20 cycles between both spark advance values was defined. Regarding the VVT system, it was configured to provide the minimum valve overlap throughout the maneuver.

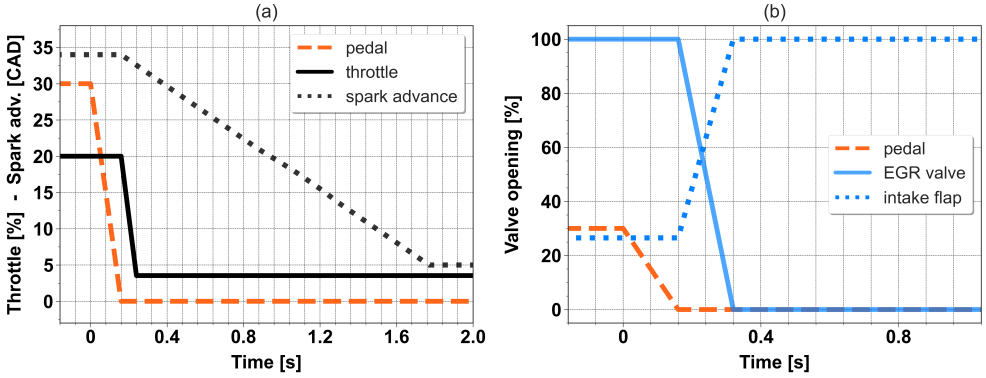

Figure 5.14: Setpoints of the throttle (a), spark advance (a), EGR valve (b) and intake flap (b) during the baseline tip-out.

Figure 5.15 provides the time evolution of the BMEP (a), IMEP (b), fuel-to-air equivalence ratio or ϕ (c), and CO and CO_2 volume fractions at the turbine outlet (d) in the baseline tip-out test. Figure 5.15**a** also includes the ideal load reduction, and Figure 5.15**b** shows the IMEP of all cylinders. From 0.4 to 0.8 s, the IMEP takes values equal to or lower than 0 bar for some engine cycles because of misfiring. This phenomenon is observed in the BMEP evolution as well. The variation of the raw CO and CO_2 emissions can be another indicator of the occurrence of misfires. Focusing on Figure 5.15**d**, firstly, a global maximum and a local minimum in the evolution of the CO and CO_2 emissions, respectively, are found at around 0.4 s. The appearance of these extrema is due to the combination of rich conditions (owing to a not accurate estimation of the air trapped into the cylinders by ECU) and combustion instabilities. Later, between 0.4 and 0.8 s, the bulk of misfire events lead to a second CO_2 reduction, but no impact on the CO concentration is noticed. The most probable explanation to this is an increase in HC and O_2

emissions. After all these results, it is confirmed that using the default throttle actuation (from the original ECU) gives rise to the occurrence of misfires.

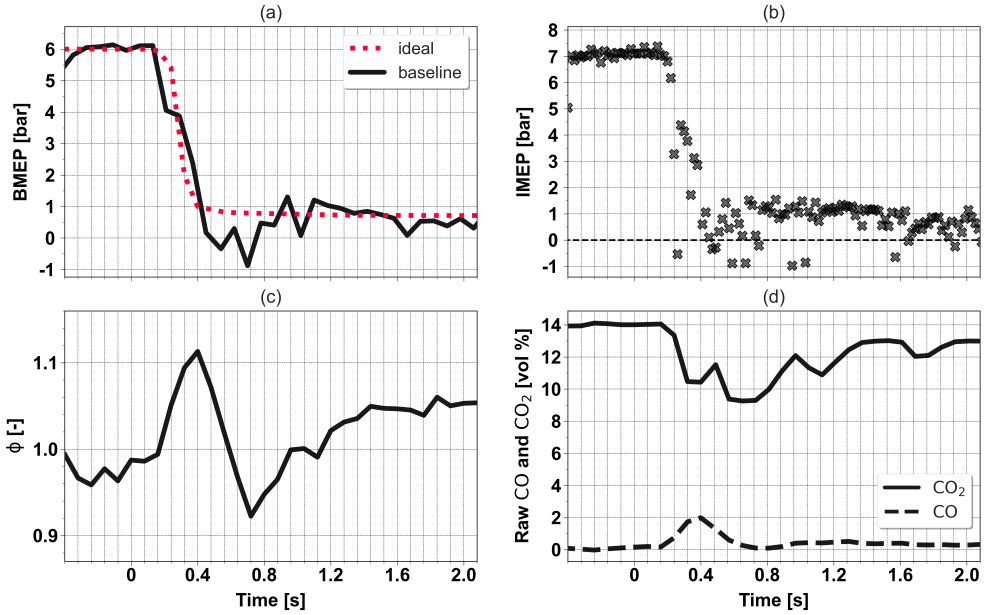

Figure 5.15: Time evolution of the BMEP (a), IMEP of the four cylinders (b), fuel-to-air equivalence ratio (c), and CO and CO_2 volume fractions at the turbine outlet (d) in the baseline tip-out test.

5.3.2 Validation of the transient 1D model response

In order to validate the 1D engine model performance under these particular transient operating conditions, three tip-outs were performed in the engine test bench using the SAP system. In these tip-outs, three throttle closure delays (2, 4 and 6 cycles regarding the pedal demand) were tested, the SAP valve was opened 20% for 6 cycles with no delay, and the fuel injection was shut off to assess how the EGR gases are evacuated from the intake path. Regarding the EGR valve, intake flap, spark advance, and VVT settings, the same actuations as in the baseline tip-out were utilized. It should be remarked that the fuel cutoff strategy was only used for the model validation. In the rest of the tip-out tests presented in Section 5.3, the fuel injection was controlled by the ECU. Figure 5.16 illustrates the throttle and SAP valve setpoints (a)

and the ϕ measurements (b) during the three tip-outs tested for the model validation.

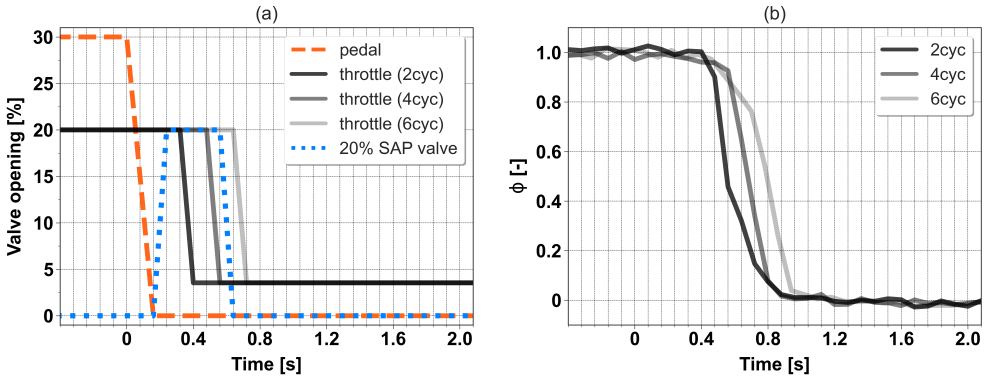

Figure 5.16: Setpoints of the throttle and SAP valve (a) and ϕ measurements (b) during the three tip-out tests used for the model validation. In the legend, the delay between the throttle closure and pedal demand is specified in the parentheses.

The three tip-out tests were replicated with the 1D model using the experimental valve actuations. Besides, the ϕ measurements were given to the model as a input, and the Wiebe function parameters were predicted by means of the ANN. Figure 5.17 provides the experimental and modeled values of the following variables during the three tip-outs with fuel cutoff used for the model validation: intake manifold pressure (a), total AMF (b), CO_2 volume fraction at the turbine outlet (c), and AMF through the SAP valve (d). The evolution of the intake manifold pressure, raw CO_2 concentration and secondary AMF is reproduced with no remarkable errors. Some slightly higher differences are found if comparing the actual and predicted values of total AMF, mainly between 0.4 and 0.8 s. These differences could simply be explained by the low-frequency sampling (20 Hz) of this variable in the test rig. In any case, in view of the results shown in Figure 5.17, it can again be affirmed that the 1D model reproduces the gas exchange process with high accuracy.

5.3.3 Delayed throttle closure and secondary air path

A parametric study was performed to calibrate the delayed throttle closure (DTC) and secondary air path (SAP) strategies. The parametric study con-

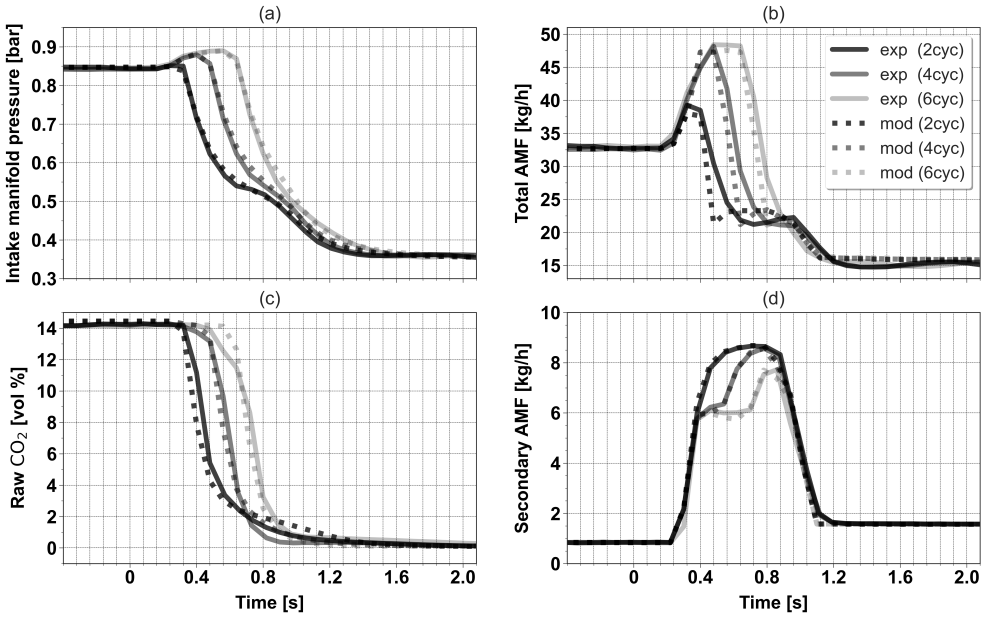

Figure 5.17: Actual and predicted values of intake manifold pressure (a), total AMF (b), raw CO_2 concentration (c), and secondary AMF (d) during the three tip-outs with fuel cutoff used for the model validation. In the legend, the first term is related to the data source (experimental or modeled), and the second (in parentheses) shows the throttle closure delay in cycles.

sists of 24 tests and simulations, in which four throttle closure delays (0, 2, 4, and 6 cycles) and five SAP valve opening percentages (0, 10, 15, 20, 25%) were investigated. A SAP valve opening time of 6 cycles was considered for all the cases, except for the tip-outs with 20% SAP valve opening, in which an opening time of 12 cycles was tried as well. It was found this opening time led to a excessive tip-out duration, so it was excluded for the rest of opening percentages. It should also be noted that testing shorter opening times than 6 cycles was not possible with the valve technology and control systems available in the engine test bench. Table 5.2 presents the different combinations of these three parameters (throttle closure delay, and SAP valve opening percentage and time) studied in this section.

Figure 5.18 shows the setpoints of the throttle and SAP valve for the following 12 tip-outs: the four cases only with the DTC strategy (SAP valve closed), and the eight cases combining the four throttle closure delays with

the best two SAP valve opening values (15 and 20%). The rest of the valve actuations used to test and simulate these tip-outs are the same as the ones for the baseline, shown in Figure 5.14. It should be remarked that the EGR valve, in all cases, was closed in 2 cycles without any delay, once the pedal demand is zero. Besides, in the 1D model, a constant ϕ equal to 1 was used, and the combustion process was simulated using the ANN. Figure 5.19 and Figure 5.20 provides the predicted values of the next variables during the 12 tip-outs mentioned above: EGR rate at the intake ports (5.19**a**), secondary AMF (5.19**b**), in-cylinder residual gas fraction 5.20**a**, and in-cylinder trapped air mass (5.20**b**). In both figures, a color gradient is utilized to distinguish the four throttle closure delays, while the type of line is related to the SAP valve opening: 0% (solid line), 15% (dashed line), and 20% (dotted line).

Table 5.2: All tip-out tests and simulations performed by combining the DTC and SAP strategies.

Number of cases	**SAP valve opening percentage (%)**	**SAP valve opening time (cycles)**	**Throttle closure delay (cycles)**	**Fuel cutoff**
4	0	0	0*, 2, 4, and 6	No
4	10	6	0, 2, 4, and 6	No
4	15	6	0, 2, 4, and 6	No
11 (**3**)	20	**6** and 12	0, **2**, **4**, and **6**	**Yes**/No
4	25	6	0, 2, 4, and 6	No

The baseline is marked with an asterisk (*), while the three cases used for the model validation are marked in bold.

Starting with the cases without SAP, it is found that delaying the throttle closure by 4 or more engine cycles leads to a faster evacuation of the EGR gases (Figure 5.19**a**); given that the intake manifold pressure and, consequently, the total mass trapped into the cylinders do not change until the throttle is closed. Regarding the cases with SAP, two facts are remarkable. On the one hand, during the first 0.6 seconds, the EGR rate into the cylinders is lower in the cases where the throttle closing is delayed by 0 and 2 cycles. This is because the AMF through the SAP is higher once the throttle is closed (Figure 5.19**b**), as a result of a larger pressure difference across the SAP valve. On the other hand, from 0.6 s, the remaining amount of EGR gases in the intake line is

smaller in the tip-outs with throttle closure delays of 4 and 6 cycles, due to a higher EGR evacuation at the maneuver beginning, before closing the throttle (as in the cases without SAP). In addition, comparing the pairs of analogous cases with 15 and 20% SAP valve opening, it is observed that a slightly faster EGR reduction is achieved with 20% opening, mainly in the first half of the tip-out.

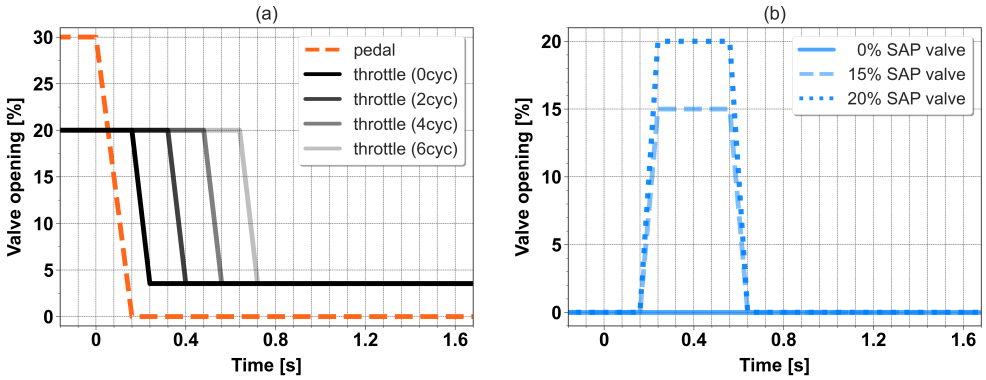

Figure 5.18: Setpoints of the throttle and SAP valve for the 12 tip-outs in which SAP valve openings of 0, 15, and 20% are combined with throttle closure delays of 0, 2, 4, and 6 cycles.

The influence of the DTC and SAP strategies on the EGR evacuation from the intake path is also reflected in the time evolution of the in-cylinder residual gas fraction (RGF). It should be stated that the RGF is calculated as the ratio between the in-cylinder trapped mass of burned gases (including external EGR) and the in-cylinder total trapped mass, both at the combustion start. In general, combining the two strategies leads to a faster reduction in RGF. The effect of SAP is predominant for the first cycles, while the opposite is observed in the final part of the maneuver (Figure 5.20**a**). Besides, a RGF peak is noticed at around 0.6 s in the cases without SAP and with a throttle closure delay of 0 and 2 cycles. These peaks are due to the abrupt pressure reduction at the intake manifold (once the throttle is closed), which causes backflows through the intake valves, even though the valve overlap is minimum, and a slow evacuation of the EGR gases. Delaying the throttle by 4 cycles is enough to avoid the RGF peaks.

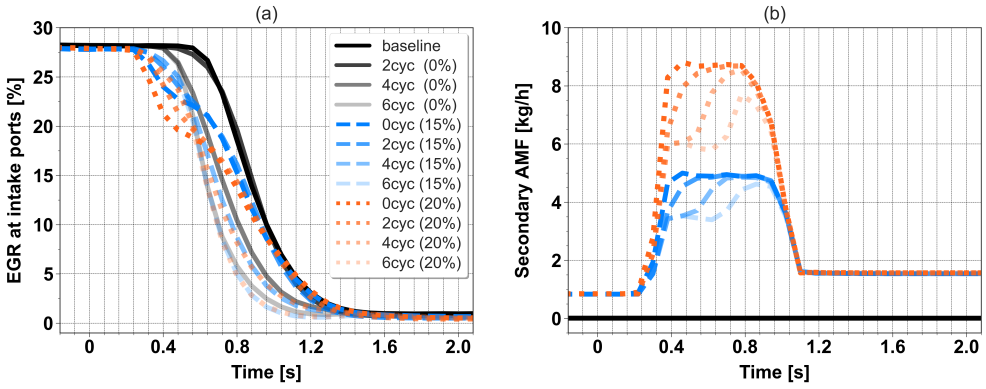

Figure 5.19: Predicted EGR rate at the intake ports (a) and secondary AMF (b) during the 12 tip-outs presented in Figure 5.18. In the legend, the first term is the throttle closure delay, and the second is the SAP valve opening percentage.

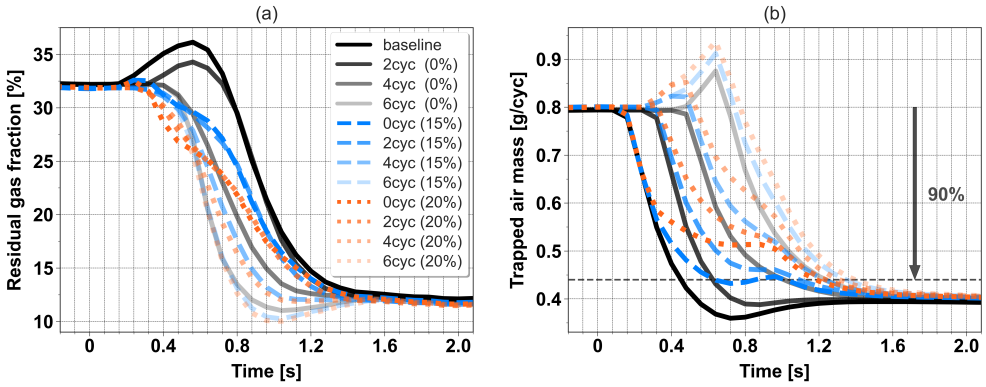

Figure 5.20: Predicted (in-cylinder) residual gas fraction (a) and trapped air mass (b) during the 12 tip-outs presented in Figure 5.18. In the legend, the first term is the throttle closure delay, and the second is the SAP valve opening percentage.

As a clear drawback, the DTC strategy induces a delay in the engine load reduction, as reflected in the evolution of the in-cylinder trapped air mass (TAM) in Figure 5.20**b**. The decrease in TAM is even slower when the SAP strategy is used as well. By taking as reference the time spent in the baseline tip-out to complete the 90% of the total TAM reduction (from 0.8 to 0.4 g/cycle), the maneuver duration is extended for a minimum of 2 cycles with 15% SAP valve opening and a minimum of 9 cycles with 20% opening. In

addition, when delaying the throttle closure by 6 cycles with and without SAP, an increase in TAM of between 10% and 18%, regarding the initial TAM value (0.8 g/cycle), is observed at around 0.6 s. Another interesting point is that no difference in TAM between the baseline and the two cases with no delay and SAP is found until 2 cycles after the throttle closing, given that the supply of fresh air by the SAP is not immediate. This can be checked if comparing the curves of secondary AMF (Figure 5.19**b**) and SAP valve setpoint (Figure 5.18**b**).

In conclusion, it seems clear that delaying the throttle closure avoids a peak of residual gases at the tip-out start and decreases the EGR dilution faster, and even faster when the DTC strategy is combined with SAP. However, both strategies also lead to a slower TAM reduction. Therefore, it can be concluded that a trade-off between a more stable combustion and better engine torque response is expected from the experiments, whose results are presented below.

The experimental analysis of combustion stability and torque response is focused on the six cases where throttle closure delays of 0, 2, and 4 cycles are combined with SAP valve openings of 0% and 15% SAP. Figure 5.21 shows the IMEP values of the four cylinders (a, b) and the CO and CO_2 volume fractions at the turbine outlet (c, d) during these six tip-out tests. Figure 5.22 provides the time evolution of the experimental BMEP (a) and ϕ (b) in the same six cases.

Firstly, focusing on the tip-outs without SAP, it can be affirmed that delaying the throttle closure by 4 cycles leads to much better combustion stability. A significant amount of misfire events (IMEP values very close to zero or negative in Figure 5.21**a**) is found in the cases in which the throttle closing is not delayed or only delayed by 2 cycles; by contrast, the number of misfires is notably lower when delaying throttle closure by 4 cycles. This combustion stability improvement is also reflected in the BMEP evolution in Figure 5.22**a** (solid black lines), but it is not enough to achieve a 100% stable torque decrease. The evolution of the raw CO and CO_2 concentrations is very similar in the three tests without SAP, as seen in Figure 5.21**c**. After 0.4 s, an increase in CO emissions and a reduction in CO_2 are observed mainly because of rich mixture operation. Then, the CO peaks disappear, and the CO_2 emissions are secondly decreased due to the occurrence of misfires. This second reduction in CO_2 also happens in the case with a 4-cycle delay, although it is probably caused by operating under lean mixture conditions (Figure 5.22**b**).

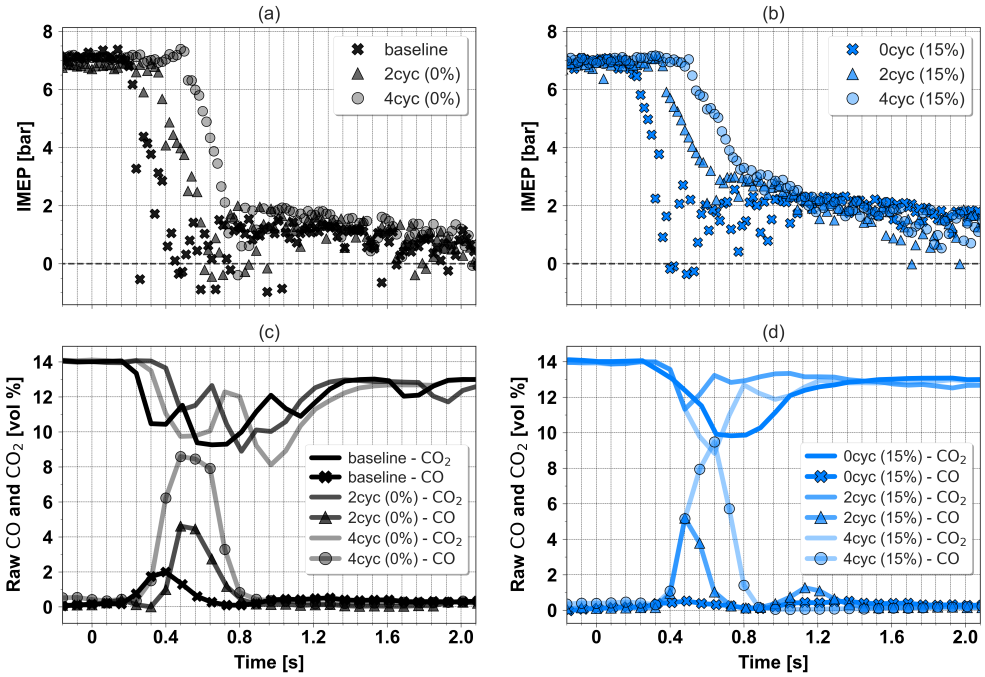

Figure 5.21: IMEP values of the four cylinders (a, b) and the CO and CO_2 volume fractions at the turbine outlet (c, d) during the six tip-out tests selected to show the real effect of the DTC and SAP strategies on combustion stability and torque response.

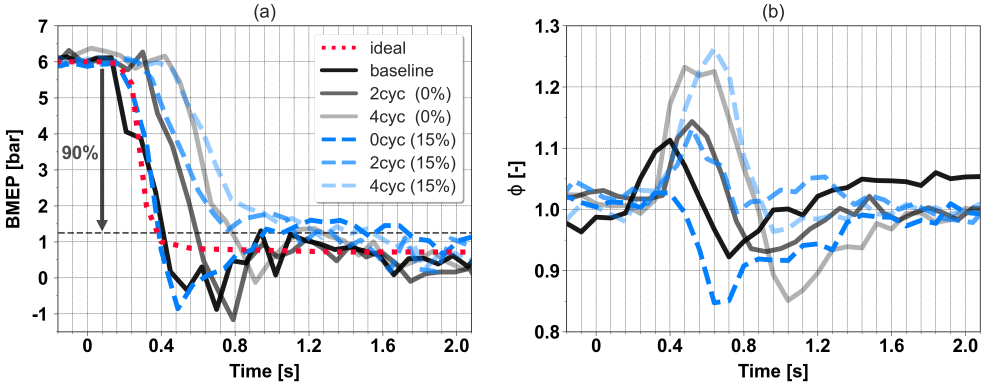

Figure 5.22: Experimental BMEP (a) and ϕ (b) during the same six tip-outs presented in Figure 5.21.

Regarding the tests with 15% SAP valve opening, it seems clear that using the SAP system improves combustion stability. Nevertheless, this strategy by itself is not enough to achieve a 100% stable load decrease. As explained before, the supply of fresh air through the SAP is not immediate, so the RGF reduction is not either, causing some misfires in the case without DTC in Figure 5.21**b**. No misfire is found in the other two cases, in which the DTC and SAP strategies are combined. The absence of misfires in these two tip-out tests is also perceived in the evolution of the CO_2 volume fraction. A reduction in CO_2 emissions is observed between 0.4 and 0.6 s, but it is caused by the lack of oxygen under rich mixture conditions (Figure 5.22**b**).

As a summary, Figure 5.23 shows the tip-out duration (x-axis), calculated as the time required to complete the 90% of the total BMEP reduction (from 6 to 0.7 bar) once the pedal demand reaches zero, and the numbers of misfires (y-axis) for the 12 cases presented in Figure 5.18. A misfire event was considered as such if the IMEP is equal to or lower than zero. The following four conclusions can be drawn from all these results:

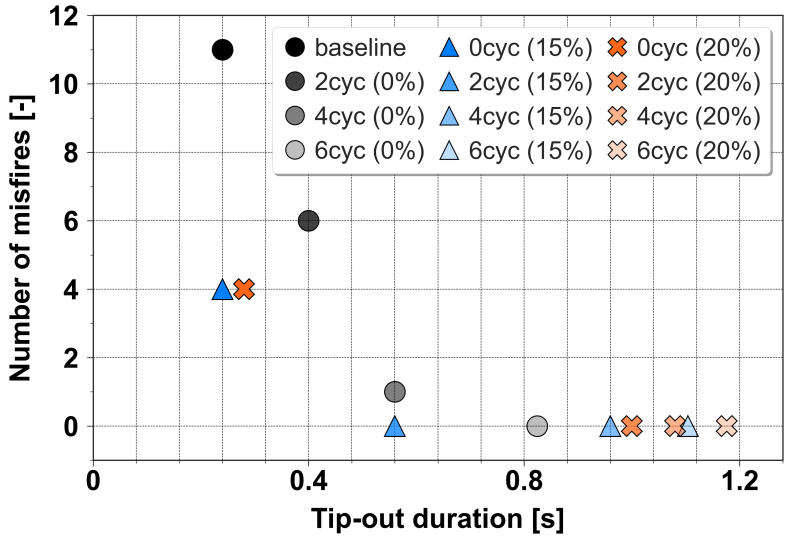

Figure 5.23: Number of misfire events versus duration of the maneuver for the 12 tip-outs presented in Figure 5.18.

- A trade-off between combustion stability and torque response must be faced, as predicted via modeling.

- Delaying the throttle closure by 4 cycles with no SAP is a practical solution that remarkably improves combustion stability (only one misfire event) without increasing costs and complexity. As a disadvantage, the tip-out duration is increased proportionally to the throttle closure delay (Figure 5.23).
- Using the SAP system is effective in enhancing combustion stability. This strategy by itself, without DTC, does not affect the tip-out duration but cannot completely prevent misfiring.
- The combination of the DTC and SAP strategies can lead to a 100% stable load decrease. The fastest torque reduction without misfiring was achieved with a throttle closure delay of 2 engine cycles and with a SAP valve opening of 15% (for 6 cycles). In this particular case, the maneuver duration is 0.56 s, 0.32 s (4 cycles) longer than in the baseline.

5.3.4 Pressurized air tank (PAT)

The potential of the PAT strategy to enhance combustion stability during tip-outs is assessed via 1D modeling in this subsection. The first step is the tank design, which is based on providing a similar amount of air to the one introduced through the SAP in the case with a throttle closure delay of 2 cycles and a SAP valve opening of 15%. In this particular tip-out, the area under the secondary AMF curve (Figure 5.19**b**) is equal to 1.5 g. To introduce this amount using the PAT, a 1-L tank of fresh air, initially at 20°C and 1.3 bar, is sufficient if opening the PAT valve by 15% for 6 cycles. The PAT valve used for this study has the same diameter as the SAP valve (DN20). Besides, it should be reminded that the tank was equipped with an anti-vacuum valve to not operate below the ambient pressure.

Four tip-out simulations were performed with the PAT strategy, in which two initial tank pressure values (1.3 and 1.8 bar) were combined with two throttle closure delays (0 and 2 cycles). The second pressure value equal to 1.8 bar was tried to increase the initial secondary AMF and, consequently, to reduce the EGR dilution more quickly in the first cycles. Before analyzing the results of these simulations, it must also be remarked that: the tank filling procedure is not be addressed in the present thesis; and there is no difference between the PAT and SAP valve actuations (same opening percentage, duration and timing) to ensure a fair comparison of both strategies.

Figure 5.24 illustrates the predicted values of EGR rate at the intake ports (a) and secondary AMF (b) during eight tip-outs: the four cases with PAT, mentioned above, and other four, formerly presented in Subsection **5.3.3**, with the most interesting combinations of the DTC and SAP strategies. Figure 5.25 shows the time evolution of the in-cylinder RGF (a) and TAM (b) in the same eight tip-out simulations. In the legend of both figures, the first term is the throttle closure delay, and the second one refers to the SAP valve opening percentage or the initial tank pressure.

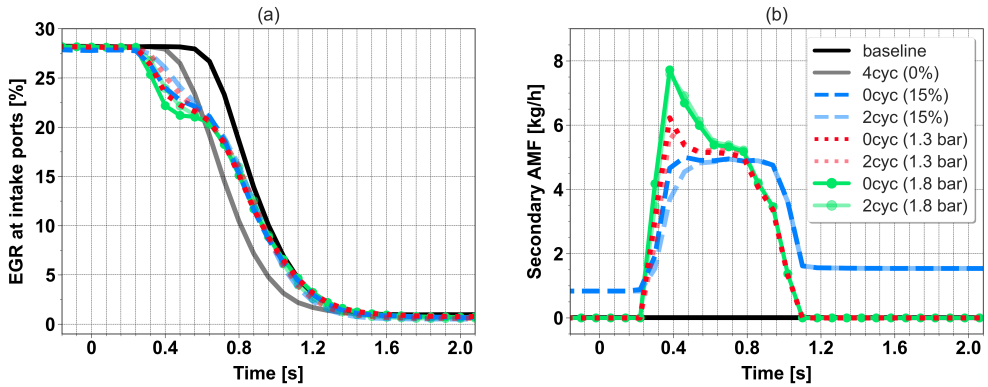

Figure 5.24: Predicted EGR rate at the intake ports (a) and secondary AMF (b) during the tip-outs used for the evaluation of the PAT strategy.

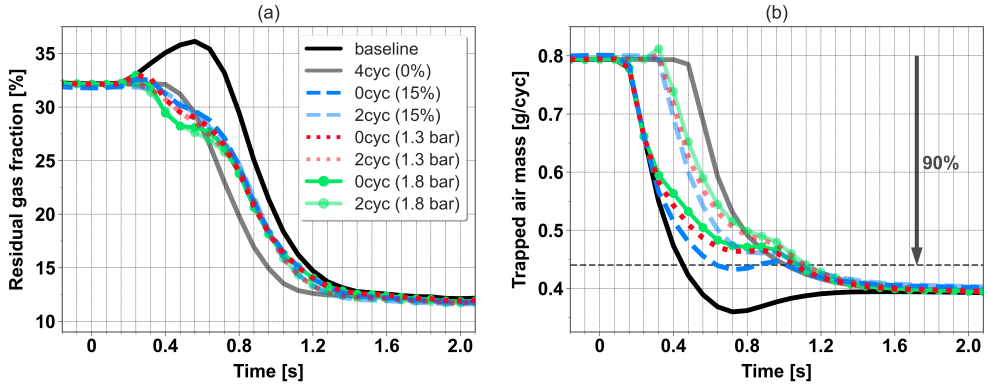

Figure 5.25: Predicted in-cylinder RGF (a) and TAM (b) during the tip-outs used for the evaluation of the PAT strategy.

The SAP and PAT systems introduce a similar amount of air throughout the tip-out but with a different time distribution: in the cases with SAP, the secondary AMF is almost constant during the whole valve opening; in contrast, in the cases with PAT, a first peak is noticed at around 0.4 s, and then the secondary AMF decreases as the tank empties (Figure 5.24**b**). Therefore, it can be affirmed that the addition of air through the PAT in the first cycles is larger and faster than through the SAP system, and even larger and faster as the initial tank pressure is increased. This is reflected in the evolution of the EGR rate and in-cylinder RGF. Both are reduced a bit more quickly, between 0.2 and 0.7 s, using the PAT. From 0.7 s, no differences in RGF between the cases with SAP and PAT are observed (Figure 5.25**a**).

Considering the above, it is concluded that combining the PAT strategy (1 liter and 1.3 bar) with a throttle closure delay of 2 cycles leads to a 100% stable load decrease without any misfire; given that this solution provides similar results in RGF and TAM to the ones obtained in the analogous case with a SAP valve opening of 15% (Figure 5.25). Nevertheless, the TAM decrease with PAT is slightly slower than with SAP (comparing the cases with the same throttle closure delay), so the engine torque response will also be.

Focusing on the tip-out with no throttle closure delay and a initial tank pressure of 1.8 bar (opaque green solid line in Figure 5.25), the values of in-cylinder RGF and TAM are respectively 3% lower and 12% higher, at around 0.48 s, than in the equivalent case with SAP (opaque blue dashed line). An increase in TAM (closely related to the engine load) leads to a better EGR dilution tolerance, so the PAT doubly decreases the probability of misfiring in the first cycles, compared to SAP. In view of these last results, it is concluded that the PAT system offers a potential solution to avoid misfires without delaying the load decrease. Anyway, it should not be forgotten that the PAT is a more complex technology than SAP. Implementing the PAT strategy would require defining a tank filling procedure, calibrating the initial tank pressure according to the operating conditions, and using an anti-vacuum valve.

5.4 Compressor surge in tip-out maneuvers

This section presents a study on compressor surge control in gasoline engines operating with EGR during aggressive tip-outs. To avoid surge in deceleration or load-decrease maneuvers, automotive turbochargers are usually equipped with an anti-surge valve (ASV), which can connect the compressor inlet and outlet to rapidly decrease the compression ratio. The objective of this study is to determine if it is feasible to remove the ASV, in the interest of reducing the turbocharger cost, without affecting compressor stability and torque response. For that purpose, two alternative strategies are investigated: optimizing the throttle closure and reducing the compressor inlet pressure. The latter can be applied, without any additional equipment, just using the intake flap (located upstream of the EGR joint).

A series of tip-outs at 1500 rpm from full to zero load were tested to research the strategies mentioned. This particular maneuver was selected because the surge margin at the initial operating conditions is minimal, so the surge tendency is very high, especially at the tip-out start. The optimum EGR rates at the initial and final working points are 5% and 0%, respectively. Regarding the surge detection, a criterion based on the analysis of the crank-angle resolved pressure signal at the compressor outlet was utilized. Using the theoretical surge line, obtained from tests in the turbocharger test rig, was rejected, given that the surge margin can significantly change under transient flow conditions.

The results of the tip-outs tests are presented in two subsections: (5.4.2) throttle closure optimization and (5.4.3) reduction of the compressor inlet pressure. Before that, the criterion used for surge detection is defined in Subsection 5.4.1.

5.4.1 Surge detection

The turbocharger was formerly tested in a gas stand according to the method described in [110], after which the compressor surge line was determined. However, this limit is not reliable once the turbocharger is coupled to the engine; given that, as explained in **Chapter 2**, surge appearance is affected by the piping geometry around the compressor [61], the engine pulsation [62], and the flow transience [63]. Instead, the compressor outlet pressure (p_2) signal,

acquired with a sampling period of 0.2 crank-angle degrees (45 kHz at 1500 rpm), was used to detect surge. The procedure followed for surge detection is explained below.

The characteristic frequency of surge is generally below 30 Hz [121], while the engine firing frequency with four cylinders at 1500 rpm is 50 Hz. Hence, to identify surge with no interference from engine pulses, the p_2 signals were processed by means of a 5^{th} order low-pass Butterworth filter [122] with a cut-off frequency (f_C) of 30 Hz. In addition, the moving average of p_2 was obtained using the same low-pass filter but with an f_C of 5 Hz, in order to eliminate the oscillations caused by the surge. The difference between the pressure filtered with an f_C of 30 Hz ($\widetilde{p_2}$) and the moving average pressure ($\overline{p_2}$) was selected as the surge indicator. For the sake of brevity, the difference between $\widetilde{p_2}$ and $\overline{p_2}$ is represented by the term $\widetilde{\overline{p_2}}$. Using this variable, the following criterion was defined for surge detection: an oscillation in the $\widetilde{\overline{p_2}}$ signal is considered a surge event if the amplitude of this oscillation is higher than 10 mbar [64, 121].

5.4.2 Throttle closure optimization

The throttle closure was optimized to decrease the engine load as fast as possible without causing compressor surge. To this end, the throttle actuation was divided into five linear transitions, and the time to complete each transition was varied to find the surge limit. Figure 5.26 shows the throttle actuation in the 20 tip-outs tested for its optimization. In all cases, the compressor ASV was disconnected, and the throttle was automatically closed from 100% (fully open) to 67% opening in just one cycle (0.08 s); given that, in this opening range, the engine intake flow is slightly modified. For each of the other four transitions, between 67, 50, 33, 17, and 5% opening (minimum value to compensate friction losses), five transition durations (1, 3, 5, 7, and 9 cycles) were tested, as seen in Figure 5.26.

Regarding the rest of valves, the VVT system was configured to provide a constant valve overlap period of 40 CAD throughout the maneuver, and the VGT mechanism was fully opened in 2 cycles from its full-load position simultaneously with the throttle closure. The EGR valve was closed from 15 to 0% opening, also in 2 cycles, and the intake flap was kept 100% open. Besides, the spark timing actuation was designed to avoid knocking and misfiring.

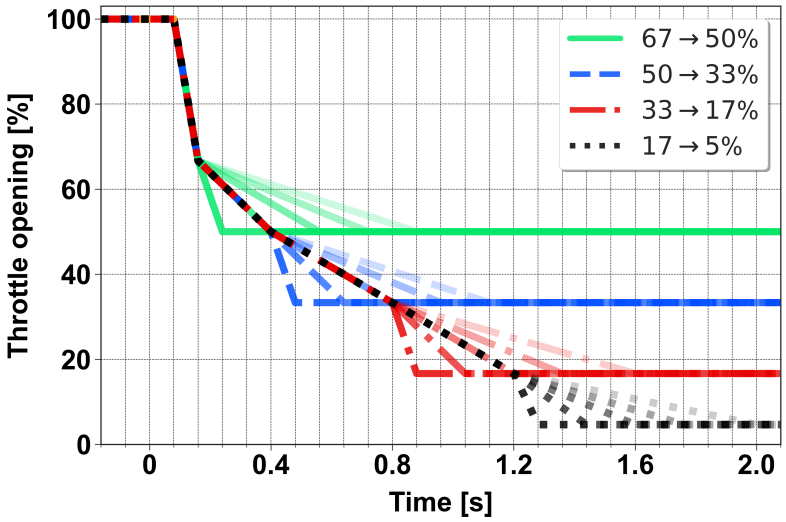

Figure 5.26: Throttle closure optimization.

For each of the four transitions optimized, Figure 5.27 provides the time evolution of the $\widetilde{p_2}$ and $\widetilde{\widetilde{p_2}}$ signals in the following two cases: in descending order of transition duration, the first case where surge is detected (solid red line) and the preceding one (dashed black line). The latter is the optimum case. According to the criterion defined in Subsection **5.4.1** for surge detection, the duration of each transition cannot be lower than 3 (from 67 to 50%), 5 (50 to 33%), 5 (33 to 17%), and 3 (17 to 5%) cycles, respectively. Thus, the total duration of the fastest "surge-free" throttle actuation is 17 engine cycles (around 1.4 s), including the 1-cycle ramp between 100% and 67% opening.

After optimizing the throttle actuation, other two tests were performed: a tip-out with the ASV activated, labeled "Case E", in which the throttle was closed in 2 cycles; and another with the ASV disconnected, labeled "Case F", where the throttle actuation was designed to obtain the closest compressor operating path to the theoretical surge line. The tip-out with the throttle closure optimized according to the criterion defined in Subsection **5.4.1** was labeled "Case G". Figure 5.28 provides the throttle actuation (a) and compressor operating path (b) in the three tip-outs mentioned: Case E, F and G. And Figure 5.29 shows the time evolution of the compressor outlet pressure (a), air mass flow at the filter outlet (b), turbocharger speed (c), and engine load (d) in Case E, F, and G.

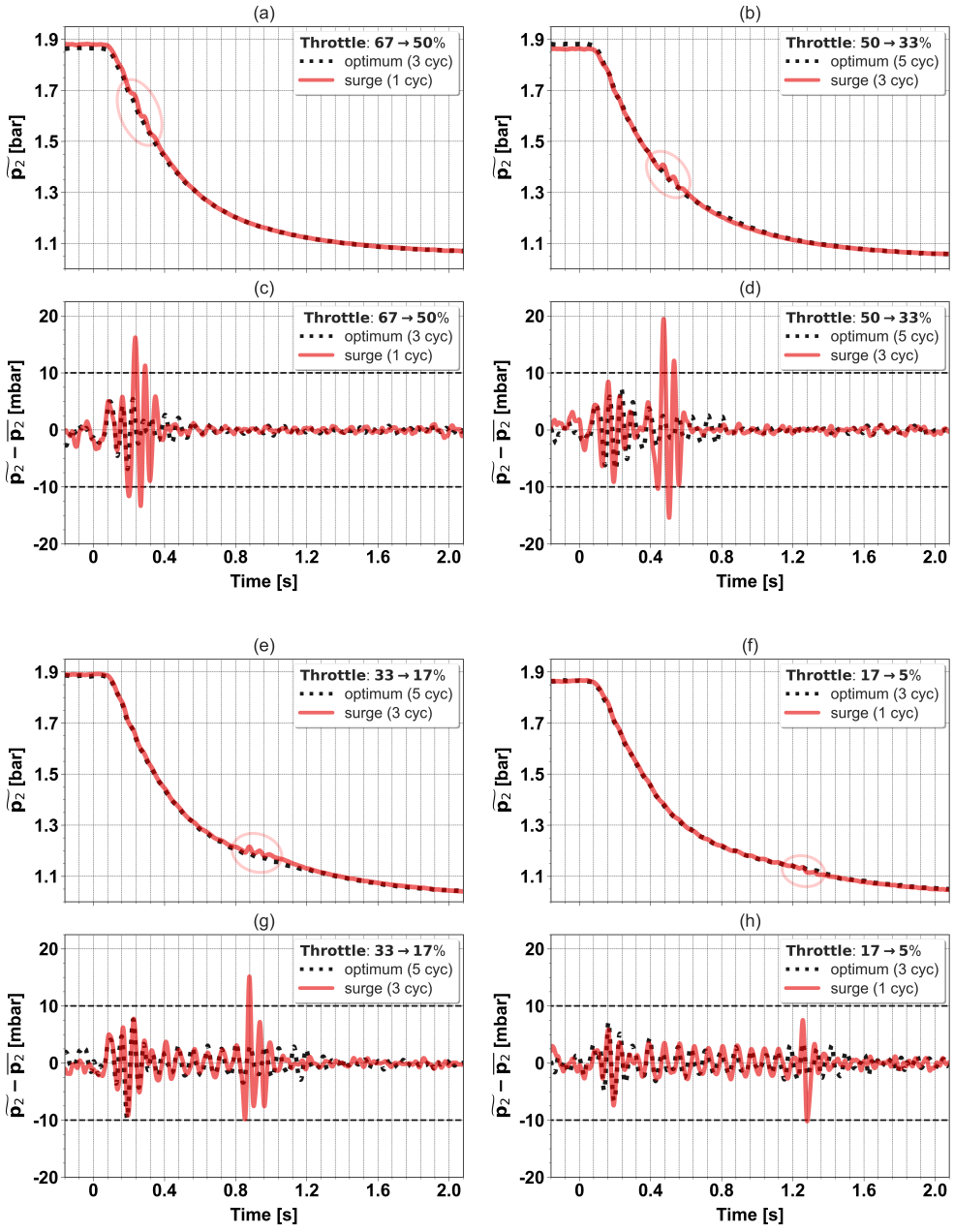

Figure 5.27: Time evolution of the $\widetilde{p_2}$ and $\widetilde{\overline{p_2}}$ signals in eight of the twenty tip-outs tested for the throttle closure optimization. In the legend of every plot, the transition under study is specified in bold letters, and the transition duration of each case is shown in parentheses.

To obtain Figure 5.28**b**, 5.30**b** and 5.30**d** (the last two will be presented later), the mass flow (MF) of gases through the compressor was calculated as explained below. Firstly, the instantaneous EGR rate was estimated by means of Equation 3.1 by utilizing the intake CO_2 measurements registered with the Cambustion NDIR500 device and, besides, by assuming that the volume fraction of CO_2 at the exhaust line was constant and equal to around 14% (Figure 5.17). Then, the compressor MF was determined using the values of AMF, measured at the filter outlet, and the estimated EGR rate.

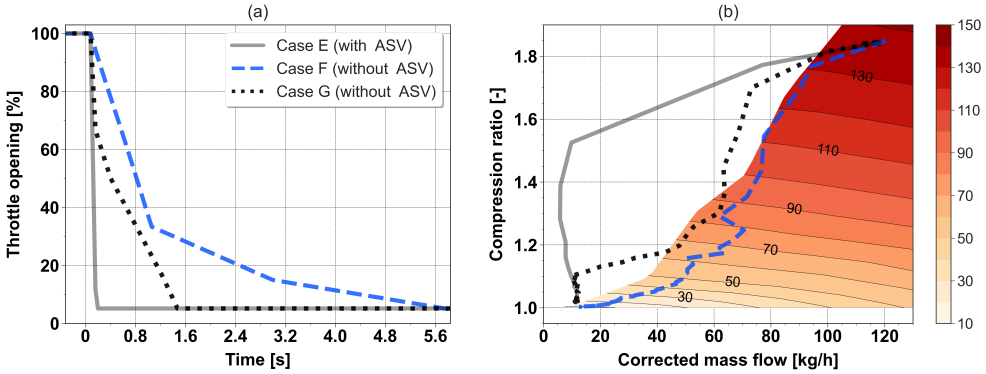

Figure 5.28: Throttle actuation (a) and compressor operating path (b) during three tip-outs: Case E (solid gray line), Case F (dashed blue), and Case G (dotted black). In the right plot, the corrected compressor speed values are given in the vertical colorbar in kRPM.

The compressor operating path in Case G is clearly located at the left side of the surge line, except for compression ratios between 1.2 and 1.4, as seen in Figure 5.28**b**. Therefore, it is confirmed that the surge line (used as the surge limit in Case F) determined by testing a turbocharger in a gas stand is not a reliable limit. Regarding Case E, it is observed that the throttle reaches its minimum opening (5%) in 0.16 s, 1.2 and 5.4 s earlier than in Case G and F, respectively. These significant differences are also reflected in the evolution of the AMF and engine load. In particular, the torque response time in Case G is around 1 s slower than in Case E (Figure 5.29**d**), if considering the time required to reach an engine load of 10% in each case. In view of these results, it is concluded that compressor surge can be avoided without the ASV by adjusting the throttle closure, but in return for a 1 s slower torque response.

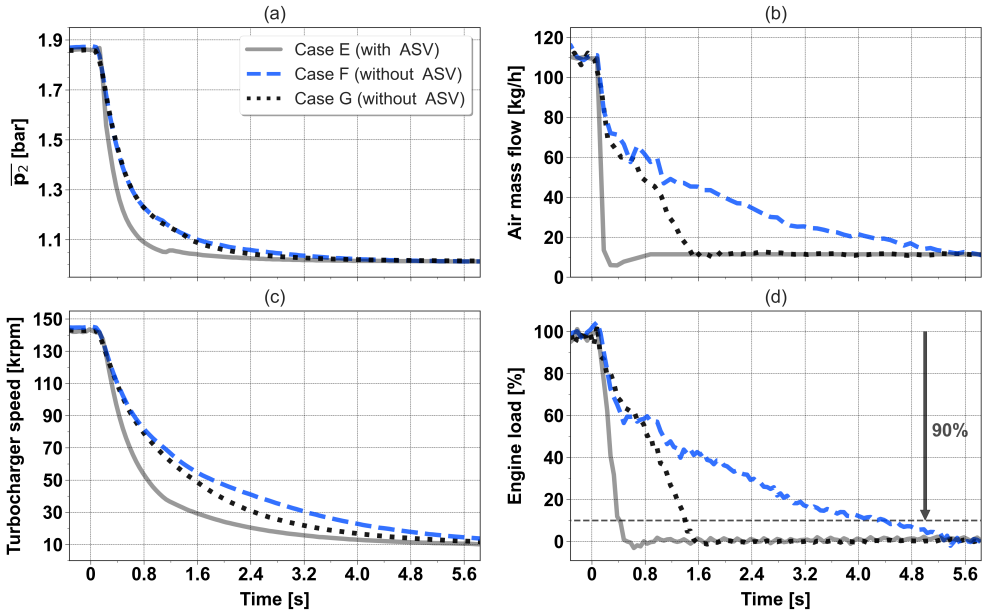

Figure 5.29: Time evolution of the compressor outlet pressure (a), AMF at the filter outlet (b), turbocharger speed (c), and engine load (d) in Case E, F, and G.

5.4.3 Reduction of the compressor inlet pressure

Reducing the compressor inlet pressure (p_1) increases the corrected mass flow and, consequently, the surge margin, given that the compressor operating point is moved to the right. Therefore, the p_1 reduction strategy can lead to a faster load decrease than the one obtained in Case G (Figure 5.29). This strategy can be applied without additional equipment and costs, given that the intake flap, located upstream the EGR joint, can be used to reduce p_1.

A tip-out, labeled "Case H", was tested using the same throttle actuation as in Case G, but now the intake flap was closed from 100 to 6% opening in two engine cycles, instead of keeping it open throughout the maneuver. Figure 5.30 shows the values of p_1 and p_2 (a), the compressor mass flow along with its corrected values (b), the turbocharger speed (c), and the compressor operating path (d) during the "Case G" and "Case H" tip-out tests, both with the ASV disconnected.

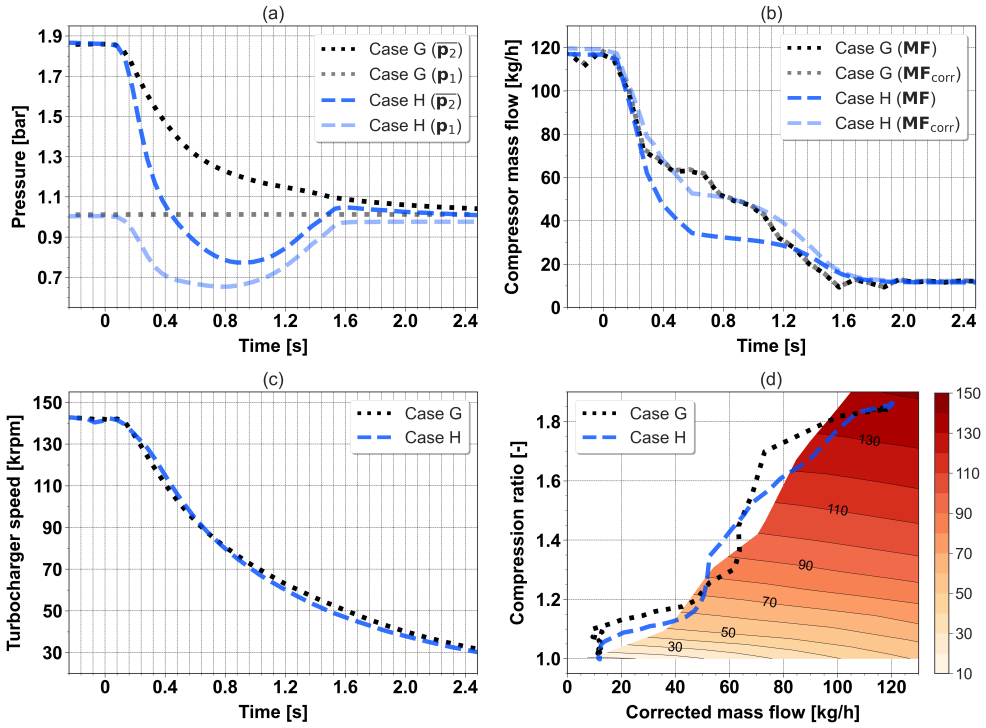

Figure 5.30: Compressor inlet and outlet pressure (a), compressor mass flow (b), turbocharger speed (c), and compressor operating path (d) during Case G and H. In the top-right plot, the corrected values of MF are also provided. And in the bottom-right plot, the corrected compressor speed values are given in the colorbar in kRPM.

As observed in Figure 5.30**a**, p_1 is decreased to a minimum value of 0.65 bar at around 0.8 s in Case H, then it is recovered as the engine intake flow is reduced. It should be noted that the intake flap is not reopened during the tip-out. Even though decreasing p_1 leads to lower compressor MF values in Case H (than in Case G) between 0.2 and 1.2 s, the evolution of the corrected MF is very similar in both cases (Figure 5.30**b**). In fact, if considering the compressor operating path in Case G as the actual surge line, it can be affirmed that there is still a margin to close the throttle faster in Case H at the beginning, before 0.4 s, and at the end, from 1 s.

Once the capability of the p_1 reduction strategy to accelerate torque response was confirmed, three p_1 levels were analyzed (considering its minimum value during the tip-out): 0.87, 0.65, and 0.33 bar. For the first two levels, the

throttle actuation was re-optimized by following a similar procedure to the one described in Figure 5.26. However, this re-optimization is not required for the last p_1 level, given the tip-out can be completed, without varying the throttle position, just by closing the intake flap. Figure 5.31 provides the time evolution of the $\widetilde{p_2}$ and $\widetilde{\widetilde{p_2}}$ signals in the following four tests: in the left plots (a,c), the tip-out with a p_1 level of 0.33 bar (Case I) and Case G; and in the right plots (b,d), two tip-outs with a p_1 level of 0.65 bar, the one with the throttle closure re-optimized (Case J) and another with a more aggressive throttle actuation (with surge), and again Case G. As noticed in Figure 5.31**c**, no surge is detected in Case I.

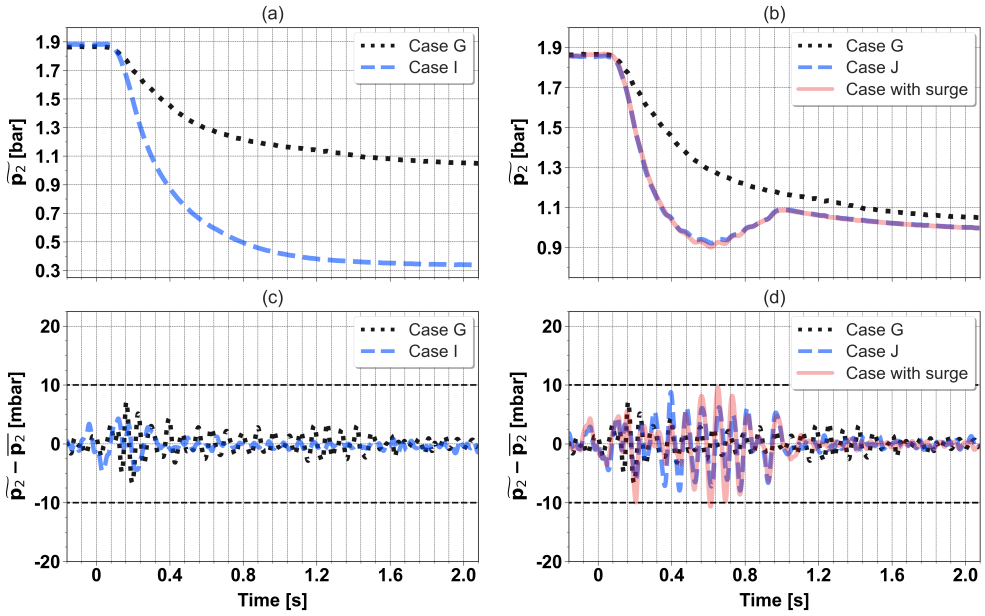

Figure 5.31: Time evolution of the $\widetilde{p_2}$ and $\widetilde{\widetilde{p_2}}$ signals in four tip-out tests: Case G (intake flap open), Case I (p_1 = 0.33 bar), Case J (p_1 = 0.65), an additional case (p_1 = 0.65) with surge.

Two more remarks must be made in relation to the tip-out tests in which the p_1 reduction strategy was used. Firstly, in all these cases, the intake flap was closed as quickly as feasible, generally in two cycles, from 100% opening to its final position (2, 6, and 12% opening, in ascending order of p_1). And secondly, no delay between the start of throttle and intake flap actuations was

applied. For the sake of readability, Table 5.3 provides a summary of the main features of the tip-out tests presented in this section, from Case E to K.

Table 5.3: Summary of the main features of Case E, F, G, H, I, J and K.

Case	**Throttle closure**	**Intake flap**	p_1 **level**	**ASV**
E	in 2 cycles (0.16 s)	fully open	ambient	Yes
F	defined to follow surge line	fully open	ambient	No
G	optimized	fully open	ambient	No
H	same as G	100 to 6% opening in 0.16 s	0.65 bar	No
I	fully open	100 to 2% opening in 0.16 s	0.33 bar	No
J	re-optimized	100 to 6% opening in 0.16 s	0.65 bar	No
K	re-optimized	100 to 12% opening in 0.16 s	0.87 bar	No

Figure 5.32 shows the throttle actuation (a) and the values of p_1 (b) during the following five tip-outs: Case E, G, I, J and K. It should be reminded that the first one was tested with the ASV activated, and the rest without it. Figure 5.33 illustrates the time evolution of the compressor outlet pressure (a), AMF at the filter outlet (b), turbocharger speed (c), and engine load (d) for these five cases.

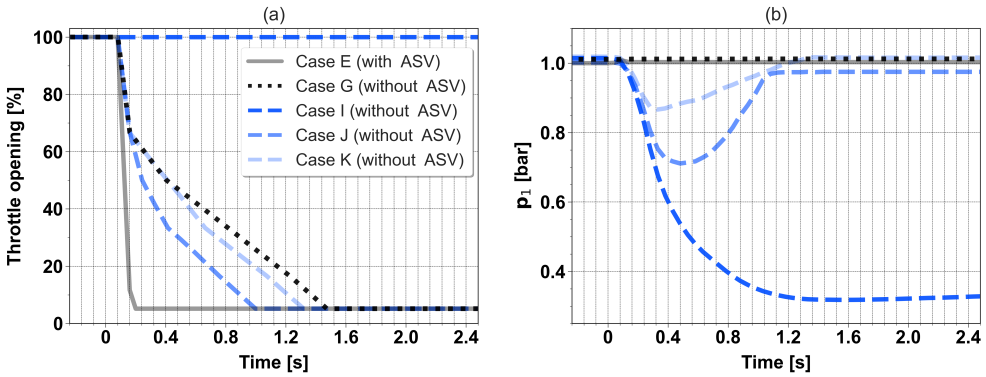

Figure 5.32: Throttle actuation (a) and compressor inlet pressure (b) during the following tip-out tests: Case E, G, I, J and K.

As seen in Figure 5.32**a**, the throttle closure in Case J and K is completed 0.48 and 0.16 s earlier, respectively, than in Case G because of the reduction in p_1. In consequence, the air mass flow and engine load in Case J and K is decreased more quickly. In particular, the torque response time in Case J is improved by around 0.6 s, compared to Case G, if considering the time required to reach an engine load of 10% in each case (Figure 5.33**d**). Besides, it should be remarked that the torque evolution in Case I ($p_1 = 0.33$ bar) is very similar to the one achieved in the reference tip-out (Case E). These results clearly reveal that the role of the anti-surge valve can be assigned to the intake flap without affecting compressor stability and torque response. However, as a potential drawback, such momentary low p_1 levels might cause oil leakages into the compressor; so it would be necessary to study how relevant they are and how to mitigate them before using the p_1 reduction strategy.

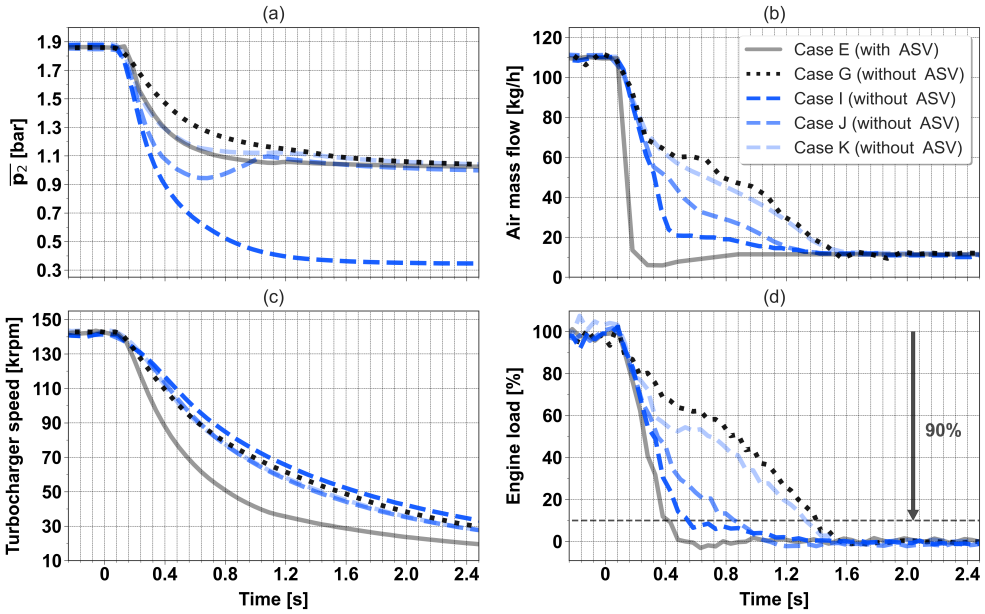

Figure 5.33: Time evolution of the compressor outlet pressure (a), AMF at the filter outlet (b), turbocharger speed (c), and engine load (d) in Case E, G, I, J and K.

Chapter 5 references

[4] J. Galindo, H. Climent, J. de la Morena, D. González-Domínguez, S. Guilain, and T. Besançon. "Compressor Surge Mitigation in Turbocharged Spark-Ignition Engines without an Anti-Surge Control System during Load-Decrease Operation". *Applied Sciences* 12.(3) (2022), p. 1751. DOI: 10.3390/app12031751. URL: https://www.mdpi.com/2076-3417/12/3/1751 (cit. on pp. xii, 89).

[61] A. Engeda, Y. Kim, R. Aungier, and G. Direnzi. "The Inlet Flow Structure of a Centrifugal Compressor Stage and Its Influence on the Compressor Performance". *ASME Journal of Fluids Engineering* 125.(5) (2003), pp. 779–785. DOI: 10.1115/1.1601255 (cit. on pp. 17, 113).

[62] J. Galindo, H. Climent, C. Guardiola, and A. Tiseira. "On the effect of pulsating flow on surge margin of small centrifugal compressors for automotive engines". *Experimental Thermal and Fluid Science* 33.(8) (2009), pp. 1163–1171. DOI: 10.1016/j.expthermflusci.2009.07.006 (cit. on pp. 17, 113).

[63] P. Podevin, A. Danlos, M. Deligant, P. Punov, A. Clenci, and G. De La Bourdonnaye. "Automotive compressor: Effect of an electric throttle in the upstream circuit on the surge limit". In: *MATEC Web of Conferences*. Vol. 234. 2018. DOI: 10.1051/matecconf/201823403006 (cit. on pp. 17, 113).

[64] J. Galindo, J. Serrano, H. Climent, and A. Tiseira. "Experiments and modelling of surge in small centrifugal compressor for automotive engines". *Experimental Thermal and Fluid Science* 32.(3) (2008), pp. 818–826. DOI: 10.1016/j.expthermflusci.2007.10.001 (cit. on pp. 17, 114).

[67] J. Lujan, J. Pastor, H. Climent, and M. Rivas. "Experimental Characterization and Modelling of a Turbocharger Gasoline Engine Compressor By-Pass Valve in Transient Operation". *SAE Technical Paper 2015-24-2524* (2015). DOI: 10.4271/2015-24-2524 (cit. on pp. 17, 89).

[103] K. Shen, Z. Xu, Z. Zhu, and L. Yang. "Combined effects of electric supercharger and LP-EGR on performance of turbocharged engine". *Energy* 244 (2022), p. 123176. DOI: 10.1016/j.energy.2022.123176. URL: https://linkinghub.elsevier.com/retrieve/pii/S0360544222000792 (cit. on pp. 27, 80).

[110] J. R. Serrano, F. J. Arnau, L. M. Garciá-Cuevas, A. Gómez-Vilanova, S. Guilain, and S. Batard. "A methodology for measuring turbocharger adiabatic maps in a gas-stand and its usage for calibrating control oriented and one-dimensional models at early ICE design stages". *ASME Journal of Energy Resources Technology* 143.(4) (2021), p. 042303. DOI: 10.1115/1.4048229 (cit. on pp. 45, 46, 113).

[118] N. Zsiga, C. Voser, C. Onder, and L. Guzzella. "Intake manifold boosting of turbocharged spark-ignited engines". *Energies* 6.(3) (2013), pp. 1746–1763. DOI: 10.3390/en6031746 (cit. on p. 80).

[119] A. Lefebvre and S. Guilain. "Transient response of a turbocharged SI engine with an electrical boost pressure supply". *SAE Technical Paper 2003-01-1844* (2003). DOI: 10.4271/2003-01-1844 (cit. on p. 80).

[120] J. R. Serrano, F. J. Arnau, J. De la Morena, A. Gómez-Vilanova, S. Guilain, and S. Batard. "A Methodology to Calibrate Gas-Dynamic Models of Turbocharged Petrol Engines With Variable Geometry Turbines and With Focus on Dynamics Prediction During Tip-in Load Transient Tests". In: *Proceedings of the ASME Turbo Expo 2020: Turbomachinery Technical Conference and Exposition (Volume 8)*. ASME, 2020. DOI: 10.1115/GT2020-15169. URL: https://asmedigitalcollection.asme.org/GT/proceedings/GT2020/84195/Virtual,Online/1095133 (cit. on p. 84).

[121] J. Galindo, J. Serrano, C. Guardiola, and C. Cervelló. "Surge limit definition in a specific test bench for the characterization of automotive turbochargers". *Experimental Thermal and Fluid Science* 30.(5) (2006), pp. 449–462. DOI: 10.1016/j.expthermflusci.2005.06.002 (cit. on p. 114).

[122] G. Ellis. "Filters in Control Systems". In: *Control System Design Guide*. Elsevier, 2012, pp. 165–183. DOI: 10.1016/B978-0-12-385920-4.00009-6. URL: https://linkinghub.elsevier.com/retrieve/pii/B9780123859204000096 (cit. on p. 114).

Chapter 6

Conclusions and future works

Contents

6.1 Summary and conclusions

Operating with high rates of cooled LP-EGR in SI gasoline engines is a proven strategy to reduce fuel consumption and CO_2 emissions. However, the use of this strategy in current SI engines, generally downsized with direct injection, can also lead to some issues during transient operation, such as poor engine responsiveness or combustion instabilities. Solving these issues is essential for automobile manufacturers, especially since the adoption of new vehicle homologation procedures, in which the number of transient maneuvers is much higher than in the preceding ones.

Knowing the above, two objectives were defined in the present thesis: firstly, analyze the influence of EGR on the performance of advanced gasoline engines during relevant transient maneuvers, and secondly, investigate technical solutions to improve the said performance. In order to achieve these objectives, a Euro-6 1.3L turbocharged DI SI gasoline engine with VVT and VGT technologies was tested and simulated. Engine tests were mainly employed to validate the 1D engine model, which, in turn, was used to assess fluid dynamics and transport phenomena. Engine tests were also utilized to evaluate torque response, combustion stability, and raw exhaust emissions.

Given that the gasoline engine mentioned above was originally designed to operate without EGR, the engine calibration with EGR had to be carried out before anything else. With the aim of reducing the costs and resources related to the experimental activity, a calibration method based on a high number of 1D simulations was applied. In particular, this method consisted of four stages: (i) 300 experiments distributed into 16 operating points were first performed to know the engine behavior under different EGR and valve overlap conditions; (ii) these 300 tests were reproduced with the 1D model to calibrate it; (iii) 150 engine simulations per operating point were done to find the EGR rate and VVT settings that minimize fuel consumption in each case; and (iv) a reduced DOE was performed to verify the findings obtained via modeling.

After this calibration process, and before studying the engine performance under transient conditions, the impact of EGR on fuel economy was analyzed. The tests and simulations for engine calibration revealed that the LP-EGR strategy led to fuel savings above 3% at medium loads when using high recirculation rates (around 25%). Such fuel savings resulted from higher knocking

resistance (which allows better combustion phasing) and lower heat and pumping losses. A maximum fuel consumption reduction of 5.9% was achieved at 2000 rpm and 15 bar BMEP, while limited advantages were observed at very low and high loads. These findings related to the use of the EGR strategy match the ones found in the literature [53, 96].

Moreover, conventional and hybrid SUV simulations were performed to evaluate the EGR benefit under WLTP driving conditions. These simulations showed that the EGR strategy decreased the fuel consumed by the conventional and hybrid SUVs by 2.6% and 5.0%, respectively. The higher impact of EGR on hybrid vehicle performance is due to the fact that hybridization enables the ICE to typically operate at medium-high loads, where both the engine thermal efficiency and the EGR benefit are maximum.

Once the potential of the EGR strategy to reduce fuel consumption and CO_2 emissions was confirmed, the objectives of this Ph.D. thesis were addressed. For that purpose, three studies were carried out to analyze and optimize the transient performance of the gasoline engine under high EGR conditions during relevant tip-in and tip-out maneuvers. All the conclusions drawn from these three studies are gathered in the following subsections: (6.1.1) engine response in tip-ins, (6.1.2) engine response in tip-outs, (6.1.3) compressor surge in tip-outs, and (6.1.4) overall conclusions.

6.1.1 Engine response in tip-ins

In this study, a series of tip-ins at 1500 rpm from 6 to 12 bar BMEP were tested to determine the influence of the EGR strategy on transient engine response. These tests were also utilized to assess the 1D model prediction under such conditions. The experimental tip-ins revealed that using EGR rates of around 22% slowed down the load increase notably, leading to a 2-s longer response time than not using EGR. This poor response with EGR is because of the slow increase in AMF, which, in turn, is derived from the need for larger turbocharger acceleration when introducing high EGR rates.

Therefore, in order to accelerate torque response, it is required to increase the engine airflow more rapidly. To this end, the following three strategies were investigated mainly with tip-in simulations (the first was also tested):

- EGR reduction strategy. The EGR dilution is reduced as fast as possible by closing the EGR valve simultaneously with the throttle opening.
- Pressurized air tank (PAT). A small (2l) tank of fresh air, initially at 3 bar and 20°C, is connected to both the intake manifold (downstream PAT) and the compressor inlet duct (upstream PAT).
- Electric supercharger. An electrically-driven supercharger is installed at the compressor outlet in series.

In addition to the engine response time, other criteria, such as fuel economy, complexity and costs, were also considered to evaluate the said strategies. In particular, the fuel consumption in each tip-in was assessed through the average BSFC in the first 20 engine cycles of the maneuver (Equation 5.3). The findings obtained from the tip-in simulations are listed below:

- The EGR reduction strategy is the simplest solution and leads to a torque response time of 0.57 s, around 0.25 s slower than with no EGR. Thus, this strategy is able to improve torque response significantly without using additional equipment. However, despite being the simplest, its implementation would not be effortless; given that the EGR valve and spark plug actuations must be adapted according to the tip-in operating conditions. This calibration work is essential to prevent torque overshoot and to ensure stable combustion.
- The downstream PAT leads to the best torque response time (0.31 s), which is even slightly better than the one achieved in the tip-in without EGR (0.32 s). In contrast, this strategy also results in higher fuel consumption and material costs. Besides, it should be noted that implementing the downstream PAT is associated with a significant increase in complexity: (i) a tank filling procedure is needed; (ii) compressor surge must be managed; and (iii) there is a trade-off between the tank capacity and the effort required to design the EGR and PAT valve actuations. If the amount of fresh air supplied by the tank is limited, it is necessary to close the EGR valve transiently (as in the tip-in with the EGR reduction strategy) and to optimize the PAT valve opening.
- The upstream PAT is a simpler solution than the preceding one. Thanks to the tank location, the compressor is not blocked during the maneuver,

and a dedicated EGR valve actuation is not needed. However, the torque response time (0.43 s) is not as fast as with the downstream tank.

- The electric supercharger provides an excellent trade-off between torque response and fuel consumption. With this boosting system, a short response time (0.41 s) can be achieved without reducing EGR dilution (the recirculation rate is kept above 22% throughout the maneuver), making a difference in fuel economy. Besides, using the e-supercharger is not associated with high complexity, given that it is enough to regulate the input power of its electric motor.

6.1.2 Engine response in tip-outs

Secondly, the impact of EGR on the performance of SI engines during tip-out maneuvers was studied. The EGR strategy was found to lead to combustion instabilities (in particular, 11 misfire events) in a tip-out test at 1500 rpm from 6 to 0.7 bar BMEP. The IMEP values of all cylinders were used as the main indicator of the occurrence of misfires. Besides, other variables, such as BMEP and raw CO and CO_2 emissions, were also analyzed to identify such stability issues. The appearance of misfires under these particular conditions is caused by a slow evacuation of the LP-EGR gases accumulated along the intake path, resulting in an excessive dilution of the air-fuel mixture once the load is decreased. In other words, the EGR dilution is reduced at a rate slower than required by the load conditions, so the solution seems clear: either to slow down the torque decrease (not desirable) or to reduce the amount of EGR gases entering the cylinders more quickly.

In order to achieve the latter, the following three strategies were investigated with tip-in tests and simulations:

- Delayed throttle closure (DTC). The throttle closure is delayed by 2, 4 and 6 engine cycles regarding the rest of the valve actuations.
- Secondary air path (SAP). A second intake path is coupled to the engine to bypass the main line, thus directly connecting the pipe upstream of the EGR joint to the intake manifold.
- Pressurized air tank (PAT). The concept is the same as the one defined in Subsection **6.1.1**, but the tank capacity is lower in this case. A 1l tank

of fresh air was connected to the intake manifold, and two initial tank pressure were considered: 1.3 and 1.8 bar. This system was investigated only via modeling.

The potential of these three strategies to enhance transient engine operation with EGR was evaluated based on two variables (related to combustion stability and engine response, respectively): the number of misfire events and the tip-out duration. The conclusions drawn from this study are given below:

- The tip-out tests and simulations performed to investigate the DTC and SAP solutions revealed a trade-off between combustion stability and torque response. Both solutions achieve to mitigate misfiring but at the expense of delaying or slowing down, to a greater or lesser degree, the load decrease.

- Delaying the throttle closure by 4 engine cycles (0.32 s) without SAP reduced the number of misfire events to 1. This improvement is attributed to a higher evacuation of EGR gases from the intake path during those first 4 cycles in which the in-cylinder trapped mass is not decreased. Therefore, it is concluded that DTC is an effective and simple solution, able to improve combustion stability without increasing complexity or costs. By contrast, delaying the throttle closure also involves postponing the torque drop.

- Installing a secondary air path was effective in mitigating combustion instabilities. However, given that the supply of air through the SAP is not instantaneous, this strategy cannot completely eliminate misfiring unless combined with DTC.

- No misfire was found during the tip-out tests in which DTC and SAP strategies were used. Nevertheless, the tip-out duration was prolonged by at least 4 cycles. Therefore, combining both strategies can lead to a stable load decrease but also slower.

- Engine simulations showed that the PAT system is able to reduce the EGR dilution more rapidly than SAP in the first 5 or 6 engine cycles. Hence, the PAT could potentially prevent misfiring without DTC and, consequently, without affecting torque response; although this should be confirmed with tests. That said, it should not be forgotten that using

the PAT is associated with a non-negligible increase in complexity and costs.

6.1.3 Compressor surge in tip-outs

A third study was done to determine if removing the compressor anti-surge valve (ASV) is feasible, with the aim of reducing turbocharger costs, without affecting compressor stability and engine response during fast load-decrease maneuvers. A series of tip-outs at 1500 rpm from full to zero load were tested to investigate two alternative strategies to ASV:

- Throttle closure optimization. The throttle actuation was divided into five linear transitions, whose durations were varied to find the surge limit. The optimum throttle closure was the fastest one that did not lead to compressor surge without the help of the ASV.
- Reduction of compressor inlet pressure (p_1). It basically consists in partially closing the intake flap (placed upstream of the EGR joint to achieve high recirculation rates) during the maneuver to decrease p_1 and increase the (compressor) corrected mass flow. This way, the load can be reduced faster without causing compressor instabilities. Three p_1 levels were analyzed: 0.33, 0.65 and 0.87 bar, considering the minimum p_1 value during the tip-out. For each of the last two levels, the throttle actuation was re-optimized by following the procedure mentioned just above. Closing the throttle was not required to reach the final load in the case with a minimum p_1 of 0.33 bar.

Instead of using the theoretical surge line, obtained from turbocharger tests in a gas stand under steady-state non-pulsating conditions, a criterion based on the crank-angle resolved pressure signal at the compressor outlet was defined for surge detection. By utilizing this criterion, the following conclusions were drawn from the tip-out tests:

- Compressor surge could be avoided without the ASV just by optimizing the throttle closure. In return, torque response was clearly penalized.
- Experimental tip-outs confirmed that the p_1 reduction strategy is effective in mitigating compressor surge, enabling a faster throttle closure.

In particular, in the case where p_1 was reduced to 0.33 bar, no surge was detected, and the torque response was very similar to the target response, the one achieved in the tip-out with the ASV activated.

- Therefore, it is concluded that compressor surge can be prevented during fast tip-out maneuvers by closing the intake flap instead of using the ASV, without any impact on engine response. Besides, it should be noted that implementing the p_1 reduction strategy is easy and does not require additional equipment or costs, but it is not 100% free of drawbacks. Reducing p_1 below the ambient pressure, even momentarily, can result in oil leakages into the compressor; so it would have to analyze the relevance of such leakages before using this strategy.

6.1.4 Overall conclusions

The test and simulation results of the first two studies demonstrated that high EGR operation adversely affects the SI gasoline engine performance during transient maneuvers, leading to slow torque response in tip-ins and unstable combustion in tip-outs. Such issues can be partially solved just by optimizing the throttle and EGR valve actuation. However, matching the transient engine response achieved without EGR requires more complex solutions, such as duplicating the intake path, using electric superchargers or air reservoirs, or any other strategy that allows the engine airflow to be increased (or the EGR dilution to be decreased) more quickly. Some of these solutions were found to be able to eliminate the penalty in engine response and combustion stability with EGR. That said, it should be considered that the better the solution is, the more complex and costly it tends to be. Therefore, understanding that engine response and, consequently, drivability cannot be penalized, manufacturers have to choose between two options: either reduce the EGR rate at certain operating conditions at the expense of not using the full EGR potential to improve fuel economy; or increase costs in design, development and manufacturing to operate with high EGR rates without affecting drivability.

Finally, the experimental results of the third study revealed that the intake flap can potentially assume the role of the compressor ASV during fast tip-out maneuvers without negative effects on compressor stability and engine response. Therefore, a reduction in turbocharger costs can be derived from high EGR operation.

6.2 Future works

The respondent is fully aware of the limitations of the studies performed in this thesis. Firstly, although the 1D engine model performance was widely validated, some of the solutions or strategies proposed (such as the pressurized air tank or electric supercharger) were investigated only with simulations. Secondly, it should be noted that the conclusions presented in Section 6.1 were drawn from engine tests and simulations under some specific transient operating conditions. Besides, the pollutant emissions were not analyzed in the studies. These limitations open the doors for the following future works:

- Testing the PAT and electric supercharger systems in order to confirm the findings obtained via modeling.
- Analyzing the EGR impact on engine response during other transient maneuvers and under real driving conditions. In this way, manufacturers could assess the worthiness of each solution more completely.
- Carrying out design and calibration tasks to utilize the strategies investigated (DTC, SAP, PAT, electric supercharger,...) over a wide range of operation. Using these strategies requires, among others, compact designs, dedicated valve and spark plug actuations, and a filling procedure for the PAT system.
- Evaluating how EGR and the other strategies affect pollutant emissions during the selected transient maneuvers.

Additionally, focusing on fuel economy, it would be interesting to explore the synergies between EGR and other relatively-new strategies, such as powertrain hybridization or advanced combustion modes:

- In this thesis, it was demonstrated with vehicle simulations that hybridization can increase the EGR benefit due to the possibility of partially decoupling engine power from driver demand. It should also be noted that the electric motor can mitigate or eliminate (depending on the level of hybridization and power demand) the drivability penalty derived from high EGR operation. Hence it would be worth studying the influence of the EGR strategy on fuel economy and drivability in different hybrid vehicle concepts.

- Turbulent jet ignition (TJI) is an advanced pre-chamber initiated combustion system that enables gasoline engines to operate with high levels of dilution [123]. The TJI strategy can extend the EGR tolerance [124] and reduce throttling. In light of this, the potential of TJI to improve the performance of gasoline engines during transient maneuvers under high EGR conditions should be studied.

Chapter 6 references

[53] T. Alger, T. Chauvet, and Z. Dimitrova. "Synergies between high EGR operation and GDI systems". *SAE International Journal of Engines* 1.(1) (2009), pp. 101–114. DOI: 10.4271/2008-01-0134 (cit. on pp. 17, 24, 25, 74, 127).

[96] K. Siokos, R. Koli, R. Prucka, J. Schwanke, and J. Miersch. "Assessment of Cooled Low Pressure EGR in a Turbocharged Direct Injection Gasoline Engine". *SAE International Journal of Engines* 8.(4) (2015), pp. 1535–1543. DOI: 10.4271/2015-01-1253 (cit. on pp. 25, 74, 127).

[123] W. P. Attard, N. Fraser, P. Parsons, and E. Toulson. "A Turbulent Jet Ignition Pre-Chamber Combustion System for Large Fuel Economy Improvements in a Modern Vehicle Powertrain". *SAE International Journal of Engines* 3.(2) (2010), pp. 20–37. DOI: 10.4271/2010-01-1457. URL: https://www.sae.org/content/2010-01-1457/ (cit. on p. 134).

[124] L. Zhou, Y. Ding, A. Q. Li, Y. Song, Z. Liu, and H. Wei. "Experimental study of gasoline engine with EGR dilution based on reactivity controlled turbulent jet ignition (RCTJI)". *Fuel* 331 (2023), p. 125744. DOI: 10.1016/j.fuel.2022.125744. URL: https://linkinghub.elsevier.com/retrieve/pii/S0016236122025728 (cit. on p. 134).

Global bibliography

[1] J. Serrano, H. Climent, R. Navarro, and D. González-Domínguez. "Methodology to Standardize and Improve the Calibration Process of a 1D Model of a GTDI Engine". *SAE Technical Paper 2020-01-1008* (2020). DOI: 10.4271/2020-01-1008. URL: https://www.sae.org/content/2020-01-1008/ (cit. on pp. xi, 60, 61, 63).

[2] J. Galindo, H. Climent, J. de la Morena, D. González-Domínguez, S. Guilain, and T. Besançon. "Experimental and modeling analysis on the optimization of combined VVT and EGR strategies in turbocharged direct-injection gasoline engines with VNT". *Proceedings of the Institution of Mechanical Engineers, Part D: Journal of Automobile Engineering* 235.(10-11) (2021). DOI: 10.1177/09544070211004502 (cit. on p. xi).

[3] J. Galindo, H. Climent, J. de la Morena, D. González-Domínguez, S. Guilain, and T. Besançon. "Assessment of air-management strategies to improve the transient performance of a gasoline engine under high EGR conditions during load-decrease operation". *International Journal of Engine Research* (2021). DOI: 10.1177/14680874211055578 (cit. on pp. xii, 5).

[4] J. Galindo, H. Climent, J. de la Morena, D. González-Domínguez, S. Guilain, and T. Besançon. "Compressor Surge Mitigation in Turbocharged Spark-Ignition Engines without an Anti-Surge Control System during Load-Decrease Operation". *Applied Sciences* 12.(3) (2022), p. 1751. DOI: 10.3390/app12031751. URL: https://www.mdpi.com/2076-3417/12/3/1751 (cit. on pp. xii, 89).

[5] H. Climent, V. Dolz, B. Pla, and D. González-Domínguez. "Analysis on the potential of EGR strategy to reduce fuel consumption in hybrid

powertrains based on advanced gasoline engines under simulated driving cycle conditions". *Energy Conversion and Management* 266 (2022), p. 115830. DOI: 10.1016/j.enconman.2022.115830 (cit. on p. xii).

[6] J. Galindo, H. Climent, J. de la Morena, D. González-Domínguez, and S. Guilain. "Assessment of air management strategies to improve the transient response of advanced gasoline engines operating under high EGR conditions". *Energy* 262 (2023), p. 125586. DOI: 10.1016/j.energy.2022.125586. URL: https://linkinghub.elsevier.com/retrieve/pii/S0360544222024720 (cit. on pp. xii, 5).

[7] C. Flynn, E. Yamasumi, S. Fisher, D. Snow, Z. Grant, M. Kirby, P. Browning, M. Rommerskirchen, and I. Russell. *Peoples' Climate Vote*. Tech. rep. United Nations Development Programme, University of Oxford and Browning Environmental Communications, 2021. URL: https://www.undp.org/publications/peoples-climate-vote (cit. on p. 2).

[8] H. Ritchie, M. Roser, and P. Rosado. "CO2 and Greenhouse Gas Emissions: by sector". *Our World in Data* (2020). URL: https://ourworldindata.org/emissions-by-sector (cit. on p. 2).

[9] Statista. *Emissions in the European Union*. Tech. rep. 2022. URL: https://www.statista.com/study/56124/emissions-in-the-european-union/ (cit. on p. 2).

[10] Statista. *Emissions in the United States*. Tech. rep. 2022. URL: https://www.statista.com/study/40176/us-ghg-emissions-statista-dossier/ (cit. on p. 2).

[11] A. Joshi. "Review of Vehicle Engine Efficiency and Emissions". *SAE Technical Paper 2021-01-0575* (2021). DOI: 10.4271/2021-01-0575. URL: https://www.sae.org/content/2021-01-0575/ (cit. on pp. 2, 3, 23).

[12] G. Fontaras, N.-G. Zacharof, and B. Ciuffo. "Fuel consumption and CO2 emissions from passenger cars in Europe – Laboratory versus real-world emissions". *Progress in Energy and Combustion Science* 60 (2017), pp. 97–131. DOI: 10.1016/j.pecs.2016.12.004. URL: https://linkinghub.elsevier.com/retrieve/pii/S0360128516300442 (cit. on p. 2).

[13] G. Fontaras, B. Ciuffo, N. Zacharof, S. Tsiakmakis, A. Marotta, J. Pavlovic, and K. Anagnostopoulos. "The difference between reported and real-world CO2 emissions: How much improvement can be expected by WLTP introduction?" *Transportation Research Procedia* 25 (2017), pp. 3933–3943. DOI: 10.1016/j.trpro.2017.05.333. URL: https://linkinghub.elsevier.com/retrieve/pii/S2352146517306403 (cit. on p. 2).

[14] European Parliament. *Fit for 55: MEPs back objective of zero emissions for cars and vans in 2035*. Tech. rep. 2022. URL: https://www.europarl.europa.eu/news/en/press-room/20220603IPR32129/fit-for-55-meps-back-objective-of-zero-emissions-for-cars-and-vans-in-2035 (cit. on p. 2).

[15] Statista. *Transportation emissions in the European Union*. Tech. rep. 2021. URL: https://www.statista.com/study/89825/eu-transportation-emissions/ (cit. on p. 2).

[16] U.S. Environmental Protection Agency (EPA). *Revised 2023 and Later Model Year Light-Duty Vehicle Greenhouse Gas Emissions Standards*. 2021. URL: https://www.epa.gov/regulations-emissions-vehicles-and-engines/final-rule-revise-existing-national-ghg-emissions (cit. on p. 3).

[17] H. Zhang, F. Zhao, H. Hao, and Z. Liu. "Effect of Chinese Corporate Average Fuel Consumption and New Energy Vehicle Dual-Credit Regulation on Passenger Cars Average Fuel Consumption Analysis". *International Journal of Environmental Research and Public Health* 18.(14) (2021), p. 7218. DOI: 10.3390/ijerph18147218. URL: https://www.mdpi.com/1660-4601/18/14/7218 (cit. on p. 3).

[18] Y. Li, Z. Wang, K. Wang, and B. Zhang. "Fuel economy of Chinese light-duty car manufacturers: An efficiency analysis perspective". *Energy* 220 (2021), p. 119622. DOI: 10.1016/j.energy.2020.119622. URL: https://linkinghub.elsevier.com/retrieve/pii/S0360544220327298 (cit. on p. 3).

[19] M. Lyu, X. Bao, R. Zhu, and R. Matthews. "State-of-the-art outlook for light-duty vehicle emission control standards and technologies in China". *Clean Technologies and Environmental Policy* 22.(4) (2020), pp. 757–771. DOI: 10.1007/s10098-020-01834-x. URL: http://link.springer.com/10.1007/s10098-020-01834-x (cit. on p. 3).

[20] T. Burton, S. Powers, C. Burns, G. Conway, F. Leach, and K. Senecal. "A Data-Driven Greenhouse Gas Emission Rate Analysis for Vehicle Comparisons". *SAE International Journal of Electrified Vehicles* 12.(1) (2022). DOI: 10.4271/14-12-01-0006. URL: https://www.sae.org/content/14-12-01-0006/ (cit. on p. 4).

[21] Q. Qiao, F. Zhao, Z. Liu, S. Jiang, and H. Hao. "Comparative Study on Life Cycle CO2 Emissions from the Production of Electric and Conventional Vehicles in China". In: *Energy Procedia*. Vol. 105. 2017, pp. 3584–3595. DOI: 10.1016/j.egypro.2017.03.827 (cit. on p. 4).

[22] P. Mock and Z. Yang. *A 2022 update on electric car sales: China taking the lead, the U.S. catching up, and Europe falling behind*. 2022. URL: https://theicct.org/2022-update-ev-sales-us-eu-ch-aug22/ (cit. on p. 4).

[23] P. Senecal and F. Leach. "Diversity in transportation: Why a mix of propulsion technologies is the way forward for the future fleet". *Results in Engineering* 4 (2019), p. 100060. DOI: 10.1016/j.rineng.2019.100060. URL: https://linkinghub.elsevier.com/retrieve/pii/S259012301930060X (cit. on p. 4).

[24] I. Boudway. *More Than Half of US Car Sales Will Be Electric by 2030*. 2022. URL: https://www.bloomberg.com/news/articles/2022-09-20/more-than-half-of-us-car-sales-will-be-electric-by-2030 (cit. on p. 4).

[25] N. Fraser, H. Blaxill, G. Lumsden, and M. Bassett. "Challenges for Increased Efficiency through Gasoline Engine Downsizing". *SAE International Journal of Engines* 2.(1) (2009), pp. 991–1008. DOI: 10.4271/2009-01-1053. URL: https://www.sae.org/content/2009-01-1053/ (cit. on pp. 4, 15).

[26] D. Coltman, J. Turner, R. Curtis, D. Blake, B. Holland, R. J. Pearson, A. Arden, and H. Nuglisch. "Project Sabre: A Close-Spaced Direct Injection 3-Cylinder Engine with Synergistic Technologies to Achieve Low CO2 Output". *SAE International Journal of Engines* 1.(1) (2008), pp. 129–146. DOI: 10.4271/2008-01-0138. URL: https://www.sae.org/content/2008-01-0138/ (cit. on pp. 4, 15).

[27] J. Luján, H. Climent, R. Novella, and M. Rivas-Perea. "Influence of a low pressure EGR loop on a gasoline turbocharged direct injection engine". *Applied Thermal Engineering* 89 (2015), pp. 432–443. DOI: 10.1016/j.applthermaleng.2015.06.039 (cit. on pp. 4, 17, 24).

[28] G. Xiao, Z. Yang, and A. Isenstadt. "Fuel-efficiency technology trend assessment for LDVs in China: Advanced engine technology". 2018. URL: https://theicct.org/publication/fuel-efficiency-technology-trend-assessment-for-ldvs-in-china-advanced-engine-technology/ (cit. on p. 14).

[29] U.S. Environmental Protection Agency (EPA). *The 2021 EPA Automotive Trends Report. Greenhouse Gas Emissions, Fuel Economy, and Technology since 1975*. Tech. rep. 2021. URL: https://www.epa.gov/automotive-trends (cit. on p. 14).

[30] B. Lecointe and G. Monnier. "Downsizing a Gasoline Engine Using Turbocharging with Direct Injection". *SAE Technical Paper 2003-01-0542* (2003). DOI: 10.4271/2003-01-0542. URL: https://www.sae.org/content/2003-01-0542/ (cit. on p. 14).

[31] R. Nozawa, Y. Morita, and M. Shimizu. "Effects of engine downsizing on friction losses and fuel economy". *Tribology International* 27.(1) (1994), pp. 31–37. DOI: 10.1016/0301-679X(94)90060-4. URL: https://linkinghub.elsevier.com/retrieve/pii/0301679X94900604 (cit. on p. 14).

[32] H. C. Watson, E. E. Milkins, K. Roberts, and W. Bryce. "Turbocharging for Fuel Efficiency". *SAE Technical Paper 830014* (1983). DOI: 10.4271/830014. URL: https://www.sae.org/content/830014/ (cit. on p. 15).

[33] G. Lumsden, D. OudeNijeweme, N. Fraser, and H. Blaxill. "Development of a Turbocharged Direct Injection Downsizing Demonstrator Engine". *SAE International Journal of Engines* 2.(1) (2009), pp. 1420–1432. DOI: 10.4271/2009-01-1503. URL: https://www.sae.org/content/2009-01-1503/ (cit. on p. 15).

[34] J. Turner et al. "Ultra Boost for Economy: Extending the Limits of Extreme Engine Downsizing". *SAE International Journal of Engines* 7.(1) (2014), pp. 387–417. DOI: 10.4271/2014-01-1185. URL: https://www.sae.org/content/2014-01-1185/ (cit. on p. 15).

[35] G. Ericsson, H.-E. Angstrom, and F. Westin. "Optimizing the Transient of an SI-Engine Equipped with Variable Cam Timing and Variable Turbine". *SAE International Journal of Engines* 3.(1) (2010), pp. 903–915. DOI: 10.4271/2010-01-1233. URL: https://www.sae.org/content/2010-01-1233/ (cit. on pp. 15, 17, 27).

[36] M. Bassett, J. Hall, B. Hibberd, S. Borman, S. Reader, K. Gray, and B. Richards. "Heavily Downsized Gasoline Demonstrator". *SAE International Journal of Engines* 9.(2) (2016), pp. 729–738. DOI: 10.4271/2016-01-0663. URL: https://www.sae.org/content/2016-01-0663/ (cit. on pp. 15, 17).

[37] S. Potteau, P. Lutz, S. Leroux, S. Moroz, and E. Tomas. "Cooled EGR for a Turbo SI Engine to Reduce Knocking and Fuel Consumption". *SAE Technical Paper 2007-01-3978* (2007). DOI: 10.4271/2007-01-3978. URL: https://www.sae.org/content/2007-01-3978/ (cit. on pp. 15, 23).

[38] Y. Wang, G. Conway, J. McDonald, and A. Birckett. "Predictive GT-Power Simulation for VNT Matching to EIVC Strategy on a 1.6 L Turbocharged GDI Engine". *SAE Technical Paper 2019-01-0192* (2019). DOI: 10.4271/2019-01-0192. URL: https://www.sae.org/content/2019-01-0192/ (cit. on p. 15).

[39] A. Li, Z. Zheng, and T. Peng. "Effect of water injection on the knock, combustion, and emissions of a direct injection gasoline engine". *Fuel* 268 (2020), p. 117376. DOI: 10.1016/j.fuel.2020.117376. URL: https://linkinghub.elsevier.com/retrieve/pii/S0016236120303719 (cit. on p. 15).

[40] Z. Han, R. D. Reitz, J. Yang, and R. W. Anderson. "Effects of Injection Timing on Air-Fuel Mixing in a Direct-Injection Spark-Ignition Engine". *SAE Technical Paper 970625* (1997). DOI: 10.4271/970625. URL: https://www.sae.org/content/970625/ (cit. on p. 15).

[41] L. P. Wyszynski, C. R. Stone, and G. T. Kalghatgi. "The Volumetric Efficiency of Direct and Port Injection Gasoline Engines with Different Fuels". *SAE Technical Paper 2002-01-0839* (2002). DOI: 10.4271/2002-01-0839. URL: https://www.sae.org/content/2002-01-0839/ (cit. on p. 15).

[42] D. Akihisa and S. Daisaku. "Research on Improving Thermal Efficiency through Variable Super-High Expansion Ratio Cycle". *SAE Technical Paper 2010-01-0174* (2010). DOI: 10.4271/2010-01-0174. URL: https://www.sae.org/content/2010-01-0174/ (cit. on p. 15).

[43] F Zhao, M.-C Lai, and D. L Harrington. "Automotive spark-ignited direct-injection gasoline engines". *Progress in Energy and Combustion Science* 25.(5) (1999), pp. 437–562. DOI: 10.1016/S0360-1285(99)

00004-0. URL: https://linkinghub.elsevier.com/retrieve/pii/S0360128599000040 (cit. on pp. 15, 16).

[44] L. Graham. "Chemical characterization of emissions from advanced technology light-duty vehicles". *Atmospheric Environment* 39.(13) (2005), pp. 2385–2398. DOI: 10.1016/j.atmosenv.2004.10.049. URL: https://linkinghub.elsevier.com/retrieve/pii/S1352231005000774 (cit. on pp. 15, 16).

[45] K. A. Confer, J. Kirwan, and N. Engineer. "Development and Vehicle Demonstration of a Systems-Level Approach to Fuel Economy Improvement Technologies". *SAE Technical Paper 2013-01-0280* (2013). DOI: 10.4271/2013-01-0280. URL: https://www.sae.org/content/2013-01-0280/ (cit. on p. 16).

[46] R. Golzari, Y. Li, and H. Zhao. "Impact of Port Fuel Injection and In-Cylinder Fuel Injection Strategies on Gasoline Engine Emissions and Fuel Economy". *SAE Technical Paper 2016-01-2174* (2016). DOI: 10.4271/2016-01-2174. URL: https://www.sae.org/content/2016-01-2174/ (cit. on p. 16).

[47] T. Han, G. Lavoie, M. Wooldridge, and A. Boehman. "Dual Fuel Injection (DI + PFI) for Knock and EGR Dilution Limit Extension in a Boosted SI Engine". *SAE Technical Paper 2018-01-1735* (2018). DOI: 10.4271/2018-01-1735. URL: https://www.sae.org/content/2018-01-1735/ (cit. on p. 16).

[48] V. Knop and E. Essayem. "Comparison of PFI and DI Operation in a Downsized Gasoline Engine". *SAE International Journal of Engines* 6.(2) (2013), pp. 941–952. DOI: 10.4271/2013-01-1103. URL: https://www.sae.org/content/2013-01-1103/ (cit. on p. 16).

[49] P. Price, R. Stone, D. OudeNijeweme, and X. Chen. "Cold Start Particulate Emissions from a Second Generation DI Gasoline Engine". *SAE Technical Paper 2007-01-1931* (2007). DOI: 10.4271/2007-01-1931. URL: https://www.sae.org/content/2007-01-1931/ (cit. on p. 16).

[50] M. Braisher, R. Stone, and P. Price. "Particle Number Emissions from a Range of European Vehicles". *SAE Technical Paper 2010-01-0786* (2010). DOI: 10.4271/2010-01-0786. URL: https://www.sae.org/content/2010-01-0786/ (cit. on p. 16).

[51] G. Saliba et al. “Comparison of Gasoline Direct-Injection (GDI) and Port Fuel Injection (PFI) Vehicle Emissions: Emission Certification Standards, Cold-Start, Secondary Organic Aerosol Formation Potential, and Potential Climate Impacts”. *Environmental Science and Technology* 51.(11) (2017), pp. 6542–6552. DOI: 10.1021/acs.est.6b06509. URL: https://pubs.acs.org/doi/10.1021/acs.est.6b06509 (cit. on p. 16).

[52] H. Mansouri and F. Ommi. “Performance prediction of aircraft gasoline turbocharged engine at high-altitudes”. *Applied Thermal Engineering* 156 (2019), pp. 587–596. DOI: 10.1016/j.applthermaleng.2019.04.116. URL: https://linkinghub.elsevier.com/retrieve/pii/S1359431118380268 (cit. on p. 16).

[53] T. Alger, T. Chauvet, and Z. Dimitrova. “Synergies between high EGR operation and GDI systems”. *SAE International Journal of Engines* 1.(1) (2009), pp. 101–114. DOI: 10.4271/2008-01-0134 (cit. on pp. 17, 24, 25, 74, 127).

[54] V. Macián, B. Tormos, V. Bermúdez, and L. Ramírez. “Assessment of the effect of low viscosity oils usage on a light duty diesel engine fuel consumption in stationary and transient conditions”. *Tribology International* 79 (2014), pp. 132–139. DOI: 10.1016/j.triboint.2014.06.003. URL: https://linkinghub.elsevier.com/retrieve/pii/S0301679X14002199 (cit. on p. 17).

[55] D. Zeppei, S. Koch, and A. Rohi. “Ball Bearing Technology for Passenger Car Turbochargers”. *MTZ worldwide* 77.(11) (2016), pp. 26–31. DOI: 10.1007/s38313-016-0109-z. URL: http://link.springer.com/10.1007/s38313-016-0109-z (cit. on p. 17).

[56] B. Hu, S. Akehurst, A. Lewis, P. Lu, D. Millwood, C. Copeland, E. Chappell, A. De Freitas, J. Shawe, and D. Burtt. “Experimental analysis of the V-Charge variable drive supercharger system on a 1.0 L GTDI engine”. *Proceedings of the Institution of Mechanical Engineers, Part D: Journal of Automobile Engineering* 232.(4) (2018), pp. 449–465. DOI: 10.1177/0954407017730464 (cit. on p. 17).

[57] J. R. Serrano, H. Climent, J. De la Morena, and A. Gómez-Vilanova. “On the impact of turbocharger thermo-mechanical limitations on new generation gasoline engines”. *Applied Thermal Engineering* 222 (2023), p. 119934. DOI: 10.1016/j.applthermaleng.2022.119934. URL:

https://linkinghub.elsevier.com/retrieve/pii/S1359431122018646 (cit. on pp. 17, 19, 25).

[58] R. Kurz and R. White. "Surge avoidance in gas compression systems". *Journal of Turbomachinery* 126.(4) (2004), pp. 501–506. DOI: 10.1115/1.1777577 (cit. on p. 17).

[59] J. Andersen, F. Lindström, and F. Westin. "Surge definitions for radial compressors in automotive turbochargers". *SAE International Journal of Engines* 1.(1) (2009), pp. 218–231. DOI: 10.4271/2008-01-0296 (cit. on p. 17).

[60] W. Oakes, P. Lawless, J. Fagan, and S. Fleeter. "High-speed centrifugal compressor surge initiation characterization". *Journal of Propulsion and Power* 18.(5) (2002), pp. 1012–1018. DOI: 10.2514/2.6049 (cit. on p. 17).

[61] A. Engeda, Y. Kim, R. Aungier, and G. Direnzi. "The Inlet Flow Structure of a Centrifugal Compressor Stage and Its Influence on the Compressor Performance". *ASME Journal of Fluids Engineering* 125.(5) (2003), pp. 779–785. DOI: 10.1115/1.1601255 (cit. on pp. 17, 113).

[62] J. Galindo, H. Climent, C. Guardiola, and A. Tiseira. "On the effect of pulsating flow on surge margin of small centrifugal compressors for automotive engines". *Experimental Thermal and Fluid Science* 33.(8) (2009), pp. 1163–1171. DOI: 10.1016/j.expthermflusci.2009.07.006 (cit. on pp. 17, 113).

[63] P. Podevin, A. Danlos, M. Deligant, P. Punov, A. Clenci, and G. De La Bourdonnaye. "Automotive compressor: Effect of an electric throttle in the upstream circuit on the surge limit". In: *MATEC Web of Conferences*. Vol. 234. 2018. DOI: 10.1051/matecconf/201823403006 (cit. on pp. 17, 113).

[64] J. Galindo, J. Serrano, H. Climent, and A. Tiseira. "Experiments and modelling of surge in small centrifugal compressor for automotive engines". *Experimental Thermal and Fluid Science* 32.(3) (2008), pp. 818–826. DOI: 10.1016/j.expthermflusci.2007.10.001 (cit. on pp. 17, 114).

[65] J. Galindo, A. Tiseira, R. Navarro, D. Tarí, and C. Meano. "Effect of the inlet geometry on performance, surge margin and noise emission of an automotive turbocharger compressor". *Applied Thermal Engineering*

110 (2017), pp. 875–882. DOI: 10.1016/j.applthermaleng.2016.08.099 (cit. on p. 17).

[66] J. Galindo, J. Serrano, X. Margot, A. Tiseira, N. Schorn, and H. Kindl. "Potential of flow pre-whirl at the compressor inlet of automotive engine turbochargers to enlarge surge margin and overcome packaging limitations". *International Journal of Heat and Fluid Flow* 28.(3) (2007), pp. 374–387. DOI: 10.1016/j.ijheatfluidflow.2006.06.002 (cit. on p. 17).

[67] J. Lujan, J. Pastor, H. Climent, and M. Rivas. "Experimental Characterization and Modelling of a Turbocharger Gasoline Engine Compressor By-Pass Valve in Transient Operation". *SAE Technical Paper 2015-24-2524* (2015). DOI: 10.4271/2015-24-2524 (cit. on pp. 17, 89).

[68] Z. Lou and G. Zhu. "Review of Advancement in Variable Valve Actuation of Internal Combustion Engines". *Applied Sciences* 10.(4) (2020), p. 1216. DOI: 10.3390/app10041216. URL: https://www.mdpi.com/2076-3417/10/4/1216 (cit. on p. 18).

[69] F. Bonatesta, G. Altamore, J. Kalsi, and M. Cary. "Fuel economy analysis of part-load variable camshaft timing strategies in two modern small-capacity spark ignition engines". *Applied Energy* 164 (2016), pp. 475–491. DOI: 10.1016/j.apenergy.2015.11.057. URL: https://linkinghub.elsevier.com/retrieve/pii/S030626191501507X (cit. on p. 19).

[70] P. Piqueras, J. D. la Morena, E. J. Sanchis, and R. Pitarch. "Impact of Exhaust Gas Recirculation on Gaseous Emissions of Turbocharged Spark-Ignition Engines". *Applied Sciences* 10.(21) (2020), p. 7634. DOI: 10.3390/app10217634. URL: https://www.mdpi.com/2076-3417/10/21/7634 (cit. on pp. 19, 25).

[71] M. Sellnau and E. Rask. "Two-Step Variable Valve Actuation for Fuel Economy, Emissions, and Performance". *SAE Technical Paper 2003-01-0029* (2003). DOI: 10.4271/2003-01-0029. URL: https://www.sae.org/content/2003-01-0029/ (cit. on p. 20).

[72] S. Hara, S. Suga, S. Watanabe, and M. Nakamura. "Variable valve actuation systems for environmentally friendly engines". *Hitachi Review* 58.(7) (2009), pp. 319–324 (cit. on p. 20).

[73] Q. Li, J. Liu, J. Fu, X. Zhou, and C. Liao. "Comparative study on the pumping losses between continuous variable valve lift (CVVL) engine and variable valve timing (VVT) engine". *Applied Thermal Engineering* 137 (2018), pp. 710–720. DOI: 10.1016/j.applthermaleng.2018.04.017. URL: https://linkinghub.elsevier.com/retrieve/pii/S1359431117351918 (cit. on p. 20).

[74] W. Shin, M. Kim, S. Oh, C. Lee, H. Hwang, H. H. Song, H. W. Kim, B. S. Kim, and K. P. Ha. "An Experimental Study on a Six-Stroke Gasoline Homogeneous Charge Compression Ignition (HCCI) Engine with Continuously Variable Valve Duration (CVVD)". *SAE Technical Paper 2021-01-0512* (2021). DOI: 10.4271/2021-01-0512. URL: https://www.sae.org/content/2021-01-0512/ (cit. on p. 20).

[75] K. Akima, K. Seko, W. Taga, K. Torii, and S. Nakamura. "Development of New Low Fuel Consumption 1.8L i-VTEC Gasoline Engine with Delayed Intake Valve Closing". *SAE Technical Paper 2006-01-0192* (2006). DOI: 10.4271/2006-01-0192. URL: https://www.sae.org/content/2006-01-0192/ (cit. on p. 20).

[76] J. B. Heywood. "Ideal Models of Engine Cycles". In: *Internal Combustion Engine Fundamentals*. 2nd. New York: McGraw-Hill Education, 2018. URL: https://www.accessengineeringlibrary.com/content/book/9781260116106 (cit. on p. 20).

[77] M. Roberts. "Benefits and Challenges of Variable Compression Ratio (VCR)". *SAE Technical Paper 2003-01-0398* (2003). DOI: 10.4271/2003-01-0398. URL: https://www.sae.org/content/2003-01-0398/ (cit. on p. 21).

[78] K. Wittek, F. Geiger, J. Andert, M. Martins, V. Cogo, and T. Lanzanova. "Experimental investigation of a variable compression ratio system applied to a gasoline passenger car engine". *Energy Conversion and Management* 183 (2019), pp. 753–763. DOI: 10.1016/j.enconman.2019.01.037. URL: https://linkinghub.elsevier.com/retrieve/pii/S0196890419300834 (cit. on p. 21).

[79] K. Fridrichová, L. Drápal, J. Vopařil, and J. Dlugoš. "Overview of the potential and limitations of cylinder deactivation". *Renewable and Sustainable Energy Reviews* 146 (2021), p. 111196. DOI: 10.1016/j.rser.2021.111196. URL: https://linkinghub.elsevier.com/retrieve/pii/S1364032121004846 (cit. on p. 21).

[80] A. Kouba, B. Hnilicka, and J. Navratil. "Downsized Gasoline Engine Cylinder Deactivation MiL Development and Validation Using Real-Time 1-D Gas Code". *SAE Technical Paper 2018-01-1244* (2018). DOI: 10.4271/2018-01-1244. URL: https://www.sae.org/content/2018-01-1244/ (cit. on p. 21).

[81] R. Golzari, H. Zhao, J. Hall, M. Bassett, J. Williams, and R. Pearson. "Impact of intake port injection of water on boosted downsized gasoline direct injection engine combustion, efficiency and emissions". *International Journal of Engine Research* 22.(1) (2021), pp. 295–315. DOI: 10.1177/1468087419832791 (cit. on p. 21).

[82] C. Tornatore, D. Siano, L. Marchitto, A. Iacobacci, G. Valentino, and F. Bozza. "Water Injection: a Technology to Improve Performance and Emissions of Downsized Turbocharged Spark Ignited Engines". *SAE International Journal of Engines* 10.(5) (2017), pp. 2319–2329. DOI: 10.4271/2017-24-0062. URL: https://www.sae.org/content/2017-24-0062/ (cit. on p. 21).

[83] M. Fratita, F. Popescu, J. Martins, F. Brito, and T. Costa. "Direct water injection and combustion time in SI engines". *Energy Reports* 7 (2021), pp. 798–803. DOI: 10.1016/j.egyr.2021.07.061. URL: https://linkinghub.elsevier.com/retrieve/pii/S2352484721005266 (cit. on p. 21).

[84] B. Ashok, A. N. Kumar, A. Jacob, and R. Vignesh. "Emission formation in IC engines". In: *NOx Emission Control Technologies in Stationary and Automotive Internal Combustion Engines*. Elsevier, 2022, pp. 1–38. DOI: 10.1016/B978-0-12-823955-1.00001-2. URL: https://linkinghub.elsevier.com/retrieve/pii/B9780128239551000012 (cit. on p. 22).

[85] S. Rood, S. Eslava, A. Manigrasso, and C. Bannister. "Recent advances in gasoline three-way catalyst formulation: A review". *Proceedings of the Institution of Mechanical Engineers, Part D: Journal of Automobile Engineering* 234.(4) (2020), pp. 936–949. DOI: 10.1177/0954407019859822. URL: http://journals.sagepub.com/doi/10.1177/0954407019859822 (cit. on p. 22).

[86] W. B. Ribbens. "The Basics of Electronic Engine Control". In: *Understanding Automotive Electronics*. Elsevier, 2017, pp. 135–182. DOI: 10.1016/B978-0-12-810434-7.00004-1. URL: https://linkinghub.elsevier.com/retrieve/pii/B9780128104347000041 (cit. on p. 22).

[87] S. Kafle, H. Valera, and A. K. Agarwal. "Evolution of Catalytic Converters for Spark Ignition Engines to Control Emissions". In: *Novel Internal Combustion Engine Technologies for Performance Improvement and Emission Reduction*. Springer, 2021, pp. 175–196. DOI: 10.1007/978-981-16-1582-5_7. URL: https://link.springer.com/10.1007/978-981-16-1582-5_7 (cit. on p. 22).

[88] A. Joshi and T. V. Johnson. "Gasoline Particulate Filters—a Review". *Emission Control Science and Technology* 4 (2018), pp. 219–239. DOI: 10.1007/s40825-018-0101-y. URL: http://link.springer.com/10.1007/s40825-018-0101-y (cit. on p. 23).

[89] K. Nam, J. Yu, and S. Cho. "Improvement of Fuel Economy and Transient Control in a Passenger Diesel Engine Using LP(Low Pressure)-EGR". *SAE Technical Paper 2011-01-0400* (2011). DOI: 10.4271/2011-01-0400. URL: https://www.sae.org/content/2011-01-0400/ (cit. on p. 23).

[90] Y. Kawabata, T. Sakonji, and T. Amano. "The Effect of NOx on Knock in Spark-ignition Engines". *SAE Technical Paper 1999-01-0572* (1999). DOI: 10.4271/1999-01-0572. URL: https://www.sae.org/content/1999-01-0572/ (cit. on p. 23).

[91] V. Macián, J. Luján, H. Climent, J. Miguel-García, S. Guilain, and R. Boubennec. "Cylinder-to-cylinder high-pressure exhaust gas recirculation dispersion effect on opacity and NOx emissions in a diesel automotive engine". *International Journal of Engine Research* 22.(4) (2021), pp. 1154–1165. DOI: 10.1177/1468087419895401 (cit. on p. 23).

[92] L. Zhong, M. Musial, R. Reese, and G. Black. "EGR Systems Evaluation in Turbocharged Engines". *SAE Technical Paper 2013-01-0936* (2013). DOI: 10.4271/2013-01-0936. URL: https://www.sae.org/content/2013-01-0936/ (cit. on pp. 23, 24).

[93] J. Luján, H. Climent, F. Arnau, and J. Miguel-García. "Analysis of low-pressure exhaust gases recirculation transport and control in transient operation of automotive diesel engines". *Applied Thermal Engineering* 137 (2018), pp. 184–192. DOI: 10.1016/j.applthermaleng.2018.03.085 (cit. on p. 24).

[94] M. E. Rivas Perea. "Assessment of fuel consumption reduction strategies on a gasoline turbocharged direct injection engine with a cooled EGR system". PhD thesis. Valencia (Spain): Universitat Politècnica

de València, 2016. DOI: 10.4995/Thesis/10251/68497. URL: https://riunet.upv.es/handle/10251/68497 (cit. on p. 24).

[95] K. Kumano and S. Yamaoka. "Analysis of Knocking Suppression Effect of Cooled EGR in Turbo-Charged Gasoline Engine". *SAE Technical Paper 2014-01-1217* (2014). DOI: 10.4271/2014-01-1217. URL: https://www.sae.org/content/2014-01-1217/ (cit. on p. 24).

[96] K. Siokos, R. Koli, R. Prucka, J. Schwanke, and J. Miersch. "Assessment of Cooled Low Pressure EGR in a Turbocharged Direct Injection Gasoline Engine". *SAE International Journal of Engines* 8.(4) (2015), pp. 1535–1543. DOI: 10.4271/2015-01-1253 (cit. on pp. 25, 74, 127).

[97] R. Shimura, H. Zhao, and X. Wang. "Expansion of external EGR effective region and influence of dilution on boosted operation of a downsized turbocharged GDI engine". *SAE Technical Paper 2019-01-2252* (2019). DOI: 10.4271/2019-01-2252 (cit. on p. 25).

[98] G. Pilla and L. Francqueville. "Stabilization of Highly Diluted Gasoline Direct Injection Engine using Innovative Ignition Systems". *SAE International Journal of Engines* 7.(4) (2014), pp. 1734–1743. DOI: 10.4271/2014-01-2598 (cit. on p. 25).

[99] K. Siokos and R. Prucka. "Transient Operation and Over-Dilution Mitigation for Low-Pressure EGR Systems in Spark-Ignition Engines". *SAE International Journal of Engines* 11.(5) (2018), pp. 525–538. DOI: 10.4271/03-11-05-0035 (cit. on p. 26).

[100] P. Davis and M. Peckham. "The Analysis of Gasoline Transient Emissions Behaviour Using Fast Response Gas Analysers". *SAE Technical Paper 2007-26-015* (2007). DOI: 10.4271/2007-26-015 (cit. on p. 26).

[101] J. Sarlashkar, S. Rengarajan, and R. Roecker. "Transient Control of a Dedicated EGR Engine". *SAE Technical Paper 2016-01-0616* (2016). DOI: 10.4271/2016-01-0616. URL: https://www.sae.org/content/2016-01-0616/ (cit. on p. 26).

[102] A. Wiese, A. Stefanopoulou, J. Buckland, and A. Y. Karnik. "Modelling and Control of Engine Torque for Short-Circuit Flow and EGR Evacuation". *SAE Technical Paper 2017-01-0606* (2017). DOI: 10.4271/2017-01-0606. URL: https://www.sae.org/content/2017-01-0606/ (cit. on p. 26).

[103] K. Shen, Z. Xu, Z. Zhu, and L. Yang. "Combined effects of electric supercharger and LP-EGR on performance of turbocharged engine". *Energy* 244 (2022), p. 123176. DOI: 10.1016/j.energy.2022.123176. URL: https://linkinghub.elsevier.com/retrieve/pii/S0360544222000792 (cit. on pp. 27, 80).

[104] F. Liu, J. M. Pfeiffer, R. Caudle, P. Marshall, and P. Olin. "Low Pressure Cooled EGR Transient Estimation and Measurement for an Turbocharged SI Engine". *SAE Technical Paper 2016-01-0618* (2016). DOI: 10.4271/2016-01-0618. URL: https://www.sae.org/content/2016-01-0618/ (cit. on p. 27).

[105] F. Payri, J. Luján, H. Climent, and B. Pla. "Effects of the intake charge distribution in HSDI engines". *SAE Technical Paper 2010-01-1119* (2010). DOI: 10.4271/2010-01-1119 (cit. on p. 43).

[106] B. Pla, J. De La Morena, P. Bares, and I. Jiménez. "Knock Analysis in the Crank Angle Domain for Low-Knocking Cycles Detection". *SAE Technical Paper 2020-01-0549* (2020). DOI: 10.4271/2020-01-0549 (cit. on pp. 43, 44).

[107] B. Pla, J. De la Morena, P. Bares, and I. Jiménez. "Cycle-to-cycle combustion variability modelling in spark ignited engines for control purposes". *International Journal of Engine Research* 21.(8) (2020), pp. 1398–1411. DOI: 10.1177/1468087419885754 (cit. on p. 44).

[108] Gamma Technologies LCC. *GT-Suite: Flow Theory Manual*. Westmont, IL (USA), 2018 (cit. on p. 45).

[109] J. Ghojel. "Review of the development and applications of the Wiebe function: A tribute to the contribution of Ivan Wiebe to engine research". *International Journal of Engine Research* 11.(4) (2010), pp. 297–312. DOI: 10.1243/14680874JER06510 (cit. on p. 45).

[110] J. R. Serrano, F. J. Arnau, L. M. Garciá-Cuevas, A. Gómez-Vilanova, S. Guilain, and S. Batard. "A methodology for measuring turbocharger adiabatic maps in a gas-stand and its usage for calibrating control oriented and one-dimensional models at early ICE design stages". *ASME Journal of Energy Resources Technology* 143.(4) (2021), p. 042303. DOI: 10.1115/1.4048229 (cit. on pp. 45, 46, 113).

[111] A. Broatch, M. Diez, J. R. Serrano, P. Olmeda, and A. Gómez-Vilanova. "An experimental methodology and model for characterizing radial centrifugal compressors of turbocharged engines from diathermal perspective". In: *IFToMM World Congress 2019: Advances in Mechanism and Machine Science*. Krakow (Poland), 2019, pp. 883–892. DOI: 10.1007/978-3-030-20131-9_88. URL: http://link.springer.com/10.1007/978-3-030-20131-9_88 (cit. on p. 46).

[112] Gamma Technologies LCC. *GT-Suite: Vehicle Driveline and HEV Application Manual*. Westmont, IL (USA), 2018 (cit. on pp. 48, 49, 51).

[113] J. M. Luján, A. García, J. Monsalve-Serrano, and S. Martínez-Boggio. "Effectiveness of hybrid powertrains to reduce the fuel consumption and NOx emissions of a Euro 6d-temp diesel engine under real-life driving conditions". *Energy Conversion and Management* 199 (2019), p. 111987. DOI: 10.1016/j.enconman.2019.111987 (cit. on p. 50).

[114] F. Zhang, L. Wang, S. Coskun, H. Pang, Y. Cui, and J. Xi. "Energy Management Strategies for Hybrid Electric Vehicles: Review, Classification, Comparison, and Outlook". *Energies* 13.(13) (2020), p. 3352. DOI: 10.3390/en13133352. URL: https://www.mdpi.com/1996-1073/13/13/3352 (cit. on p. 51).

[115] G. Lavoie, E. Ortiz-Soto, A. Babajimopoulos, J. Martz, and D. Assanis. "Thermodynamic sweet spot for highefficiency, dilute, boosted gasoline engines". *International Journal of Engine Research* 14.(3) (2013), pp. 260–278. DOI: 10.1177/1468087412455372 (cit. on p. 60).

[116] J. Benajes, A. García, J. Monsalve-Serrano, and S. Martínez-Boggio. "Optimization of the parallel and mild hybrid vehicle platforms operating under conventional and advanced combustion modes". *Energy Conversion and Management* 190 (2019), pp. 73–90. DOI: 10.1016/j.enconman.2019.04.010 (cit. on p. 72).

[117] A. Pesaran. "Battery Requirements for Plug-In Hybrid Electric Vehicles: Analysis and Rationale". In: *23rd International Electric Vehicles Symposium and Exposition (EVS 23), Sustainability: The Future of Transportation*. Anaheim, California (USA), 2007. URL: https://www.osti.gov/biblio/923227 (cit. on p. 72).

[118] N. Zsiga, C. Voser, C. Onder, and L. Guzzella. "Intake manifold boosting of turbocharged spark-ignited engines". *Energies* 6.(3) (2013), pp. 1746–1763. DOI: 10.3390/en6031746 (cit. on p. 80).

[119] A. Lefebvre and S. Guilain. "Transient response of a turbocharged SI engine with an electrical boost pressure supply". *SAE Technical Paper 2003-01-1844* (2003). DOI: 10.4271/2003-01-1844 (cit. on p. 80).

[120] J. R. Serrano, F. J. Arnau, J. De la Morena, A. Gómez-Vilanova, S. Guilain, and S. Batard. "A Methodology to Calibrate Gas-Dynamic Models of Turbocharged Petrol Engines With Variable Geometry Turbines and With Focus on Dynamics Prediction During Tip-in Load Transient Tests". In: *Proceedings of the ASME Turbo Expo 2020: Turbomachinery Technical Conference and Exposition (Volume 8)*. ASME, 2020. DOI: 10.1115/GT2020-15169. URL: https://asmedigitalcollection.asme.org/GT/proceedings/GT2020/84195/Virtual,Online/1095133 (cit. on p. 84).

[121] J. Galindo, J. Serrano, C. Guardiola, and C. Cervelló. "Surge limit definition in a specific test bench for the characterization of automotive turbochargers". *Experimental Thermal and Fluid Science* 30.(5) (2006), pp. 449–462. DOI: 10.1016/j.expthermflusci.2005.06.002 (cit. on p. 114).

[122] G. Ellis. "Filters in Control Systems". In: *Control System Design Guide*. Elsevier, 2012, pp. 165–183. DOI: 10.1016/B978-0-12-385920-4.00009-6. URL: https://linkinghub.elsevier.com/retrieve/pii/B9780123859204000096 (cit. on p. 114).

[123] W. P. Attard, N. Fraser, P. Parsons, and E. Toulson. "A Turbulent Jet Ignition Pre-Chamber Combustion System for Large Fuel Economy Improvements in a Modern Vehicle Powertrain". *SAE International Journal of Engines* 3.(2) (2010), pp. 20–37. DOI: 10.4271/2010-01-1457. URL: https://www.sae.org/content/2010-01-1457/ (cit. on p. 134).

[124] L. Zhou, Y. Ding, A. Q. Li, Y. Song, Z. Liu, and H. Wei. "Experimental study of gasoline engine with EGR dilution based on reactivity controlled turbulent jet ignition (RCTJI)". *Fuel* 331 (2023), p. 125744. DOI: 10.1016/j.fuel.2022.125744. URL: https://linkinghub.elsevier.com/retrieve/pii/S0016236122025728 (cit. on p. 134).